Available online at www.sciencedirect.com

ScienceDirect

Advances in Space Research xxx (xxxx) xxx

ADVANCES IN SPACE RESEARCH (a COSPAR publication)

www.elsevier.com/locate/asr

Earth's geomagnetic environment—progress and gaps in understanding, prediction, and impacts

Hermann J. Opgenoorth [a,b,*], Robert Robinson [c,d], Chigomezyo M. Ngwira [c,d], Katherine Garcia Sage [c,d], Maria Kuznetsova [d], Mostafa El Alaoui [c,d], David Boteler [e], Jennifer Gannon [f], James Weygand [g], Viacheslav Merkin [h], Katariina Nykyri [d], Burcu Kosar [c], Daniel Welling [i], Jonathan Eastwood [j], Joseph Eggington [j], Michael Heyns [j], Norah Kaggwa Kwagala [k], Dibyendu Sur [c,d], Jesper Gjerloev [h]

[a] Dept. of Physics, Umeå University, SE-90187 Umeå, Sweden
[b] Dept. of Physics and Astronomy, Univ. of Leicester, University Road, LE17RH, Leicester, UK
[c] Dept. of Physics, Cath. Univ. of America, 620 Michigan Ave NE, Washington DC 20064, USA
[d] NASA Goddard Space Flight Center, 8800 Greenbelt Rd, Greenbelt, MD 20771, USA
[e] Natural Resources Canada, 2617 Anderson Rd., Ottawa, Ontario K1A E7, Canada
[f] Computational Physics Inc., 337 E Simpson St, Suite 200, Lafayette, CO 80026, USA
[g] Dept. of Earth, Planet. and Space Sci., Univ. of California, Los Angeles, CA, USA
[h] Johns Hopkins Univ., Appl. Physics Lab., 11100 Johns Hopkins Rd., Laurel, MD 20723, USA
[i] Dept. of Climate and Space Sci. and Engin., Univ. of Michigan, 2455 Hayward St., Ann Arbor, MI 48109, USA
[j] Space and Atm. Phys. Group, Imp. Coll. London, Prince Consort Rd., London, SW72AZ, UK
[k] Dept. of Physics and Technology, Univ. of Bergen, PO Box 7803, 5020 Bergen, Norway

Received 21 September 2023; received in revised form 26 April 2024; accepted 8 May 2024

Abstract

Understanding of Earth's geomagnetic environment is critical to mitigating the space weather impacts caused by disruptive geoelectric fields in power lines and other conductors on Earth's surface. These impacts are the result of a chain of processes driven by the solar wind and linking Earth's magnetosphere, ionosphere, thermosphere and Earth's surface. Tremendous progress has been made over the last two decades in understanding the solar wind driving mechanisms, the coupling mechanisms connecting the magnetically controlled regions of near-Earth space, and the impacts of these collective processes on human technologies on Earth's surface. Studies of solar wind drivers have been focused on understanding the responses of the geomagnetic environment to spatial and temporal variations in the solar wind associated with Coronal Mass Ejections, Corotating Interaction Regions, Interplanetary Shocks, High-Speed Streams, and other interplanetary magnetic field structures. Increasingly sophisticated numerical models are able to simulate the magnetospheric response to the solar wind forcing associated with these structures. Magnetosphere-ionosphere-thermosphere coupling remains a great challenge, although new observations and sophisticated models that can assimilate disparate data sets have improved the ability to specify the electrodynamic properties of the high latitude ionosphere. The temporal and spatial resolution needed to predict the electric fields, conductivities, and currents in the ionosphere is driving the need for further advances. These parameters are intricately tied to auroral phenomena—energy deposition due to Joule heating and precipitating particles, motions of the auroral boundary, and ion outflow. A new view of these auroral processes is emerging that focuses on small-scale structures in the magnetosphere and their ionospheric effects, which may include the rapid variations in current associated with geomagnetically induced currents and the resulting perturbations to geoelectric fields on Earth's surface. Improvements in model development have paralleled the advancements in understanding, yielding coupled models that better replicate the spatial and temporal scales needed to simulate the interconnected domains. Many realizations of

* Corresponding author at: Dept. of Physics, Umeå University, SE-90187 Umeå, Sweden.
E-mail address: hermann.opgenoorth@umu.se (H.J. Opgenoorth).

https://doi.org/10.1016/j.asr.2024.05.016
0273-1177/

such multi-component systems are under development, each with its own limitations and advantages. Challenges remain in the ability of models to quantify uncertainties introduced by propagation of solar wind parameters, to account for numerical effects in model codes, and to handle the special conditions occurring during extreme events. The impacts to technical systems on the ground are highly sensitive to the local electric properties of Earth's surface, as well as to the specific technology at risk. Current research is focused on understanding the characteristics of geomagnetic disturbances that are important for geomagnetically induced currents, the development of earth conductivity models, the calculation of geoelectric fields, and the modeling of induced currents in the different affected systems. Assessing and mitigating the risks to technical systems requires quantitative knowledge of the range of values to be expected under all possible geomagnetic and technical conditions. Considering the progress that has been made in studying the chain of events leading to hazardous geomagnetic disturbances, the path forward will require concerted efforts to reveal missing physics, improve modeling capabilities, and deploy new observational assets. New understanding should be targeted to accurately quantify solar wind driving, magnetosphere-iono sphere-thermosphere coupling, and the impacts on specific technologies. The research, modeling, and observations highlighted here provide a framework for constructing a plan by which the international science community can comprehensively address the growing threat to human technologies caused by geomagnetic disturbances.

1. Introduction

The geomagnetic environment refers to those regions of the near-Earth solar wind, the magnetosphere, and the ionosphere that are strongly influenced by the presence of magnetic fields. These regions are host to a number of physical phenomena that link them together, exchanging plasmas and fields on a wide range of spatial and temporal scales.

Space weather encompasses a broad range of physical processes from the Sun's atmosphere to Earth's surface. These produce intense radiation, energetic particle fluxes, disturbances in the solar wind, spatial and temporal variations of Earth's ionosphere, heating and expansion of the neutral atmosphere, electric currents, and geomagnetic disturbances. Technologies affected include electric power grids, communications, satellite infrastructure, global navigation systems, and aviation (Eastwood et al., 2017). The International Space Weather Action Teams (ISWAT) convened by the Committee on Space Research (COSPAR) were organized to assess progress and gaps across all space weather domains and affected technologies. In this paper, we focus on the physical processes and hazards associated with geomagnetic disturbances. Other space weather impacts are addressed in contributions from other ISWAT participants.

From a space weather perspective, disturbances in the geomagnetic environment are important because they may lead to disruptive geoelectric fields in power lines and other conductors on Earth's surface. The most dramatic geomagnetic disturbances are those associated with geomagnetic storms and substorms, which represent large-scale reconfigurations of the geomagnetic environment caused by electric currents in the magnetosphere, ionosphere, and along magnetic field lines connecting the two regions. However, hazardous perturbations to the geoelectric field can occur at other times, and the full chain of events that connect variations in the geomagnetic environment to terrestrial electric field perturbations remain to be elucidated. Success in mitigating the space weather effects stemming from disturbances in the geomagnetic environment depends on the fundamental understanding of the physical processes that underlie their occurrence.

This review summarizes the progress that has been made in the last 10 to 20 years in understanding the geomagnetic environment and forecasting the disturbances in the geoelectric field that represent the greatest potential threats to technical systems. The paper is organized to address in turn the solar wind driving mechanisms for geomagnetic disturbances, the coupling mechanisms that link the magnetically controlled regions of near-Earth space, and finally the impacts of these collective processes.

We begin with an analysis of solar wind drivers of geomagnetic disturbances, including a description and evaluation of past extreme events that illuminate both what we know and what we have yet to understand to mitigate geomagnetic and related hazards to technical systems. We then focus on the improvements in specifying auroral precipitation, high latitude electrodynamics, and the geomagnetic currents that have been achieved with global observations and assimilative models. Then we describe and critically assess the physics-based, modeling systems that have been developed to simulate solar disturbances and their magnetospheric and ionospheric effects. Finally, we discuss geoelectric fields and the geomagnetically induced currents that produce the direct impacts on vulnerable technical systems. We conclude with a summary of the remaining gaps in our ability to mitigate hazards from geomagnetic disturbances in terms of scientific understanding, modeling capabilities, and observations.

2. Solar wind driving

Understanding and modeling the transport of the Sun's energy carried by the solar wind into geospace is one of the most fundamental challenges for improving geomagnetic environment specification and forecasting. The Earth's magnetosphere results from the interaction of the solar wind plasma and interplanetary magnetic field (IMF) with the geomagnetic field. During this interaction, the shocked

solar wind impinging on the magnetosphere first interacts with the geomagnetic field on the dayside magnetopause located on average around 10 R_E from the Earth's center. During storms the magnetopause can be pushed inside the geosynchronous orbit. The magnetopause boundary is not in direct contact with the solar wind itself, but with the magnetosheath plasma which is located between the magnetopause and the bowshock. For typical solar wind conditions, quiet or disturbed, the bowshock lies only a few R_E sunward of the magnetopause. However, for low solar wind Mach number (e.g., during times of low solar wind density) the bow shock can be located much farther towards the Sun. A characteristic feature of the shocked magnetosheath plasma and foreshock region is the presence of waves and turbulence, which may change the orientation of the magnetic field in the magnetosheath and significantly affect the magnetosphere response to the solar wind. The effect of turbulence on magnetospheric dynamics is facilitated by the major physical processes operating at the magnetopause, high-altitude cusps and magnetotail. These processes are both impacted by the "seed" turbulence properties, and they also self-generate turbulence (Nykyri et al., 2006; Hasegawa et al., 2020; Stawarz et al., 2016). For example, it has been shown via MHD simulations that Kelvin-Helmholtz (KH) waves reach a larger size and produce more plasma transport into the magnetosphere when the magnetosheath seed turbulence of the plasma velocity field has dominating frequency close to the frequency of the theroretical fastest growing KH mode and has a higher amplitude (Nykyri, 2017). The fully kinetic simulations provide similar results and have shown that "when the amplitude level of turbulent magnetic field fluctuations is sufficiently high, the initial fluctuations can cause a faster evolution of the KH instability, leading to a more efficient plasma mixing within the vortex layer" (Nakamura et al., 2020). When IMF has a southward component, the solar wind energy is convected to the night side where it is temporarily stored as electromagnetic energy in the magnetotail before being released through magnetic reconnection in the magnetotail current sheet, often violently, and via accelerated plasma ejected tailward and towards the Earth. The magnetotail current sheet, when sufficiently thin, may also be impacted by turbulence properties in the plasma sheet and tail-lobes, and may more easily reconnect and lead to substorm onset, e.g., via transient flux loading produced by magnetosheath jets (Nykyri et al., 2019). It would be important to systematically study the effect of the enhanced magnetopause turbulence (e.g, those driven by KH waves) at the flank magnetopause on magnetotail reconnection dynamics and its dependence of solar wind and IMF properties.

To accurately model and predict the relationship between the solar wind and the response of the geospace system, it is vital that we understand which solar wind conditions cause the most intense geomagnetic disturbances, which conditions do not, and why. Here, we focus mainly on Coronal Mass Ejections (CMEs) and other interplanetary transients like Corotating Interaction Regions, (CIRs), Interplanetary Shocks (IPSs), and High-Speed Streams, (HSSs), which arrive first at L1 and then at the terrestrial magnetopause, and couple to the dynamic geospace system. In this paper, we use the term geospace to encompass the magnetosphere, plasmasphere, ionosphere, and thermosphere, which are electrically, dynamically, and chemically linked through coupling processes that remain to be understood.

Solar wind features, as recorded by different spacecraft at L1, provide information about the composition of CMEs or other solar wind transients (external driving conditions) that are critical for fundamental space weather research (Akasofu, 1981; Borovsky 2003; Echer et al., 2008), and for forecasting and prediction services (Pulkkinen et al., 2013; Tóth et al., 2014; Vourlidas, 2021). Solar wind interaction with the Earth's geospace regions is a complex process that is central to the initiation and development of dynamic geospace processes (Tsurutani et al., 2015, Borovsky and Valdinia, 2018). Note that the interplanetary solar wind origins and properties are discussed in a parallel accompanying paper by Temmer et al (2023, in this issue).

Storms driven by Coronal Mass Ejections (CMEs) are widely believed to be the most effective at producing large variations in the geomagnetic response (Gopalswamy et al., 2007; Huttunen et al., 2008; Ngwira et al., 2015). However, identifying whether the solar wind drivers and/or geospace processes that produce moderate to intense geomagnetic activity can be reproduced during extreme events is still an active area of research (Nagatsuma et al., 2015). One of the major hindrances to understanding the geospace dynamic processes is that the physical interactions within the solar wind, magnetosphere, ionosphere, and thermosphere exist at multiple scales, ranging from small scales of around 1 km to global scales of 300 km (Borovsky and Valdinia, 2018).

A fast CME can interact with a slow CME. These interplanetary CMEs (ICMEs) are known to be sources of intense geomagnetic activity (Mishra et al., 2015; Mostl et al., 2015). To fully appreciate the solar wind/geospace coupling and the geomagnetic response, we need to also understand the role of prehistory or preconditioning of the magnetosphere in the current state (Borovsky and Valdinia, 2018). The sequence of CMEs of various strengths will result in markedly different responses of the geospace system. The time scales over which preconditioning becomes important remain to be identified. Addressing these effects is also critical to strengthening modeling and forecasting of extreme events.

One of the most critical needs of the space weather community is to correctly predict the orientation of the IMF Bz component. This is because Bz orientation is the most important parameter in the coupling of the solar wind to the geospace system. Predicting IMF Bz is considered the "holy grail" of space weather, and Tsurutani et al., (2020) suggest that this task is more important than pre-

dicting the CME time of release, its speed, direction, and time of arrival.

There are many studies that have attempted to predict IMF Bz using different techniques, or in some cases a combination of two or more techniques (Savani et al., 2015; Riley et al., 2017; Kay and Gopalswamy, 2017; Möstl et al., 2018; Jackson et al., 2019; Sarkar et al., 2020). Unfortunately, even up to now, it is difficult to correctly predict the IMF Bz orientation. Any meaningful advances in the prediction of the IMF Bz orientation or space weather in general will require a concerted community effort, the identification of new observational techniques, and potentially also larger investments in new observational platforms at more locations. At present upstream observations beyond the L1 position (e.g., Solar Probe or Solar Orbiter) could help shed more light on this topic.

Although most geomagnetic disturbances originate from variations in the IMF Bz (Dungey, 1961; Yermolaev et al., 2018), magnetospheric compression caused by interplanetary shocks can significantly enhance the magnetopause current. Compression of the magnetosphere also plays a major role during sudden storm commencement (SSC) and can lead to increased magnetic perturbations at all latitudes. There has been some progress in the last 5–8 years on our understanding of the shock impact. Recent works have shown that the solar wind impact angle is also very important for geomagnetic response levels (Oliveira et al., 2018; Oliveira et al., 2021). These works suggest that shock impact angle is a key aspect of the interplanetary driving conditions, which affects the intensity and location of magnetic variations during geomagnetic storm activities. For instance, Oliveira et al., (2021) show that nearly frontal shocks can trigger intense substorm activity within 10 min of the impact, while inclined shocks take approximately an hour to produce substorms with lesser intensity.

Another difficulty in fully understanding solar wind drivers of magnetospheric responses stems from the existence of large-scale and mesoscale structures in the solar wind (Nykyri et al., 2019; Raptis et al., 2022). Such variations can be formed due to kinetic effects at the bow shock and/or processes in the sheath region of incoming CMEs. Nykyri et al., (2019) showed how during large-scale poloidal Alfvenic fluctuations, L1 solar wind monitors observed northward Bz, while the Geotail spacecraft –- just upstream of the Earth's bow shock –- observed a strong radial IMF. This radial IMF interval resulted in high dynamic pressure magnetosheath jets, which modified the preexisting sheath magnetic field (which was mostly in negative y-direction) and produced several bursts of −30 to −40 nT southward Bz in the sheath. The lineup of satellites including ARTEMIS, Time History of Events and Macroscale Interactions during Substorms (THEMIS), Magnetospheric Multi-Scale (MMS), Geotail, and Defense Meteorological Satellite Program (DMSP), as well as ground-based observations allowed accurate mapping of the time history of this event. The DMSP data indicated that these jets initiated dayside reconnection and produced additional magnetic flux-loading into the magnetotail current sheet, eventually leading to substorm onset (Nykyri et al., 2019). Using just a single L1 monitor would have misidentified this event as a substorm initiation during northward IMF.

As the dayside magnetospheric scale is about 40 Re, the IMF and solar wind structure at this scale can have surprising consequences on solar wind – magnetosphere driving. For example, instead of having the typical quasi-parallel shock at the dawn-sector and quasi-perpendicular shock at dusk sector for Parker-Spiral IMF, certain structures in the IMF can lead to two quasi-parallel shocks or two quasi-perpendicular shocks. Therefore, it will be crucial when performing statistical studies of the magnetospheric state or training neural networks for predicting various geomagnetic indices, one classifies how structured the IMF and solar wind is. A novel method has been recently developed where three L1 monitors orbiting the Earth-Sun L1 point were used to measure this structure (Burkholder et al., 2020). However, as it only takes ~ 1 hr with a typical solar wind speed to reach the Earth from L1, this does not provide much warning time for satellite or launch operators.

In recent years, our understanding of solar wind driving has been tested through simulations of extreme events. Several definitions of extreme events exist within the space weather community depending on the field of interest and space weather technological impact. Buzulukova (2018) has reviewed the origins, predictability, and impacts of extreme events. For the geomagnetic research community, the definition of an extreme event must align with geomagnetic activity specifications. The level of geomagnetic activity can be quantified using one of the several indices, which have been defined for different purposes. Some have been used by the scientific communities for decades. Each of the geomagnetic indices is basically derived from ground-based magnetometer data and aims to measure the intensity of a specific geospace current system (Borovsky and Valdinia, 2018). For example, prior studies (Cid et al., 2014, 2020; Ngwira and Pulkkinen, 2018) have shown that traditional storm indices like Dst (disturbance storm time) and Kp index, which are mostly influenced by the low latitude magnetic field of the ring current, are useful for providing information about general storm strength, but have not been so useful as indicators of geomagnetic disturbances, which is rather related to auroral zone current electrojet systems, which are better (but not sufficiently) well reflected by the Auroral Electrojet (AE) index. The Dst index is a measure of the intensity of geomagnetic ring current, while the planetary 3-hour range Kp index quantifies the level of disturbance in the horizontal geomagnetic field component, which of course also mostly depends on the ring current intensity, given the latitude choice of stations used to determine the KP index.

Geomagnetic indices are not always available to assess the potential impacts of an extreme event. In July 2012, the STEREO spacecraft observed solar wind conditions

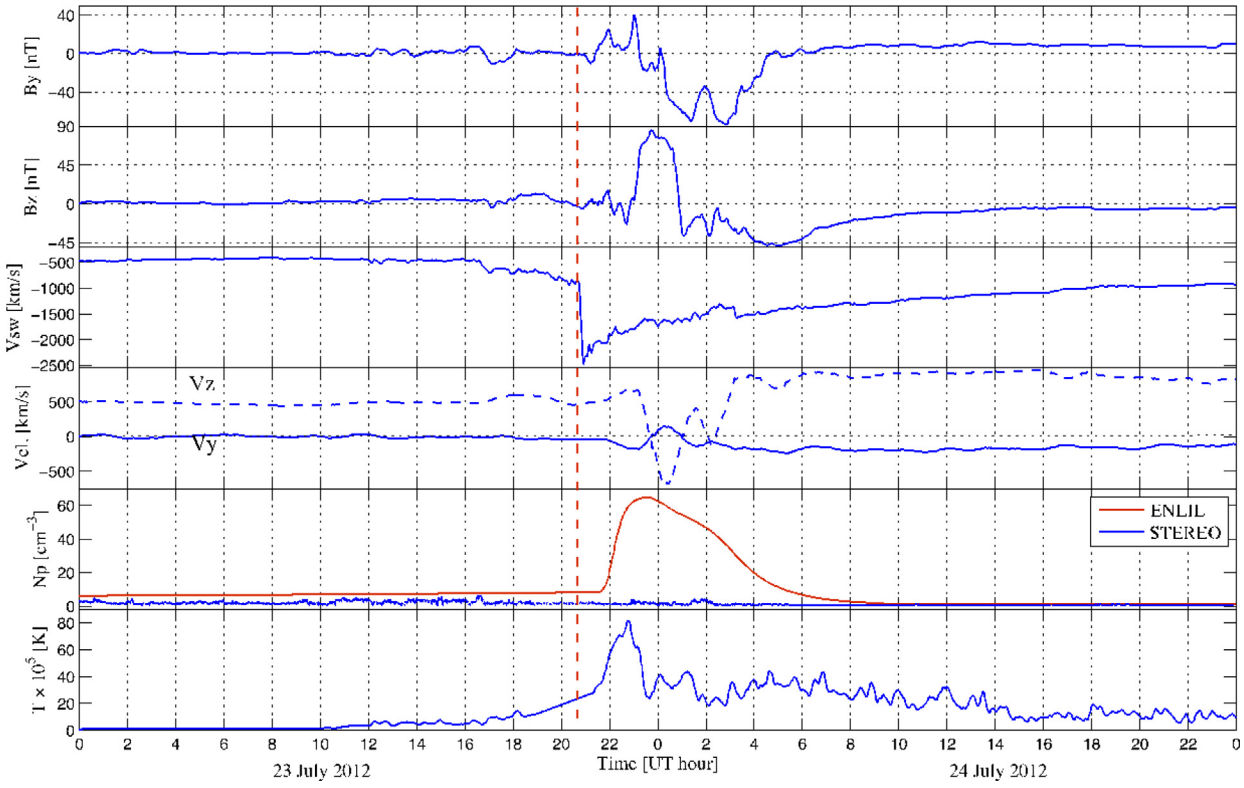

Fig. 1. In situ solar wind observations by the STEREO-A spacecraft on 12 July 2012. From top to bottom are the IMF By and Bz, and the solar wind plasma bulk speed (Vsw), velocity Vy (solid) and Vz (dashed), density (Np), and temperature (Temp). In the absence of actual measurements, the solar wind density (red trace) was obtained from the WSA-ENLIL 3-D MHD heliosphere model simulation. Adapted from Ngwira et al., (2013b).

associated with an extremely intense CME that missed the Earth. Fig. 1 shows the solar wind properties for this event modeled by Ngwira et al., (2013b) and Baker et al., (2013). The study by Baker et al., (2013) showed that the geomagnetic response at Earth, as determined by the Dst index, could have been comparable to the Carrington event of 1859 had this CME been Earth-directed. It is important to note that a comprehensive study of the Earth's response to solar influences is subject to the availability of observations. While the Carrington storm ranks as the largest storm on record, a very limited set of observations exist. However, the 20th and 21st century have been characterized by an increase in observations. Odenwald (2015) provides a thorough account of observed storms during these eras including the November 1903, September 1909, March 1918, May 1921, March 1924, September 1941, August 1972, March 1989, and the October 2003 Halloween storms, etc. Reportedly, most of these storms were associated with some level of impact on technological systems (Odenwald, 2015). In addition, Winter (2019) discusses the observed GIC effects of eight extreme storms during the period from 1859 to 2004. Two of the most recent extreme storms, i.e., March 1989 and October 2003, have well documented impacts and have received wide attention (Bolduc, 2002; Boteler, 2019; Pulkkinen et al., 2005; Wik et al., 2009).

Generally, extreme events are rare, but they can produce dramatic geomagnetic disturbances that have a detrimental impact on ground systems. Due to this occurrence limitation, extreme events pose a serious challenge to modeling efforts arising from insufficient observations and availability of much needed data for scientific analysis, and consequently for driving the relevant models. In addition, the whole solar wind-geospace coupled system is highly complex with varying physical processes acting at different spatiotemporal scales, as earlier mentioned. For example, we must consider and understand time scales such as the ~ 27 days solar rotation period, ~2–3 days Sun-Earth propagation, ~1 h propagation from L1, about 10 min for geospace reconfiguration, and ~ 1-minute geomagnetic field fluctuations. On top of these time scales of the direct magnetospheric responses, the energetic particles created in the ring currents and radiation belts, and the coupling of currents to the neutral atmosphere act like gigantic memory banks of previous solar wind impacts, influencing the subsequent magnetospheric responses to new driving events. This makes it very challenging to predict certain phenomena, for instance, the small scales and rapid geomagnetic field variations, which in the end will be responsible for the majority of the really serious space weather impacts.

3. Geospace coupling

Understanding the geospace response to solar wind driving is closely tied to untangling the current systems that

couple the two regions, manifested in the appearance of aurora caused by precipitating particles, as well as the flow of plasma between the two regions in the form of ion upwelling and outflow. The last ten years have seen enormous progress in the ability to specify auroral precipitating particle fluxes, high-latitude electrodynamics, and ion outflow, largely due to the deployment and operation of global observing systems, the development of improved assimilative models, and better understanding of the underlying physical processes that couple the magnetosphere and ionosphere. We begin here with a short description of how electrodynamic parameters of the high latitude ionosphere are related. We then describe the state of the art in determining these parameters from observations and models, concentrating on those aspects directly relevant to the occurrence and properties of geomagnetic disturbances.

Note that this section focuses primarily on coupling between the magnetosphere and ionosphere. Coupling with the thermosphere is integral to these processes, but is dealt with in a separate paper in this special issue. While recognizing that separating these discussions is part of the problem in dealing with the entire system holistically, we confine the scope of this section to avoid overlap and redundancy with other contributions. The discussion in Section 4 on modeling encompasses the entire geospace system using coupled models that effectively integrate the physical processes connecting the space weather domains.

3.1. Auroral electrodynamics

The current J in the ionosphere perpendicular to the magnetic field B is given by

$$\underline{J}_{\perp} = \Sigma_P \underline{E} - \Sigma_H (\underline{E} \times \underline{B})/|B| \quad (1)$$

where E is the electric field and Σ_P and Σ_H are the height-integrated Pedersen and Hall conductivities (conductances), respectively. Eq. (1) is derived by integrating the Ohm's Law relationship over altitude, assuming the electric fields and currents do not change with altitude in the range 80 to 200 km. This allows the height-dependent conductivity values to be expressed as the height-integrated values Σ_P and Σ_H. Eq. (1) also assumes there is no neutral wind in the altitude range where the conductivities are significant. In the presence of a horizontal neutral wind in the ionosphere, Eq. (1) holds if the electric field is replaced with the effective electric field given by $\underline{E}_{eff} = \underline{E} - \underline{U} \times \underline{B}$, where U is the horizontal neutral wind. Various studies have shown that the neutral wind can be an important contributor to auroral currents in some situations. Furthermore, the neutral wind can have significant shears in the altitude range of interest, requiring the use of the altitude-dependent version of Eq. (1).

The field-aligned currents that connect ionospheric currents and electric fields to magnetospheric sources can be calculated by taking the divergence of the horizontal currents. Using current continuity,

$$\nabla \cdot \underline{J} = 0 \quad (2)$$

Eq. (1) becomes

$$J_{\parallel} = \nabla \cdot J_{\perp} = \nabla \cdot (\bar{\Sigma} \underline{E}) \quad (3)$$

The two main sources of energy input to the auroral regions are particle precipitation and Joule heating. The Joule heating produced by the ionospheric currents is given by

$$JH = \underline{J} \cdot \underline{E} = \Sigma_P E^2 \quad (4)$$

Energy input from particle precipitation is not included explicitly in the electrodynamic relationships above. However, the energy flux from precipitating particles is closely related to the conductances. Energy flux is calculated from the volume energy deposition of particles impacting the ionosphere and thermosphere, while conductances are calculated using the electron density resulting from the energy deposition.

Written in the form of Eq. (1), Ohm's Law in the ionosphere relates three unknowns: the conductances, the electric field, and the current. Thus, if any two of the unknowns in Eq. (1) are determined, the third can be calculated, resulting in a complete specification of all electrodynamic parameters (see Fig. 2). Note that the magnetic field is assumed to be known from models such as the International Geomagnetic Reference Field (IGRF, Thébault et al., 2015). These models are expansions of spherical harmonic or other orthogonal basis functions of global measurements of Earth's field from space-based and ground-based magnetometers. Some models represent only Earth's internal magnetic field, while others incorporate variations in the field caused by external current systems in the ionosphere and magnetosphere (e. g. Tsyganenko and Sitnov, 2007). The magnitude of the magnetic field at ionospheric altitudes from these empirical models do not differ by more than a fraction of a percent, much smaller than the uncertainties in the other parameters represented in the equations above. Similarly, secular variations of Earth's magnetic field are estimated to be about 3nT/year (Finlay et al., 2016), which are not large enough to produce significant uncertainties in derived electrodynamic parameters. Furthermore, measurements of magnetic perturbations made by magnetometers in space and on the ground are detrended to eliminate background fields. Thus, in situ measurements of geomagnetic disturbances are not dependent on the absolute value of Earth's magnetic field.

The challenge in achieving an accurate, global specification of auroral electrodynamic and energy input parameters is the difficulty in making direct measurements of the relevant parameters throughout the high latitude ionosphere. Such observations are not only important in specifying auroral parameters, but also in conducting the research needed to achieve a better understanding of the relevant physical processes. The remainder of this section documents the progress that has been made, particularly in the past ten years, in improving the accuracy, timeliness,

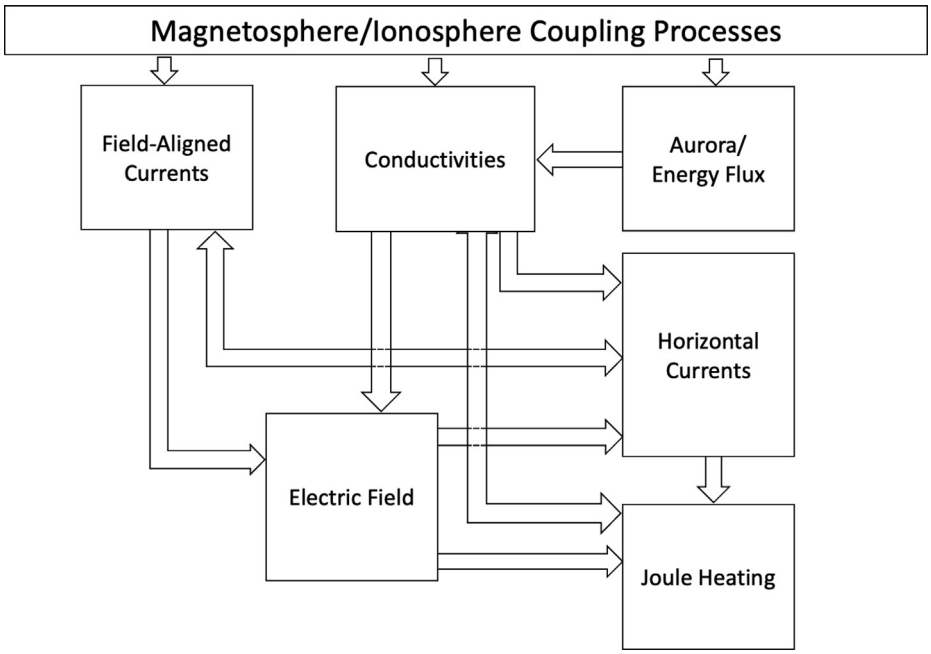

Fig. 2. Relationship between auroral electrodynamic quantities resulting from magnetosphere/ionosphere coupling processes. Arrows indicate which parameters are needed to determine other parameters. Neutral winds are taken into account by expressing the electric field in the reference frame of the neutrals.

and global extent of auroral electrodynamic parameter specification.

3.2. Energy flux and conductance

Quantifying auroral particle precipitation has been a longstanding challenge, beginning with early studies based on ground-based, optical information. Subsequent studies were based on more sophisticated optical techniques, and later in situ measurements made by sounding rockets or low-Earth orbiting satellites. Knowing the characteristics of precipitating particles is important for studies of the origin of the precipitation, quantifying the energy influx into Earth's upper atmosphere, and for accurate calculation of ionospheric electric conductivities. The challenge to a complete specification of auroral particle precipitation is that a number of different types of particles contribute, and the full particle energy spectrum must be known to accurately determine the amount of energy deposited and its location, both vertically and horizontally. Precipitating particles include energetic ions and electrons, but interaction with the atmosphere can produce secondary electrons, energetic neutral atoms, and bremsstrahlung X-rays, which also contribute to the total energy deposition. Even if particle precipitation can be characterized locally by combining data from various observational techniques, a global specification has not yet been achieved except by using empirical models based on long-term data sets, and/or theoretical models to fill in gaps between sparsely sampled measurements.

The most common approach to specifying global energy deposition by precipitating particles is based on optical auroral imaging from spacecraft. Far ultraviolet imaging allows for detection of emissions under sunlit conditions, and the ratios of selected bands provide information about the mean energy of the precipitation. Interpretation of the observations requires assumptions about the type of particles producing the emission and their energy spectrum. This begins with forward modeling of the height distribution of energy deposition using various first-principles techniques or more efficient implementations of those results (Rees, 1963; Strickland et al., 1976, 1983; Solomon, 2001; Fang et al., 2008, 2010, 2013).

FUV emissions produced below about 100 km are partially absorbed by the atmosphere above. This absorption makes it difficult to accurately estimate the high energy component of the particle spectral distribution. Bremsstrahlung X-ray emissions have been used to estimate the high energy component, but the mass of X-ray detectors makes it difficult to incorporate these instruments into satellite payloads.

Global imaging from satellites is limited in spatial or temporal coverage depending on the altitude of the spacecraft. High altitude satellites can image the entire auroral zone at one time, but not continuously. Imagers in low Earth orbit cannot image the entire auroral oval. A global specification is constructed from successive orbits or combined with a model to fill in gaps in coverage. Because of the limitations of global auroral imaging, empirical models have been used to specify the mean energy and energy flux

of particle precipitation from statistical averages of in situ measurements (Spiro et al., 1982; Hardy et al., 1985; Hardy et al., 1989; Fuller-Rowell and Evans, 1987; Newell et al., 2009, 2010; Redmon et al., 2017). Newell et al., (2014) developed an empirical model called OVATION based on DMSP electron and proton spectrometer data that accounts for the different types of auroral precipitation occurring in association with varying solar wind parameters. This approach improves the ability to replicate some of the smaller-scale structures in auroral precipitation during geomagnetically active periods.

For many applications, it is not necessary to know the global distribution. It is sufficient to know the total energy deposition from precipitating particles. This is specified separately for the northern and southern hemispheres by a quantity referred to as the hemispheric power index (HPI) (Evans, 1987). It was originally calculated from the empirical energy flux maps determined from statistical studies of in situ precipitating particle fluxes. More recently, the HPI has been determined from satellite-based measurements combined with models (Newell et al., 2009, Luan et al., 2010, 2011).

Ionospheric electrical conductivity is a key parameter for accurate specification of high latitude electrodynamic properties such as electric fields, currents, and Joule heating. While the contribution of ionospheric conductivity from solar illumination is well understood (Robinson and Vondrak, 1984; Brekke and Moen, 1993), the high spatial and temporal variability of energetic particle precipitation associated with aurora remains a challenge. A number of studies have used analytic expressions relating conductances to energetic particle precipitation parameters from the empirical particle precipitation models described above (e. g. Wallis and Budzinski, 1981; Vickrey et al., 1981; Spiro et al., 1982; Reiff, 1984; Robinson et al., 1987; and Kaeppler et al., 2015).

Conductances have also been mapped using FUV observations from numerous satellite missions. Lummerzheim et al., (1991) used broadband FUV observations from the Dynamics Explorer-1 satellite. With better spectral resolution, the intensity and ratios of selected Lyman-Birge-Hopfield bands of molecular nitrogen can be used to determine both the Pedersen and Hall conductances (Germany et al., 1994). Brittnacher et al., (1997) used FUV imaging data from the Polar satellite, which stopped operating in 2008. Coumans et al., (2004) used data from the IMAGE spacecraft, which operated from 2000 to 2005. Scanning FUV sensors on the Thermosphere Ionosphere Mesosphere Energetics and Dynamics (TIMED) satellite Global Ultraviolet Imaging (GUVI) instrument and the DMSP Special Sensor Ultraviolet Spectrographic Imager (SSUSI) provide images of FUV emissions in a broad swath over the polar regions, but not the entire auroral zone (see, for example, Christensen et al., 2003; Zhang and Paxton, 2008).

Other approaches to specifying conductances have been developed using ground-based observations. Ahn et al., (1998) correlated ionospheric conductances measured by incoherent scatter radar with ground-based magnetic perturbations. This approach has the advantage of replicating local enhancements in conductivity that other empirical models are often unable to capture. The Ahn et al., (1998) results were incorporated into the Assimilative Mapping of Ionospheric Electrodynamics (AMIE) model, which uses ground-based magnetometer and local measurements to produce an optimum specification of ionospheric conductivities (Richmond, 1992; Crowley and Hackert, 2001). Cousins et al., (2015) have shown that conductivities can be derived from ground-based measurements of electric fields from the Super Dual Auroral Radar Network (SuperDARN) combined with measurements of field-aligned currents from the Active Magnetosphere and Planetary Electrodynamics Response Experiment (AMPERE). Other ground-based instruments have been used to estimate auroral conductance, including methods based on all-sky imaging data (Kosch et al., 1998; Lam et al., 2019). Single wavelength or single bandpass imagers provide only the Pedersen conductance, while multispectral imagers offer the means to estimate both Hall and Pedersen conductances from the precipitating particle energy flux and average energy inferred from the optical emissions (e.g., Grubbs II et al., 2018). These methods offer the advantage of higher spatial and temporal resolution, but only over limited regions. Riometer measurements in combination with optical observations have also been used to deduce Hall and Pedersen conductances (Senior et al., 2008).

In the absence of global observations, modelers have used other methods to infer conductances. Ridley et al., (2004) and Wiltberger et al., (2009) derived conductances from field-aligned currents, with different relationships for upward and downward currents. This approach has the advantage of ensuring that aurorally enhanced conductances are collocated with upward current regions because those currents are well correlated with downward electron fluxes that produce conductivity enhancements. This connection was confirmed by Korth et al., (2014), who used TIMED GUVI observations to relate FUV emissions to large-scale regions of upward field-aligned currents determined from magnetometer data from the Iridium satellite constellation (the predecessor to AMPERE). More recently, Robinson et al., (2018) used AMPERE data with TIMED GUVI observations to show that field-aligned currents correlate with precipitating particle energy fluxes in both upward and downward current regions. The scaling between the two quantities was found to be a function of magnetic local time (MLT). A follow-on study based on AMPERE data combined with Poker Flat Incoherent Scatter Radar data showed similar linear relationships between field-aligned currents and conductances (Robinson et al., 2020). Relations between field-aligned currents and conductances have also been derived by Wang and Zou (2022) and Mukhopadhyay et al., (2020). McGranaghan et al., (2015a, b, and 2016) have applied machine learning

techniques for global specification of ionospheric conductances. Conductance models utilized in geospace coupled modeling systems are discussed in Section 4.

3.3. Electric fields

Early empirical models of high latitude convection were constructed by measurements of electric fields made by double probes and ion drift meters over many years. Weimer (2001) used satellite observations to develop a model of convection as a function of the direction of the interplanetary magnetic field. This has proven to be a mainstay for studies of solar wind-magnetosphere-iono sphere-thermosphere coupling and has been used in many different kinds of models for simulating the entire system.

Auroral electric fields can also be measured from the ground using incoherent scatter radars such as the European Incoherent Scatter Radar (EISCAT, Williams et al., 1984) and the Poker Flat Incoherent Scatter Radar (Nicolls et al., 2014). The high frequency (HF) radars that comprise the SuperDARN network (Greenwald et al., 1995) also measure plasma drifts from which electric fields can be derived. To overcome the limited spatial coverage of these measurements, long-term observations have been used to construct empirical models of high latitude convection (Holt et al., 1984, 1987; Foster et al., 1986a, 1986b), Gjerloev et al., 2018, Thomas and Shepherd, 2018).

Each of these empirical models has strengths and weaknesses. They all successfully capture the large-scale features of high latitude plasma convection and how it responds to changes in IMF. However, all are limited in their ability to replicate the small-scale variations in electric fields that in situ observations show are always present. Recently, Langmuir probe measurements from the SWARM satellites have been used to study the global distribution of plasma irregularities (De Michelis et al., 2021; Jin et al., 2019). In the future, EISCAT 3D will provide unprecedented volumetric measurements of electric fields and other ionospheric parameters (McCrea et al., 2015; Stamm et al., 2023) with a resolution that will enable measurements of kilometer scale structure. These small-scale variations in electric fields, can have dramatic effects on the electrical coupling between the magnetosphere and ionosphere that are not yet well understood. As discussed below, Joule heating is proportional to the square of the electric field. Thus, positive and negative values of the electric field might average to zero in empirical models, resulting in significant underestimates of the Joule heating rate.

As yet, there is no way to produce an instantaneous image of the high latitude electric fields or the associated plasma convection pattern. Thus, empirical models have been the primary means for specifying electric fields in global space weather simulations. Robinson et al., (2021) calculated the electric field from the field-aligned currents and conductances using $E=-\nabla\phi$ in Eq. (3) with the field-aligned currents determined from AMPERE and the conductance derived from Robinson et al., (2020). Thus, maps of electric potential and electric fields in the northern and southern hemispheres can be produced at the two-minute cadence of the AMPERE field-aligned current maps. This technique remains to be validated, but its success at duplicating the ground-based magnetic perturbations measured by the SuperMAG network offers promising results. The implication of this capability is that global space weather models need only specify the field-aligned currents correctly and the conductances, electric fields, and currents can be accurately and self-consistently determined.

Global maps of electric fields and other auroral electrodynamic parameters are also available through the open-source Assimilative Mapping of Geospace Observations (AMGeO) model, which extends the data assimilative approach of the AMIE model (Matsuo, 2020). By assimilating SuperDARN, AMPERE, SuperMAG, and other observations, AMGeO provides optimal specification of auroral electrodynamic parameters globally (Cousins et al., 2015).

3.4. Ionospheric and field-aligned currents

Generally, the direct impact on the magnetosphere from solar wind driving is most easily seen in the data from ground-based magnetometers, which measure the magnetic fields from ionospheric current systems connected to and driven by the three-dimensional currents in the magnetosphere. Typically, the auroral zone current systems in both hemispheres are quite stable, but nevertheless variable in response to solar wind driving. They generally consist of eastward directed auroral electrojets in the evening sector and westward directed electrojets in the morning sector, with some sunward closure current over the polar caps (Gjerloev, 2009; Gjerloev et al., 2010; 2011; and Shore et al., 2019). This current system, which is typically referred to as Disturbance Polar type 2 or DP2, is associated with the global ionospheric convection pattern in the opposite direction, which can easily be detected and monitored with HF coherent radar systems like SuperDARN (Lester, 2003). Both the convection and the current systems are directly driven by the reconnection of the terrestrial magnetosphere with the solar wind IMF component and are therefore mostly responding to the negative IMF Bz component, which controls subsolar reconnection. The system is balanced by nightside reconnection in the deep tail of the magnetosphere, closing the convection and current circuits (Dungey, 1961, Nishida, 1966, 1968a, b, Nishida and Maezawa, 1971). The DP2 system is global in its nature and exhibits relatively slow, less dramatic responses to solar wind driving than the related DP1 current system, which consists of a strong —- more or less localized —- westward electrojet enhancement in the midnight sector, appearing and disappearing in connection with so-called auroral or geomagnetic substorms. (Akasofu, 1964).

A thorough discussion of the magnetospheric processes that produce all the observed substorm phenomena, both

in space and in the ionosphere, has been ongoing for almost 50 years. It is now generally understood (Shore et al., 2019) that the localized enhanced westward electrojet, which is the ionospheric part of the of 3-dimensional substorm current wedge (the DP1current system) is typically superimposed on the preexisting eastward and westward electrojets of the convection driven DP2 current system. Thus, it can result in both an enhancement of the midnight and morning sector westward electrojet and a decrease (or turning) of the evening or pre-midnight sector eastward electrojet. McPherron et al., (1973) originally identified this superposition of a three-dimensional substorm current wedge by analyzing distant effects of the involved localized field-aligned currents at midlatitude magnetometer stations.

Obviously the DP2 system also responds globally to the local substorm onset in the nighttime sector due to the associated global magnetospheric dipolarization and related particle precipitation, which increases the ionospheric conductivity all along the auroral oval (Boraelv et al., 2000). Due to the sporadic and localized nature of the substorm current wedge, it is sometimes hard to determine the detailed nature of the new substorm DP1 current system on top of the changing and intensifying DP2 current system. It has generally been concluded (Morley et al., 2007) that the DP2 current system is directly driven by the solar wind-magnetosphere interaction, while the DP1 system is sporadically occurring, and due to an internal magnetospheric instability causing excess energy release. Thus, it has also clearly been shown that the prediction of geomagnetic disturbances on the basis of solar wind input data is reasonably good for the DP2 currents, but very hard, if not impossible for the DP1 currents (Newell et al., 2007).

A global specification of horizontal currents can be obtained by analyzing the magnetic perturbations caused by the currents as measured by ground-based magnetometers (Weygand et al., 2012; Weygand and Wing, 2020; Weygand, 2021). These studies were based on the Spherical Elementary Current System (SECS) technique, which allows determination of equivalent ionospheric currents from ground magnetic observations. The magnetic perturbation sums the contributions from all parts of the magnetosphere-ionosphere current system. In fact, Fukushima (1976) has shown that for a uniform conducting ionosphere the perturbation produced by the Pedersen component of the current is zero. Thus, the Hall currents primarily contribute to the ground-based magnetic perturbations. However, the derivation of the ionospheric currents from the ground-based measurements is difficult because the magnetometer integrates the contributions from a broad distribution of currents. Nevertheless, this method of deducing currents has continuously improved through the years owing to a denser array of magnetometer stations, more sophisticated deconvolution algorithms, and better accuracy and time resolution of the magnetic measurements. Although the global network of magnetometer stations continues to grow, specification of currents over locations without magnetometer stations remains a limiting factor.

Another method for determining ionospheric currents is based on "differential equivalent current vectors", which allows separation of newly occurring magnetic disturbances from the preexisting background fields. This method has yielded important new details about the substorm current wedge. First observed at high latitudes by Opgenoorth et al. (1980) and Baumjohann et al. (1981), it was originally understood as the signature of an onset of near-Earth reconnection or a large-scale dipolarization associated with a spontaneous short-circuiting of the unstable growth-phase cross-tail current in the magnetosphere (Sergeev et al., 2011; 2014; and references therein). Merkin et al., (2019) have shown that substorms are envelopes of the accumulative effects of multiple so-called bursty bulk flows (BBFs), containing small *meso*-scale dipolarizing bundles of magnetic flux (DFBs). When these arrive at the near-Earth inner edge of the magnetospheric plasma sheet and get braked there, they will cause DP1-like current wedges or even a multitude of smaller wedgelets (Rostoker, 1991; Liu et al., 2015). On the other hand, Ohtani and Gjerloev (2020) analyzed substorm magnetic perturbations measured by the SuperMAG network of magnetometers that contradict the wedgelet view. The formation of small-scale field aligned current wedges ("wedgelets") at the flanks of plasmasheet bursty-bulk-flow events as they get braked at the inner edge of the near-Earth plasmasheet has extensively been modelled by Birn et al., (2009), El-Alaoui et al., (2013), Wiltberger et al., (2017), Sorathia et al., (2020). These model results and their potential to represent the really occurring magnetospheric currents structures will be discussed at the end of Section 4 below. Kepko et al., (2015) have reviewed the current understanding of the substorm current wedge and associated features.

Detailed studies by Palin et al., (2015, 2016) and Weygand et al., (2022) using dense networks of ground-based magnetometers in conjunction with space-based data from THEMIS and Cluster have shown that basically all localized auroral intensifications, including breakups and even pseudo-breakups, are caused by such three-dimensional current wedgelets. An example is shown in Fig. 3 from Palin et al., (2016). It is possible that even large substorm current wedges in the sense of McPherron (1973) and Sergeev et al., (2011; 2014) may develop through an ensemble of repeated current intensifications caused by a large number of individual wedgelets or bursty bulk flows (as originally suggested by Liu et al., 2015), until the pattern results in the well-known "envelope" magnetic bay. It is this magnetic bay or substorm excursion in the ground-based magnetograms that has, over the last 50 years, given rise to the general concept of the substorm expansion phase.

Another method of observing horizontal currents in the ionosphere include incoherent scatter radars (ISR), which

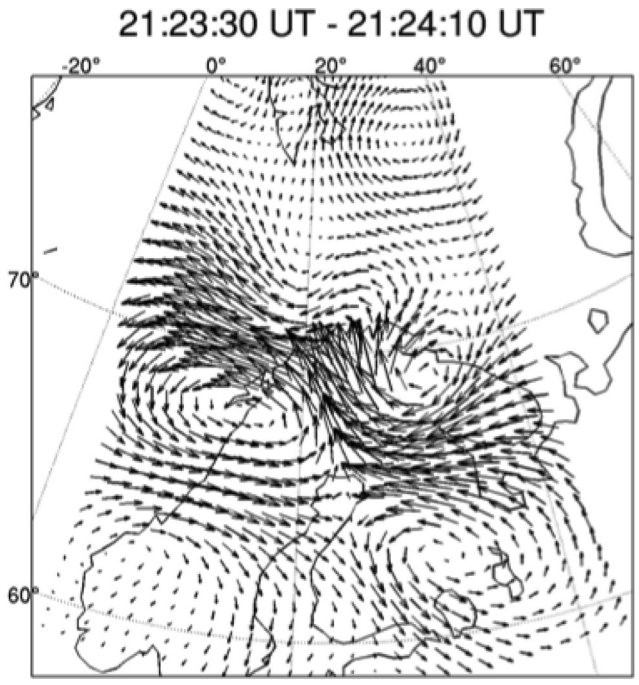

Fig. 3. Example of wedgelet-type, small scale current system reconstructed from ground magnetic observations (from Palin et al., 2016).

can directly measure conductivities and electric fields. The measured height profile of ionospheric electron density can be combined with model atmosphere parameters to determine both the altitude dependent and height-integrated conductivities. The electric fields are determined from the measured plasma drift velocities through $E = -V \times B$. The conductances and electric fields are used in Eq. (1) to calculate the current. The limitation to this method for calculating current is that ISRs are located at only a few sites around the globe, and most are not operated continuously. While important for studying the electrodynamics associated with specific localized events, their usefulness in a global specification is limited.

A new proof of concept experiment is being developed that provides a third way of measuring ionospheric currents. The EZIE cubesat mission makes use of the Zeeman splitting of atomic oxygen lines to estimate the local magnetic perturbations caused by nearby currents (Yee et al., 2017, 2021; Laundal et al., 2021). This offers a future capability of using a fleet of small satellites to measure currents globally and continuously.

Recent advances in understanding the current systems associated with geomagnetic disturbances have been made using observations of the field-aligned currents that link magnetospheric and ionospheric current systems. As indicated by Eq. (3), field-aligned currents can be determined from the divergence of the horizontal currents. This requires the two-dimensional distribution of horizontal currents, which may be possible locally with a tightly knit array of ground-based magnetometers, but global specification is not possible.

Over the past two decades, a technique for determining the global distribution of field-aligned currents using the Iridium satellite constellation has been developed. The Active Magnetosphere and Planetary Electrodynamics Response Experiment (AMPERE) is based on earlier studies that used magnetometer data from this constellation of 66 polar-orbiting satellites at 780 km altitude (Anderson et al., 2000; Waters et al., 2001). The improvement in the spatial and temporal resolution of the observations enabled by the AMPERE project has been described by Coxon et al., (2018). The field-aligned currents are computed from the horizontal magnetic perturbations measured at the Iridium satellite altitudes mapped to the ionosphere using a factor to account for the convergence of magnetic field lines (Anderson et al., 2014). With the assumption that the horizontal magnetic field perturbations are poloidal (curl-free) and that field-aligned currents are static over 10 min, the field-aligned currents can be computed from the associated potential function. To account for the uneven sampling of the Iridium magnetometer data, the measurements are fit by spherical harmonic expansion (Waters et al., 2020). Field-aligned current values are derived in a magnetic coordinate grid, with one degree spacing in latitude and one hour spacing in local time.

Although AMPERE provides a global view of the field-aligned current distribution routinely over both hemispheres, the limitations to its spatial and temporal resolution call for other techniques to study currents in more dynamic situations. Merkin et al., (2013) used model calculations to examine the effects of time variations in field-aligned currents on time scales of 10 min. Studies based on the SWARM satellite constellation have revealed a rich variety of field-aligned current structures associated with auroral precipitation (Wu et al., 2017). Despite its limitations, AMPERE has proven extremely useful for global specification of auroral energy fluxes and electrodynamic parameters for model input and validation (Robinson et al., 2018, 2020, 2021; Robinson and Zanetti, 2019).

The geomagnetic disturbances that represent hazards to power lines and long-line conductors on Earth's surface are those caused by intense and rapidly varying currents in the ionosphere. These variable currents result in large dB/dt values on the ground, causing geomagnetically induced currents (GICs) and geoelectric fields in conducting media. The sources and impacts of these time varying currents are described in Section 5.

3.5. Joule heating and Poynting flux

An important component of the auroral energy budget, particularly during geomagnetically active periods, is resistive heating from ionospheric currents (Joule heating). Joule heating is typically determined from the electric field and either the Pedersen conductance or altitude-integrated Pedersen current. Complete specification of Joule heating also includes dependence on neutral wind velocity (Thayer, 1998). Accurate Joule heating estimation depends

on the spatial and temporal resolution of the method or model used. Huang et al., (2012) compared Joule heat derived from the large-scale Weimer empirical model 2005 (Weimer, 2005) with that obtained using the Assimilative Mapping of Ionospheric Electrodynamics Model (AMIE) model. They showed that Joule heat derived from AMIE was about 40 % to 80 % higher than Joule heat derived from the empirical model. Similarly, Codrescu et al., (1995) and Matsuo and Richmond (2008) showed that intrinsic sub-grid variability of ionospheric electric field can lead to underestimation of Joule heat by large-scale models. This result indicates that dynamic variability and mesoscale structuring that are resolved in the data assimilation procedure (but not in the empirical model) are important factors affecting determinations of high-latitude heating.

It is important to note that modeling and data assimilative approaches may use different definitions of the Joule heating (Thayer and Semeter, 2004). The Thermosphere Ionosphere Electrodynamics General Circulation Model (TIEGCM) of the upper atmosphere (Qian et al., 2014; Richmond et al., 1992) and AMIE calculate the Joule heating as ohmic heating caused by current dissipation using the current and conductivity (Lu et al., 1996; Rastätter, et al., 2016). This approach does not account for neutral wind contribution. The Global Ionosphere Thermosphere Model (GITM) defines the Joule heating as frictional heating estimated directly from the relative ion-neutral drift velocities (Schunk and Nagy, 2009; Ridley et al., 2006; Zhu and Ridley, 2016). This discrepancy complicates direct comparison of Joule heating estimates across different data sources and model outputs (Verkhoglyadova et al., 2016; 2017).

A variety of observational techniques has been applied to validating estimates of Joule heating from models. Cosgrove at el. (2009) compared Joule heating derived from Sondrestrom Incoherent Scatter Radar measurements with those derived from the AMIE model. They found that the AMIE procedure provided estimates that are $\sim$ 30 % less than those of the ISR. They attributed the discrepancy to a difference in spatial resolution as predicted by Codrescu et al., (1995) and Matsuo and Richmond (2008).

Thayer (1998) examined the dependence of Joule heating altitude variations using electric field and neutral wind velocity measurements through the E region from the Sondrestrom incoherent scatter radar. The measurement was based on the steady state ion equation of motion applied to the measured ion drift velocity and electric field. The results showed a strong dependence of the altitudinal profile of Joule heating on neutral winds. The height-integrated Joule heating was dependent on neutral winds to a lesser degree.

Incoherent scatter radar has the capability to infer ionospheric heating locally with high resolution. Sojka et al., (2009) used ionospheric temperature measurements by the Poker Flat Incoherent Scatter Radar (PFISR) and EISCAT Svalbard Radar (ESR) to analyze heating in the polar cap and auroral region during High-Speed Streams. These measurements did not distinguish between heating due to particle precipitation and Joule heating. Further efforts are needed to separate these two sources. Combined use of incoherent scatter radar measurements of heating and auroral imaging can be a promising approach (Baker et al., 2004). This approach uses an empirical model to calculate neutral wind velocity in the absence of collocated measurements. Neutral wind divergence can contribute to high-latitude electrodynamics and is closely related to localized heating due to auroral precipitation (Mannucci et al., 2018). Collocated estimations of ionospheric electrodynamic parameters and neutral winds, for instance, with incoherent scatter radar can improve the Joule heating estimates.

In some cases, Joule heating cannot be measured directly, but is calculated from other validated measurements under certain assumptions, (Thayer, 1998; Cosgrove et al., 2014). Empirical models can constrain the values of auroral electrodynamic quantities if measurements are not readily available. Evaluation of several empirical models shows promising results (Lane et al., 2015) and their outputs can be compared with direct measurements and data assimilation products as a part of the assessment. When the ground-truth data is model-dependent, all the model assumptions must be thoroughly documented for future review and possible revision.

3.6. Auroral boundaries

Accurate identification of auroral boundaries is important for isolating the physical processes responsible for geomagnetic disturbances. Both poleward and equatorward boundaries are often necessary, and boundaries may differ depending on the process or phenomenon that is most important to the application. Boundary identification algorithms have been described by Longden et al., (2010) to identify the inner and outer edges of the auroral emission using optical data from the IMAGE satellite. Zhang et al., (2010) developed an automated technique to determine auroral boundaries using far ultraviolet data from the Global Ultraviolet Imager (GUVI) on the Thermosphere Ionosphere Mesosphere Energetics and Dynamics (TIMED) satellite (Christensen et al., (2003). In a study of extreme events, Ngwira et al., (2013a) determined auroral boundaries for geomagnetically induced current applications from DMSP precipitating particle flux data over the nine high-energy channels using the technique developed by Redmon et al., (2010). Weygand et al., (2023) determined equatorward auroral boundaries using field-aligned currents derived from ground-based magnetometer data.

The Aurorasaurus project database (MacDonald et al., 2015) offers a collection of geo-tagged and time-stamped signals of auroral visibility collected from citizen scientists. This ground-truth data provides detailed information about the observed aurora such as: colors, morphological

features, relative strength of the ongoing activity, the location in the sky, and often an image of the aurora. The number of reports submitted to the project increases proportionally with the intensity of the geomagnetic storm (Case et al., 2015a, b), thus leading to an abundance of data during large storms that can potentially be used to supplement and validate predictions of existing models. Since late 2014, the database compiled approximately 10,000 raw observations that are further validated and quality-controlled by the Aurorasaurus team using a method described in Case et al., (2016c). These validated and quality controlled real-time aurora sightings have been integrated into auroral research and utilized to quantitatively improve knowledge of auroral visibility and real-time alerts (Case et al., 2016b), as well as to help validate different sources of data and empirical models.

Recently, Kosar et al., (2018a) performed a study comparing equatorial boundaries at a fixed flux level obtained from two empirical models, the solar wind driven OVATION Prime 2013 (Newell et al., 2014) and the Kp-dependent Zhang-Paxton (Zhang and Paxton, 2008), with a subset of citizen science observations collected by the project. Previously, Case et al., (2016a) compared this data with the operational auroral forecast product of NOAA's Space Weather Prediction Center (SWPC) and found that $\sim$ 60 % of reports fall equatorward of the view-line (the estimated most equatorward latitude of the visible aurora) predicted by SWPC. The Aurorasaurus data are available and a publication to encourage its integration into auroral research by the scientific community is underway (Kosar et al., 2018b). With the continuous growth of the Aurorasaurus user community, the project database is likely to continue to expand in the near future, offering increasingly global data coverage. A future direction for the Aurorasaurus project includes development of an assimilative model that will allow full use of this new data source and will potentially lead to an improved knowledge of auroral specification.

Empirical models of auroral precipitation can be useful inputs for ionosphere-thermosphere models if measurements are not readily available, as for space weather forecasting. Evaluation of several models showed promising results (Lane et al., 2015), and their outputs can be also compared against direct measurements and data assimilation products as a part of the assessment.

3.7. Subauroral phenomena

Dramatic plasma convection enhancements occur during geomagnetic storms and substorms in the subauroral regions of geospace. These are typically latitudinally narrow regions of very strong westward plasma flows of sometimes more than 5 km/sec, which have been called many different names, often depending on the applied observation technique or the author group, such as polarization jet PJ, subauroral ion drift SAID, or subauroral electric fields SAEF.

Such narrow ionospheric plasma flow channels are proposed to be driven by a poleward polarization electric field located equatorward of the auroral electron precipitation region due to the radial separation between the inner plasma sheet electrons and ions, and similar explanations have been proposed for the broader regions of enhanced plasma convection that were regularly observed during geomagnetic storms. As a result, an encompassing term of "Sub-Auroral Polarization Streams", SAPS, has been proposed to include both the narrow PJ/SAID forms and any broader plasma stream regions. For more details on the nomenclature, and more importantly the underlying individual studies, see the excellent review on SAPS by Nishitani et al., (2019).

Of course, the question of the nomenclature is ultimately related to the question of the physical origins and magnetospheric/ionospheric driving mechanisms. The radial charge separation and the associated polarization electric field in the magnetosphere are widely accepted to be one of the two main drivers, with the other one being positive feedback between the magnetospheric electric field and ionospheric conductance. Another often advocated process that could produce SAPS is the sudden penetration of high latitude magnetospheric convection electric fields to subauroral regions, due to over- or under-shielding of the inner magnetosphere during rapid changes of the IMF Bz (Ebihara et al., 2008; Kikuchi et al., 2010). But even if there is now a general consensus on the importance of these rather large-scale magnetospheric processes for SAPS formation and evolution, there appears to be a growing realization that these do not explain some characteristics of narrow SAID and other more detailed observations of internal SAPS structure. The global SuperDARN radar network typically observes SAPS as a multiscale phenomenon from large regions of subauroral westward convection seen simultaneously by multiple radars to small-scale flow enhancements within only a few range gates.

The longitudinal structure of SAPS in the subauroral and midlatitude region has been investigated using the SuperDARN radars systems. For example, Oksavik et al., (2006) examined a SAPS flow channel equatorward of 60° MLAT that was observed for several hours by a single SuperDARN radar. Another similar observation was presented by Clausen et al., (2012), who studied the spatiotemporal evolution of a SAPS flow channel, as a narrow (few degrees wide) channel of westward flow extending over 6 h of MLT and through the fields of view of six midlatitude SuperDARN radars. Comparison with a GPS total electron content (TEC) map reveals that the SAPS channel was associated in latitude with the position of the ionospheric trough over this wide range of MLT.

SAPS have been observed more often, and with faster flow speeds and at lower latitudes with increasing geomagnetic activity level, which suggests that SAPS are closely controlled by solar wind conditions as well as by the ring current. A detailed examination by Grocott et al., (2011) showed that the latitudinal location of SAID varies on sim-

ilar time scales to those of the interplanetary magnetic field and auroral activity, while variations in its flow speed are more closely related to ring current dynamics. These results are consistent with the idea that the poleward electric field of SAPS/SAID is caused by the shielding effect of the ring current coupled with the ionosphere through the Region 2 FAC system.

SAPS are observed at all levels of geomagnetic disturbance, but with a dependence on disturbance level (characterized by Dst) such that quiet times have low occurrence rates (~10 %) while storm times have very high rates (approaching 100 %) (Kunduri et al., 2017). The SAPS feature is often clearly defined against a background of lower latitude, low velocity, subauroral scatter. Many SAPS events have been unambiguously related to substorm activity (Mishin et al., 2017). Large-scale variations of SAPS speed are not accompanied by variations of SAPS flow direction which remain extremely stable throughout the course of the event at given longitudes. SuperDARN observations of SAPS in conjunction with global auroral observations have demonstrated the important role played by auroral dynamics on the spatiotemporal evolution of SAPS. It has been demonstrated that any equatorward motion of the aurora can effectively compress the SAPS flow channel into its narrow SAID form while simultaneously strengthening it (Grocott et al., 2011).

Another recently discovered -- and much discussed – subauroral phenomenon is a new type of extended subauroral narrow region of pinkish auroral emissions. This phenomenon, which was named STEVE (Strong Thermal Emission Velocity Enhancement), may well be related to SAPS, or even more likely to the narrow form of SAPS, SAIDs. According to Gallardo-Lacourt et al. (2018), Nishimura et al. (2019) and other references within these papers, the occurrence frequency and general behavior of STEVE relates closely to those of SAIDs, and the emission characteristics of STEVE are closely related to the production mechanism of SAIDs. The observed plasma flow speeds are even higher than in SAIDs, close to 6 km/s.

For the purpose of this review, we conclude that SAPS and STEVE are mainly ionospheric phenomena in consequence of magnetospheric processes, caused by polarization electric fields set up by three-dimensional current systems. Thus, they are relevant for this chapter, but their potential space weather impact remains unclear for the time being. Considering their relation to strong electric fields, causing strong ions drifts, with a considerable impact on local electron density structures as well as TEC, one can, however, not exclude considerable space weather effects on GNSS systems by these phenomena.

3.8. Ion outflow

High latitude processes in the magnetosphere and ionosphere lead not only to electrodynamic coupling but also mass exchange between the two regions, both of which can be underlying factors in the location and timing of geomagnetic disturbances. The ionosphere, with denser and cooler plasma than the magnetosphere, undergoes a variety of energization processes that lead to escape of ions into the magnetosphere. An overview of mass loss processes, including the ion escape processes that are dominant at Earth, can be found in Gronoff et al., (2020). "Polar wind"-type outflow, so named by analogy with the solar wind, involves the escape of thermal ionospheric ions accelerated in bulk to supersonic escape velocities by ambipolar electric fields (Banks and Holzer, 1968). This type of outflow is primarily composed of H^+ and is a less variable source than the outflow processes described in the following paragraph. Along with energetic and heavy ion outflow processes, it is increasingly included as an ionospheric source in global magnetospheric modeling (e.g. Glocer et al., 2009, 2013) and has been shown to influence a variety of magnetospheric processes in global magnetosphere models (Welling and Liemohn, 2016). See Section 4 for more discussion of coupled geospace modeling systems.

The detection of O^+ in the magnetosphere indicated the presence of additional acceleration mechanisms that, unlike typical ambipolar fields in the ionosphere, are capable of accelerating heavy ions to escape energies (Shelley et al., 1972; Moore et al., 1984). O^+ plasma can make up a significant component of the plasma in the magnetosphere during geomagnetic storms (Nosé et al., 2003), where it influences the structure and dynamics of the magnetosphere and its processes (Lotko, 2007 and references therein). Such components are now included in multifluid magnetospheric models (Garcia et al., 2010; Brambles et al., 2011), in many cases with physics-based outflow models providing the multifluid outflow boundary conditions (Glocer et al., 2009; Varney et al., 2016b). The outflow processes that lead to heavy ion escape include (but are by no means limited to) soft electron precipitation (Redmon et al., 2014; Shen et al., 2016), convection-driven Joule heating (Varney et al., 2015), and wave-particle interactions that transversely accelerate ions, which are then reflected upward by the mirror force (Retterer et al., 1987; Bouhram et al., 2004). A more complete treatment of the possible mechanisms of ionospheric outflow can be found in Section 2.4 of Gronoff et al., (2020) and in Yau et al., (2011). The exact mechanisms that operate in a given region may combine and may vary over time, and the time history of the field line should be taken into account to accurately predict ion upflow and escape (Redmon et al., 2012). New research is showing that some of the outflow previously believed to be O^+ is actually N^+ (Lin et al., 2020), and new outflow modeling efforts are including N^+ upflow and escape in addition to O^+ (Lin et al., 2022).

Outflow models are coupled with other components of the coupled geospace modeling system (see Section 4). Examples include fully coupled ionosphere-thermosphere models for self-consistent magnetospheric dynamics, ion outflow, and electrodynamics (Pham et al., 2022), or models with kinetic processes providing wave particle interac-

tion physics (Glocer et al., 2018). However, a major limitation of these models is not the numerics or physics of the models themselves but our lack of knowledge of the wave processes in the ionosphere, their origin, or the wave spectral details that determine which processes are most effective in providing perpendicular or field-aligned acceleration for a given region or time period (Moore and Khazanov, 2010; Varney et al., 2016a, Glocer et al., 2018). Additional observations are needed in order to provide the necessary constraints and inputs to make improvements to outflow models and understand this important source of magnetospheric plasma.

4. Coupled models of the geomagnetic environment

4.1. Coupled geospace modeling

Solar wind impact on the magnetosphere results in dynamic transport of plasmas and fields from the dayside magnetopause to the magnetotail. Fast magnetotail reconnection causes the relatively steady earthward convection to be punctuated by strong, variable plasma energy flows in the form of bursty bulk flows (BBF) in the plasma sheet (Angelopoulos et al., 1992, 1994). Some of the earthward flowing energy is channeled into the ionosphere, but most is deposited in the inner magnetosphere and the reconnected magnetic flux is transported back to the dayside. The earthward directed energy accelerates particles into the ionosphere and excites auroral emissions. Energy and momentum are transferred between the magnetotail and the ionosphere resulting in coupling between these different physical domains. The scales involved in these transport processes range from hundreds of Earth radii (R_E) down to tens to hundreds of kilometers, as determined by the local electron and ion inertial lengths. This range of spatial and temporal scales, energies and processes makes modeling the Earth's geospace region challenging. Addressing this challenge requires coupled multicomponent modeling systems with each component utilizing modeling approaches tailored for the underlying physical processes.

The Global Magnetosphere (GM) is the largest domain and the central component of the tightly coupled geospace modeling system illustrated in Fig. 4. The GM component typically utilizes ideal or resistive magnetohydrodynamic (MHD) approaches. It has been more than 40 years since the first global MHD codes were developed to treat the large-scale dynamical response of the magnetosphere to changing solar wind conditions (Brecht et al., 1982; Ogino et al., 1985; Lyon et al., 1981; Tanaka, 1995; Frank et al., 1995; Raeder et al., 1998; Powell et al., 1999; El-Alaoui, 2001, Wiltberger et al., 2000; Gombosi et al., 2003, Palmroth et al., 2003). These studies have shown that global MHD models provide a reasonable description of the large-scale structure of Earth's magnetosphere.

The fluid MHD equations can be written in different forms, which are all mathematically equivalent, but generally lead to different numerical methods (Raeder, 2003; Gombosi et al., 2003; Lyon et al., 2004). They can be written in nonconservative (primitive variable) formalism, full conservative formalism, and semiconservative (gas dynamic conservative) formalism. The full conservative formulation allows the application of conservative finite volume schemes that strictly conserve mass, momentum, energy, and magnetic flux (Powell et al., 1999; Gombosi et al., 2003). In the semiconservative formulation, the equations are written in a form in which the gasdynamic terms are put in divergence form, and the electromagnetic terms in the momentum and energy equations are treated as source terms (Lyon et al., 2004; Raeder et al., 1998). This formulation allows for different schemes that numerically conserve mass, momentum, and plasma energy, but with no strict conservation of total energy. Examples of numerical schemes and other features utilized by different GM models are summarized in (Honkonen et al., 2013, p. 316, Table 1). The trend of modern geospace modeling systems is to utilize finer spatial resolution and less diffusive numerical schemes, and to move beyond single fluid MHD approach.

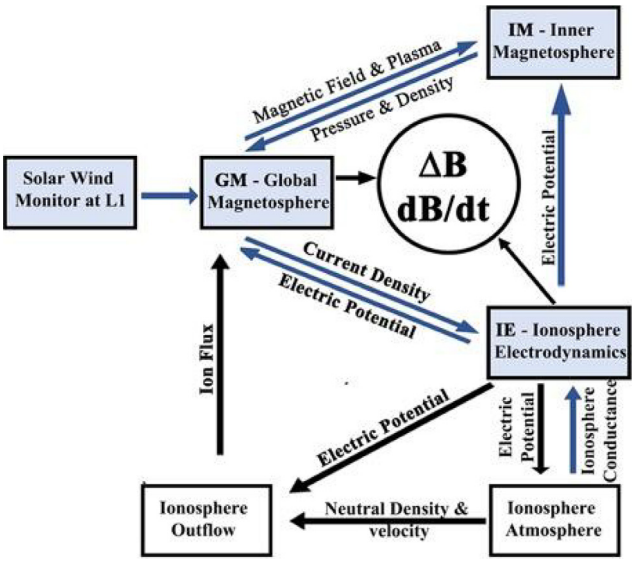

Fig. 4. Basic components of modern coupled geospace modeling systems and information passed between domains. The two-letter identifiers for the model components are those introduced in the Space Weather Modeling Framework (SWMF) (Toth et al., 2005, 2012). Components shaded in blue are included in the SWMF/Geospace model system running operationally at NOAA SWPC. Note that some geospace modeling systems include additional components that are not shown in the scheme (e.g., plasmasphere).

The GM simulation domain extends from roughly 30 R_E in the sunward direction to hundreds of Re in the nightside. The location of the upstream boundary is set further sunward if there is a need to accommodate special conditions such as low solar wind Mach number. Arbitrary or measured plasma and field solar wind parameters are imposed as boundary conditions at the upstream boundary of the GM simulation domain. For data driven modeling,

observed solar wind parameters are usually propagated from solar wind monitors at L1 (about 200 Re from the Earth) utilizing different propagation approaches. Solar wind parameters are updated and distributed uniformly at the inflow boundary or at an oblique plane. For all other outer boundaries, free flow conditions are assumed. The inner boundary of the GM domain is typically imposed at 2–3 Re from the Earth's center. However, it can be moved closer to the Earth for extreme solar wind driving. The Alfven velocity becomes too large closer to the Earth to allow a reasonable time step for explicit numerical schemes. A frequently used approach to address this issue is implementation of semi-relativistic MHD equations with a Boris factor that artificially reduces the speed of light (Boris, 1970; Lyon et al., 1986; 2004; Raeder, 2003; Gombosi et al., 2002, Toth et al., 2011). Typical values of the Boris factor are 0.01 to 0.02, which set the speed of light to 3,000 km/s to 6,000 km/s, respectively. Details of plasma and field boundary conditions at the inner boundary is a major source of uncertainties and differences between various geospace modeling systems (Xi et al., 2015).

The Ionosphere Electrodynamics (IE) modeling component approximates the ionosphere as a sphere at an altitude of about 110 km. IE plays a critical role in defining conditions at the inner boundary of the GM domain and is included in all geospace modeling systems. IE solves a Poison equation for current continuity:

$$\nabla(\Sigma \cdot \nabla\Phi) = j_{//} sin(I) \quad (5)$$

where Φ is the ionospheric potential, Σ is the height integrated conductance tensor, $j_{//}$ is the field aligned current (FAC) density mapped from the inner boundary of the GM domain along dipole field lines, and I is the inclination angle of the field line. The IE component typically utilizes the geomagnetic coordinate system, and Eq. (5) is solved separately in northern and southern hemispheres in regions between magnetic poles and equatorward boundaries that are typically set at 10–40 deg from the geomagnetic equator.

The height-integrated ionospheric conductance defined in the entire IE domain is a critical factor in regulating the closure of magnetospheric field-aligned currents (FACs) through the ionosphere as Hall and Pedersen currents (see also the discussion in Section 3). To calculate the electric potential, modelers have used various techniques to infer conductances (Raeder et al., 2001; 2008; Merkin and Lyon, 2010; Wiltberger et al., 2009; El-Alaoui et al., 2023; Ridley et al., 2003, 2004; Robinson et al., 2018, 2020; Wang and Zou, 2022; Mukhopadhyay et al., 2020). The simplest approach is to set constant Hall and Pederson conductances equal or different in northern and southern hemispheres. More sophisticated conductance models incorporate several contributions including conductance driven by solar EUV ionization and auroral conductances derived from FACs, with different relationships for upward and downward currents. Several geospace modeling systems include coupling with global ionosphere/atmosphere models that utilize ionospheric potential and FACs as inputs and return conductances based on first-principle calculations (Raeder et al., 2008; Tan et al., 2022; Lin et al., 2021; Lin et al., 2022; Pham et al., 2022). Utilization of different ionosphere conductance models can result in significant differences in simulated geomagnetic disturbances.

The derived electrical potential is then mapped back along field lines to the inner boundary of the GM domain, where it is used to set the plasma tangential velocity as a boundary condition. IE also provides electric fields to all other modeling components shown in Fig. 4, thus serving as a hub for the entire geospace modeling system.

Outputs of GM and IE components are utilized to compute magnetic perturbations ΔB and the rate of magnetic field changes dB/dt at the ground. ΔB and dB/dt are essential space environment quantities that are linked to space environment impacts on power grids (geoelectric fields and GICs) and can be compared to observations at magnetometers on the ground. To enable model-data comparisons that can demonstrate the potential of new geomagnetic environment modeling efforts to improve GIC estimates, the Community Coordinated Modeling Center (CCMC) developed a CalcDeltaB tool utilized as a post-processing tool for any geospace modeling system ((Rastätter et al., 2014). The ΔB values are calculated from three contributions: 1) the current densities in the global magnetosphere by using the Bio-Savart formula, 2) the height-integrated horizontal current densities derived in the IE component, 3) the field-aligned currents that connect the GM and IE solutions. It was demonstrated that the results are in good agreement with the outputs from similar calculations (Yu et al., 2010) that are implemented in the Space Weather Modeling Framework (Tóth et al., 2005, 2012).

In the GM domain, the MHD approximation fails in the inner magnetosphere within the geosynchronous orbit as it does not include the particle drift and ring current physics. To address this issue, modern geomagnetic environment modeling systems include an inner magnetosphere (IM) component that incorporates non-MHD physics in closed field line regions typically within 6–8 Re from the Earth. IM ring current models break the plasma into different populations, solve bounce-averaged Boltzmann equations, and calculate gradient-curvature drifts separately for each population. Advanced IM models usually include embedded plasmasphere models. The IM component utilizes 3D magnetic field and plasma distributions from the GM domain and electric fields from the IE component and returns total plasma pressure and density which are used to update the MHD solution in the near-Earth region where GM and IM domains overlap. Through frequent exchange of parameters between GM, IE and IM components, the coupled geospace modeling system produces a global magnetosphere with a realistic ring current and improved geomagnetic environment modeling.

An outflow of plasma from the ionosphere into the magnetosphere along magnetic field lines is another important process that can impact the dynamics of the geomagnetic environment (see Section 3.7). Ionospheric outflow has been shown to be a significant contributor to the plasma population of the magnetosphere during active geomagnetic conditions (Glocer et al., 2009; Redmon et al., 2010; Artemyev et al., 2019). An ionosphere outflow modeling component serves as a bridge spanning the gap between ionosphere and the inner boundary of the GM domain. Ionosphere outflow models (Glocer et al., 2009, 2018, 2020; Zhang et al., 2016, Varney et al., 2015, 2016 a, b) utilize neutral density and velocity from ionosphere/thermosphere models, calculate the transport of plasma from the ionosphere, and set the supply for the magnetosphere. Simulations that include an ionosphere outflow component demonstrated development of strong, periodic geomagnetic disturbances during periods of steady solar wind driving, such as earthward propagating plasmoids and bursty bulk flows (Zhang et al., 2016; Garcia-Sage et al., 2015) and sawtooth oscillations (Varney et al., 2016b). For coupled systems that also include an IM component it was demonstrated that ionosphere outflow also impacts the ring current system (Welling et al., 2015). Complex and dynamic particle and field environments and current systems in the near-Earth region of geospace are discussed in the accompanying review paper by Zheng et al., (2023, this special issue).

4.2. Examples of modern multicomponent systems for geomagnetic environment modeling

4.2.1. Space weather modeling framework (SWMF/Geospace)

The SWMF is a flexible software framework developed at the University of Michigan (Toth et al., 2005, 2012) that allows integration of various models into a coherent system. The framework incorporates physics models with minimal changes and can be extended with new models and components. The SWMF/Geospace part of the framework includes all basic elements of the coupled geospace system scheme shown in Fig. 4.

The GM component, BATSRUS (Block – Adaptive – Tree – Solarwind – Roe – Upwind – Scheme), is a high-performance, generalized code with adaptive mesh refinement that can be configured to solve the governing equations of ideal and resistive MHD, anisotropic, Hall, multi-species, multifluid, and MHD with embedded particle-in-cell (MHD-EPIC).

In the 2023 version of the SWMF, the IE component, RIM (Ridley Ionosphere Model), incorporates solar EUV and enables multiple options for auroral conductance:

- Ridley Legacy Model (RML) uses an inverse-exponential fitting function derived from assimilative maps to specify auroral conductance based on FAC strength. Conductances are further enhanced in regions of high FACs using an empirical auroral oval (Ridley et al., 2004).
- Conductance Model for Extreme Events (CMEE) is designed for stronger solar wind drivers to improve simulated ground-based magnetic perturbation during extreme events (Mukhopadhyay et al., 2020).
- COnductance Model based on PFISR And SWARM Satellite (COMPASS) utilizes conjugate FACs measured by SWARM and conductance derived from PFISR observations (Wang and Zou, 2022).
- AMPERE-Derived Electrodynamic Parameters of the High Latitude Ionosphere (ADELPHI) utilizes dependent linear relationships between the AMPERE-measured FACs and PFISR derived conductances (Robinson et al., 2020).

For all auroral conductance models, the fitting parameters depend on the polarity of FAC and MLT. Most models also introduce low-latitude boundaries and thresholds on conductances for the stability of the ionospheric electrodynamics solver. Modular configuration of the SWMF/IE enables adding more options to facilitate testing of new conductance models.

SWMF/Geospace was the first geospace modeling system that successfully implemented coupling with the Rice Convection Model (RCM) (De Zeeuw et al., 2004; Toffoletto et al., 2003; Sazykin et al., 2002; Wolf, 1983). Community-wide geospace model validation efforts demonstrated that incorporation of the ring current system significantly improves modeling of ground magnetic perturbation (Pulkkinen et al., 2013). These findings were used as a basis for selection of the first physics-based geospace model for transition to operations. The SWMF/Geospace with GM = BATSRUS, IM = RCM, and IE = RIM with RLM ionosphere conductance is running operationally at NOAA/SWPC since 2016 and is providing regional magnetic perturbations on a five-by-five degree global grid. In 2021 the operational SWMF/Geospace has been upgraded with improved simulation scheme, increased resolution near the inner boundary, improved auroral oval specification and more realistic representation of magnetospheric current systems. In addition to RCM, the SWMF/Geospace can be configured with other IM models, e.g., the Comprehensive Inner-Magnetosphere Ionosphere (CIMI) model [that recently replaced the Comprehensive Ring Current Model (CRCM) (Glocer et al., 2013)], the Ring current Atmosphere interaction Model with Self-Consistently calculated 3D Magnetic field (RAM-SCB) (Jordanova et al., 2014, Welling at al, 2018), and the Hot Electron and Ion Drift Integrator (HEIDI) (Ilie et al., 2012, 2014). Other components of the SWMF/Geospace include: Global Ionosphere Thermosphere Model (GITM) (Ridley et al., 2006) and Polar Wind Outflow Model (PWOM) (Glocer et al.,2009). Ionosphere outflow can also be introduced at the inner boundary through empirical formulas, (e.g., Strangeway et al., 2005).

The SWMF/GM + IE was the first physics-based geospace model implemented at the CCMC. Over more than 20 years, the model has been heavily used through the CCMC Runs-on-Request service, resulting in hundreds of publications. There have been multiple upgrades, including incorporation of several IM components: RCM, CRCM, CIMI. The latest SWMF/Geospace implementation for Runs-on-Request (V2023) offers preset and custom run types. This system offers a broad range of options that enables community engagement in testing the impact of different factors on results of geomagnetic environment modeling.

4.2.2. Open geospace general circulation model (OpenGGCM)

The global magnetosphere component of the Open Geospace General Circulation Model (OpenGGCM) coupled modeling system solves the MHD equations on a stretched cartesian grid that is computed prior to the run. The magnetic induction equation is solved using the Constrained Transport (CT) method (Evans and Hawley, 1988), which uses staggered grids for the magnetic and electric field, so that the magnetic field components are placed on the center of cell faces, and the electric field on the centers of the cell edges. This CT method allows preservation of $\nabla \cdot \mathbf{B} = 0$ to roundoff error. Since the use of a high-order hybrid scheme with increased spatial resolution minimizes numerical dissipation in the computation, the code includes a resistive term in Ohm's law, where the resistivity (η) is a nonlinear function of the local current density such that $\eta = aj^2$. To avoid spurious dissipation, the code includes a threshold, which is a function of the local normalized current density. This threshold is calibrated such that explicit resistivity is switched on at a very few grid points in strong current sheets, rather than being spread uniformly over the entire box or being applied to smaller regions such as the plasma sheet (Raeder et al., 1998, 2001, 2003).

The ionospheric electrodynamics component of the OpenGGCM utilizes either empirical formulations or the NOAA Coupled Thermosphere Ionosphere Model (CTIM) (Fuller-Rowell et al., 1996; Raeder et al., 2001). Three sources are assumed in computing the height-integrated ionospheric Hall and Pedersen conductivities that make up the conductance tensor. The first component results from solar EUV ionization and uses the Moen and Brekke (1993) empirical model based on the solar 10.7 cm flux ($F_{10.7}$) and the solar zenith angle. The second source is made up of accelerated auroral electron precipitation associated with upward FACs, which is modeled by using the Knight relationship (Knight, 1973). The third contribution comes from diffuse electron precipitation (pitch angle scattering of hot magnetospheric electrons). The Pedersen and Hall conductances can then be computed either by using the empirical formulas from the Robinson et al., (1987) model, or by feeding the precipitation parameters, along with the potential, into CTIM, which then computes the conductances self-consistently based on electron neutral collisions. Raeder at al (2008) demonstrated that using the CTIM conductances, as opposed to using conductances from empirical models, significantly affects the simulation results.

The OpenGGCM and its precursor, UCLA-GGCM, have been used successfully in reproducing the intricate details of the magnetopause boundary layer (Raeder et al., 1995; Frank et al., 1995). Frank et al., (1995) carried out the first direct comparisons of simulated plasmas and magnetic fields observed by the Geotail spacecraft in the distant tail. For example, the OpenGGCM results were used to identify the source of cold ion beams observed by the spacecraft. The model has also been used in successfully modeling substorm dynamics (Raeder et al., 2001, 2008; El-Alaoui et al., 2009).

The OpenGGCM precursor, UCLA-GGCM, was one of the first models implemented at the CCMC for Runs-on-Request. and request runs were started in 2001. The model has been used to study different regions of the magnetosphere, in particular for ionospheric electrodynamics studies. Recently OpenGGCM has implemented coupling with RCM. This version was made available through CCMC to the research community in 2020 (Cramer et al., 2017).

4.2.3. Multiscale atmosphere geospace environment (MAGE)

Multiscale Atmosphere-Geospace Environment (MAGE) modeling system is under development by the NASA DRIVE Science Center for Geospace Storms (CGS). The long-term vision for MAGE includes the components shown in Fig. 4 and more. The current working version of the model, MAGE 1.0 (Lin et al., 2021, 2022; Pham et al., 2022) consists of the GM component GAMERA (Grid Agnostic MHD with Extended Research Applications) (Sorathia et al., 2020; Zhang et al., 2019), the IE component REMIX (RE-developed Magnetosphere-Ionosphere Coupler/Solver) (Merkin and Lyon, 2010), the IM component RCM (Toffoletto et al., 2003), and TIEGCM (Thermospheric Ionosphere Electrodynamics General Circulation Model) (Richmond et al., 1992; Qian et al., 2014)

GAMERA is the next generation model built upon the high-heritage Lyon-Fedder-Mobarry (LFM) code (Lyon et al., 2004). GAMERA utilizes a finite volume method with high-order spatial reconstruction on curvilinear, nonorthogonal grids. GAMERA uses the constrained transport method (Evans and Hawley, 1988; Lyon et al., 2004) to maintain divergence-free magnetic fields to machine precision. An extensive description of the MHD numerics used in GAMERA, including comprehensive testing, was provided by Zhang et al., (2019), while the first magnetospheric applications were reported by Sorathia et al., (2020) and Michael et al. (2021). GAMERA is also being used for simulation of space plasma environments beyond the terrestrial magnetosphere, including solar wind (Mostafavi et al., 2022), planetary (Zhang et al., 2021;

Dang et al., 2023) and exoplanetary (Sciola et al., 2021) magnetospheres. The auroral conductance model in REMIX combines contributions from diffuse and monoenergetic electron precipitation (Lin et al., 2021; Lin et al., 2022) whereby diffuse precipitation is derived from the drifting electron population simulated by the RCM and the monoenergetic population is calculated similarly to the original LFM formulation (Fedder et al., 1995). To derive the diffuse precipitation, the RCM electrons are scattered into the loss cone by using empirical models of chorus and hiss waves similarly to (Chen et al., 2019). In addition, efforts are underway to include broadband and direct-entry cusp precipitation (Zhang et al., 2015). The auroral conductance is then computed using the Robinson et al., (1987) or Kaeppler et al., (2015) formulas and is combined with the background ionospheric conductance. When not coupled with an IT model, the background conductance can be computed using an empirical EUV model. By default, the model by Moen & Brekke (1993) is used, modified to avoid sharp gradients at the terminator (Laundal et al., 2022). When coupled with an IT model, such as the TIEGCM, the background ionosphere is specified by that model. The GAMERA-RCM coupling largely follows the methodology described earlier for the LFM-RCM coupling (Pembroke et al., 2012) but with important differences detailed by Sciola et al. (2023) and Sorathia et al. (2023). RCM coupling also enables incorporation of a dynamic plasmasphere into the model whereby the plasmasphere is evolved via the zeroth energy RCM channel. The dynamic plasmasphere is used in part to modulate the empirical wave models mentioned above (e.g., hiss waves would trigger inside the plasmasphere, while chorus waves outside the plasmasphere).

The GAMERA + REMIX + RCM (MAGE 0.75) modeling system is currently being implemented at the CCMC for Runs-on-Request service, to be followed by MAGE 1.0, which adds the TIEGCM. Recent high resolution MAGE simulations reproduced strong turbulence and BBFs during disturbed geomagnetic conditions (Fig. 5).

Longer term plans for MAGE include incorporation of Ionosphere/Generalized polar wind model (IPWM; Varney et al., 2016a,b), now redeveloped as the High-latitude Ionosphere Dynamics for Research Applications (HIDRA) model (Albarran et al., 2023), SAMI3 ionosphere/plasmasphere model (Huba & Krall, 2013a,b), the Whole Atmosphere Community Climate Model with thermosphere and ionosphere extension (WACCM-X; Liu et al., 2018), and other modeling components.

4.2.4. Gorgon

The Gorgon model is a more recent global magnetospheric MHD code developed at Imperial College London derived from a strong heritage of laboratory plasma simulations (Ciardi et al., 2007). It is distinct from other MHD codes in the community through its use of the magnetic vector potential to solve the resistive semiconservative MHD equations, and hence via a staggered cartesian grid achieves divergence-free magnetic field to machine precision. The equations are solved using a 3rd order van Leer advection scheme (van Leer, 1997) with variable time stepping via a second-order Runge-Kutta scheme. After being adapted to simulate the magnetospheres of Neptune (Mejnertsen et al., 2016) and Earth (Mejnertsen et al., 2018), Gorgon now provides space weather modeling capability through a coupled thin-shell ionosphere model with a split dipole approximation (Eggington et al., 2020, 2022) and integrated test particle simulations (Desai et al., 2021). Similar to other models within the community, ionospheric conductances are prescribed by a combination of background conductance, solar EUV ionization and particle precipitation derived from magnetospheric quantities at the inner boundary. Currently there is no coupling with an inner magnetosphere model.

Owing to its highly efficient parallelization, recent Gorgon development has included a shift towards real-time operational modeling with activity in several recent and ongoing projects within the UK and European domain. Part of these activities has been the development of inline parallelized ground geomagnetic field estimation through an adapted Biot-Savart integration based on CalcDeltaB (Rastätter et al., 2014) and an alternative estimation using the complex image method (CIM) (Pirjola et al., 1998), which can include induced ground current contributions in geomagnetic field estimation. The operational version of Gorgon and postprocessing suite are being delivered to the UK Met Office as part of the SWIMMR Activities in Ground Effects (SAGE) project's ensemble of forecasting models, with integrated test particle simulations providing extremal forecast constraints in the SWIMMR SatRisk project. A similar multi-model forecasting capability is being delivered to ESA in collaboration with the University of Bergen, which is leading an operational SWMF deployment. Gorgon (as 'Gorgon-Space') has further been coupled to an upstream heliospheric model (EUHFORIA) in the latest phase of ESA's Virtual Space Weather Modelling Centre (VSWMC) (Poedts et al., 2020). The VSWMC provides runs on request to end-users for chains of coupled models, and in the case of magnetospheric models these may include driving from measured or modeled L1 data.

4.2.5. Grand Unified Magnetosphere-Ionosphere coupling simulation (GUMICS)

The Grand Unified Magnetosphere-Ionosphere Coupling Simulation (GUMICS) model, first developed in the 1990s by the Finnish Meteorological Institute, has been through multiple iterations in the past three decades (Janhunen and Huuskonen, 1993; Janhunen, 1996; Janhunen et al., 2012; Honkonen et al., 2022). The most recent version developed, GUMICS-5, is a real-time-capable parallelized code version based on GUMICS-4. Both GUMICS-4 and GUMICS-5 solve the ideal MHD equations using conservative first-order finite volume schemes on an adaptive cartesian grid with a split dipole implementation. A triangularly discretized, thin-shell iono-

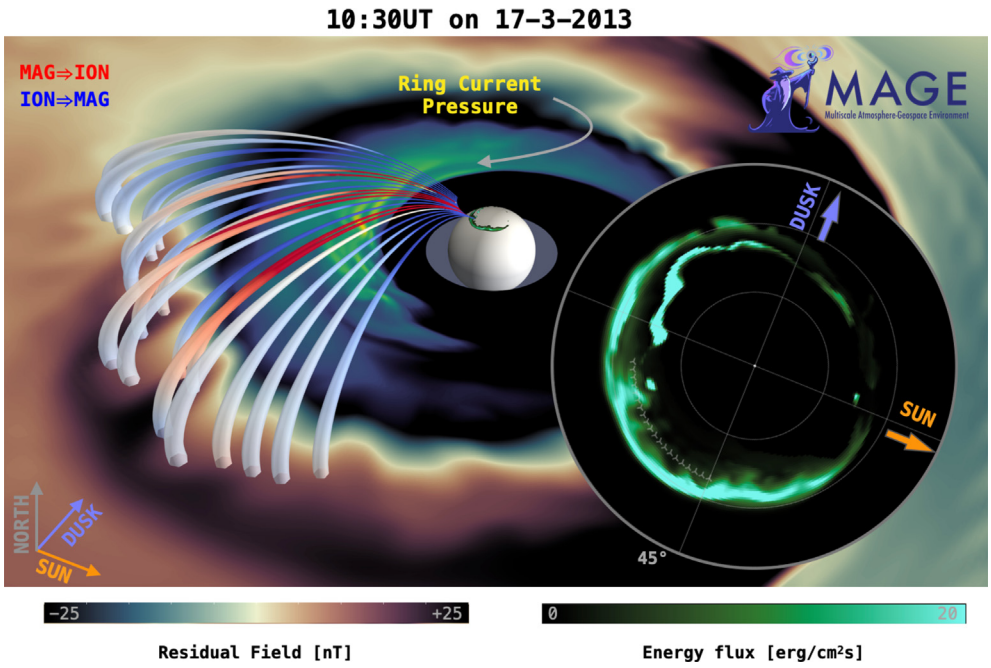

Fig. 5. MAGE model simulations of bursty bulk flows and omega bands in the dawn sector. Field-aligned currents connecting the ionosphere and magnetosphere are shown in this 3D rendering, along with the associated precipitating electron energy flux.

sphere model is used for magnetosphere-ionosphere coupling, with conductances determined by a background conductance, solar EUV flux, and electron precipitation flux controlled by magnetospheric inner boundary quantities (temperature and mass density) and a parameterized loss cone filling rate. No inner magnetospheric model is currently included in GUMICS. The previous (serial) version GUMICS-4 has recently been deployed as part of ESA's Virtual Space Weather Modelling Centre (VSWMC), providing runs on request with coupled driving from in-situ or modeled L1 data, albeit not in real-time.

4.2.6. Reproduce plasma universe (REPPU)

The REPPU model, originally developed in Japan (Tanaka, 1994, Tanaka et al., 2010; 2017), has been widely used to reproduce observed features of the substorm onset in the ionosphere. This model utilizes an unstructured grid with very high spatial resolution in the inner magnetosphere (up to 0.06 Re) and ionosphere (<0.5 deg) with focus on resolving in detail the field-aligned currents. The modeling approach quantifies numerical viscosity and introduces reconnection viscosity coupled with X-point detection. It was demonstrated that localization of reconnection viscosity near X-points produces a considerable effect on the behavior of the plasma sheet. Currently there is no coupling with an inner magnetosphere model.

4.3. Progress in kinetic modeling of global magnetosphere

The importance of the kinetic effects on structure and dynamics of the global magnetosphere stimulated an extensive body of work focused on constructing global models that go beyond MHD. Kinetic simulations, such as hybrid codes (Chen et al., 2012) moment expansion methods (Dong et al., 2019), and the global hybrid-Vlasov code Vlasiator (Palmroth et al., 2018; von Alfthan et al., 2014) have advanced greatly over the past decades. We now have 3D particle-in-cell (PIC) simulations and hybrid simulations that are producing magnetospheric-like results (Lin et al., 2013; Lin et al., 2014). Recently techniques have been developed in which an implicit PIC simulation was embedded within a global MHD simulation of the magnetosphere (Chen et al., 2017). The MHD simulation provides the global configuration of the magnetosphere, while the kinetic models allow large regions of the magnetosphere to be modeled in a fully kinetic state. To address numerical limitations modelers compromise on the physical parameters, such as the ratio of electron to ion mass or in the case of hybrid codes the ratio of ion kinetic scale and Earth's radius. NASA's Living with a Star Strategic Capability program specifically designed a focus topic for developing the next generation of reliable, stable, and accurate global models. This includes coupled models that allow a more realistic assessment of small-scale processes on the global magnetosphere system (and vice versa) that will address needs for both basic and applied research.

For example, kinetic models have been used to address turbulent processes in the foreshock and magnetosheath (Omelchenko et al., 2021; Chen et al., 2021; Ng et al., 2022) as illustrated in Fig. 6 in Geocentric Solar Magnetospheric (GSM) coordinates. In the GSM coordinate system, the x-axis points from the Earth toward the Sun, the y-axis points in the dawn-dusk direction, and the z-axis completes the right-handed system. The two left panels show the central meridional (GSM x-z) plane for the GSM Bz component of magnetic field (panel a) and the

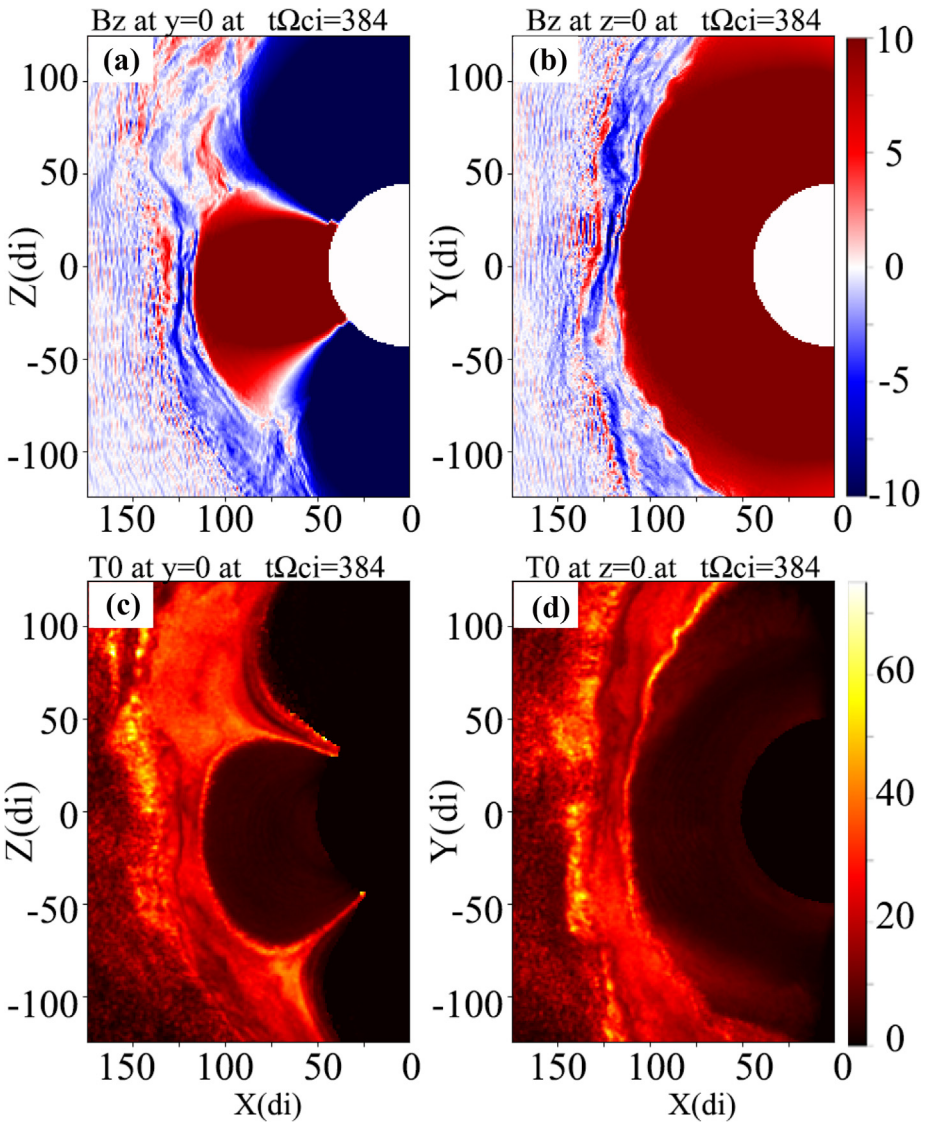

Fig. 6. Results of kinetic model simulations of turbulence in the magnetosheath as discussed by Omelchenko et al., (2021) and Ng et al., 2022. See text for details.

ion (proton) temperature T0 (panel c). The two right panels show the equatorial (GSM *x-y*) plane for Bz (panel b) and T0 (panel d). These simulation snapshots were taken at t $\Omega_{ci\ =38}$, where Ω_{ci} is the ion cyclotron frequency computed with respect to the IMF (Interplanetary Magnetic Field) value. The positions (x,y,z) are normalized by the solar wind ion inertial length (di). The magnetic field, Bz is normalized by the IMF value. The ion temperature, T0 is normalized by the characteristic ion kinetic energy, computed with respect to the upstream solar wind Alfven speed. This hybrid simulation captures the important kinetic physics of magnetosheath turbulence arising under quasi-radial IMF conditions.

4.4. Caveats and uncertainties

Uncertainties in drivers and internal assumptions can significantly impact predictive capabilities of the geomagnetic environment, especially in timing and location of localized impulsive phenomena such as spikes in geomagnetic disturbances.

4.4.1. Uncertainties introduced by propagation of solar wind plasma and field parameters

A challenge in geospace modeling comes from the driving data used, which typically is either measured or modeled L1 data. In the case of modeled solar wind data, there may be significant uncertainty in the plasma and interplanetary magnetic field parameters, all of which may influence resulting models. In the case of measured data from L1, there is significant uncertainty in the bulk solar wind structure, which may not be sampled adequately. The propagation of individual L1 data typically assumes planar phase fronts on scales below which important solar wind structure may exist. For time-critical operational modeling, there is a further challenge that

interactions between such phase fronts are not fully considered (Cash et al., 2016, Cameron and Jackel, 2019). Most typically, ballistic propagation is used, with geospace simulations rewinding and re-run if a previous in-situ measurement would be overtaken by a faster phase front. An alternative is to 'blindly' model with raw L1 data directly, neglecting plasma interactions but maintaining temporal ordering and allowing for continuous runtime, with the caveat that associated forecast lead time estimates must be included. When using real-time data, there are additional challenges relating to data availability, data gaps, and data quality (Smith et al., 2022, Loto'aniu et al., 2022). In these cases, there is often a failover to an alternative spacecraft, the most typical being DSCOVR or ACE. Although these switchovers aim to provide continuous data, they often introduce artificial shocks due to differences in the spacecraft position and instrumentation. These artificial shocks will create an immediate linear response in geospace models, but could cause nonlinear responses only seen much later in the simulation.

4.4.2. Impact of spatial resolution in global magnetosphere modeling

Dimmock et al., (2021) analyzed the effects of spatial resolution in the GM component of the SWMF with RCM and CMEE ionospheric conductance on simulated geomagnetic response over Fennoscandia to the September 6–8, 2017 event. The lowest resolution setting utilized one million grid cells with 1/4 Re inter-cell spacing near the inner boundary, and the medium resolution setting utilized two million grid cells with 1/8 Re intercell spacing. Simulation settings with the highest resolution utilized a simulation grid with 8 million cells and a minimum spacing of 1/16 Re, allowing the code to better resolve field-aligned currents and to produce simulated geomagnetic perturbations with higher amplitude than lower resolution runs. It was demonstrated that at low to midlatitudes where substorm effects are not as dominant, higher spatial resolution produced noticeably improved dBdt and GICs in terms of both amplitude and timing. At higher latitudes increased spatial resolution does not lead to improvement in modeling of dB/dt spikes likely associated with substorms.

Vandegriff et al., (2022) performed further analysis of high resolution SWMF simulations of the September 6–8, 2017, storm focusing on the second half of the storm when substorm activity is seen in observational data. The model simulated textbook signatures of tail dynamics during a substorm in conjunction with the real-world substorm signatures: formation of near-Earth reconnection line around 20 Re downtail, spiraling field lines corresponding to a plasmoid, subsequent plasmoid release, and dipolarization of the newly reconnected closed field lines. Despite very good overall model-observation association, the model does not capture signatures of extremely localized ground magnetic perturbations in Fennoscandia. The problems could be related to slower rate of magnetotail reconnection supported only by numerical dissipation in the ideal MHD approach. Increased spatial resolution may not help to reproduce physical phenomena if the underlying physical process is missing in the modeling approach.

Substorms remain a significant challenge that prevents geospace modeling systems with GM component based on the ideal MHD approach to accurately simulate localized ground magnetic perturbations at high latitudes. Statistical analysis of substorms demonstrated that substorms occur in a periodic fashion with a period of 1–3 h (Borovsky and Yakymenko, 2017; Keiling et al., 2022). Understanding and modeling periodic substorms and their impact on magnetic perturbations on the ground is an even bigger challenge.

4.4.3. Uncertainties in simulation settings

Several model-model comparison studies for several GM + IE modeling systems discussed in this section with a comparable grid resolution and using the same set of inputs demonstrated that different models display a systematically different global behavior (Ridley et al., 2016; Gordeev et al., 2017; Mukhopadhyay et al., 2021).

Major differences in simulation results for models utilizing the same first principles are likely related to differences in details of conditions at the inner boundary, including ionospheric conductance models; density and temperature imposed at the inner boundary, and the type of boundary conditions for the magnetic field (e.g., floating or reflecting). There is a need for detailed uncertainty assessment associated with these model limitations.

4.4.4. Missing physics for modeling key physical processes

Single fluid ideal MHD approximation is not applicable for modeling key processes controlling global geospace dynamics, such as fast magnetotail reconnection, periodic sub-storms, and turbulence in the foreshock region. It was demonstrated that incorporation of kinetic effects in some parts of the computation domain may significantly influence the geospace system behavior (Chen et al., 2017). Parameterization of kinetic effects and incorporation of localized corrections into MHD equations is one of the low-cost ways to improve modeling of global magnetosphere dynamics (Kuznetsova et al., 2007; Tanaka et al., 2010, Raeder et al., 2008). For example, it was demonstrated by Kuznetsova et al., (2007) that dynamic incorporation of localized kinetic corrections into the SWMF near reconnection sites reproduces the dynamic quasiperiodic response to the steady southward IMF driving conditions that generate strong flow and magnetic field perturbations at the flanks of the magnetosphere.

Global kinetic modeling approaches discussed in the previous section that ultimately include additional physics and help describe and understand the complex and multiscale system generate an enormous amount of data and require significant computational resources to run, making it currently challenging to deploy in the operational arena. One of the promising pathways is incorporation of a kinetic description into small dynamically changing com-

putational subdomains in regions satisfying relevant physics-based criteria (Shou et al., 2021). Another relatively low-cost option is to utilize outputs of hybrid simulations of foreshock turbulence.

4.4.5. Numerical effects

Numerical diffusion in the GM domain affects the amplitude of the field-aligned currents used for dB/dt calculations. Quantitative estimates of numerical resistivity and diffusivity are usually absent. Numerical noise can also generate artificial spikes in temporal variations (Dimmock et al., 2021). Impact of numerical effects is a concern even for relatively high-resolution simulation grids and relatively low diffusion schemes. Quantification of deviation from ideal MHD approximation is important prior to incorporation of non-MHD effects. GM-IM coupling aimed to incorporate important physics can also introduce coupling artifacts due to modification of plasma pressure in the GM domain and crossfield numerical diffusion near the IM boundary.

5. Space weather impacts of geomagnetic disturbances

Geomagnetic disturbances (GMDs), geoelectric fields, and geomagnetically induced currents (GICs) result from the driving and coupling processes described in the previous chapters. Fig. 7 is a summary of the space weather chain of events, often described as from 'Sun to Mud', which leads to problems for technological systems on the ground. The GIC problem can be broken down into two independent steps (Pirjola, 2002): (1) the geophysical step involving the magnetometer data and Earth conductivity information to determine the geoelectric fields at the Earth's surface, and (2) the engineering step involving the use of these geoelectric fields as input to engineering models of the ground networks (power systems, pipelines, railways and submarine cables) to calculate the GICs and voltages that can affect the operation of those systems. In this chapter, we consider the characteristics of GMDs that are important for GIC effects, the development of earth conductivity models, the calculation of geoelectric fields, and the modelling of GIC in the different affected systems.

5.1. Geomagnetic disturbance field variations

The rapidly-changing geomagnetic fields and large dB/dt levels associated with geomagnetic storms have been studied in detail for decades. Geomagnetic storms occur when the interplanetary magnetic field turns southward and remains southward for a prolonged period of time. These geomagnetic storms on average last several days and typically begin with a storm sudden commencement (SSC), which is followed by a main phase and recovery phase associated with the growth and decay of the ring current. Large dB/dt are not produced by the storm main phase itself but by the faster variations, SSCs, substorms, and magnetic perturbation events (MPEs) associated with the storm.

Because SSC are often produced by the shock on the magnetosphere produced by the impact of a CME, SSCs are valuable as precursor signals of a magnetic storm. SSC have also been identified as a risk factor for GIC and, because of their global signature, raise concerns for power systems at low and mid latitudes. Smith et al., (2021) found that most large dB/dt at low latitudes were associated with SSC, whereas they represent only a small percentage of the issues encountered at high latitudes where substorms are the main contributor to geomagnetic activity. An analysis by Fiori et al., (2014) showed that SSC associated with higher speed CMEs can also have a higher latitude enhancement due to an accompanying surge in magnetospheric convection.

Substorms are one of the fundamental processes within the magnetosphere, involving acceleration of particles from the magnetotail into the auroral region producing auroral displays and the electric currents that produce magnetic disturbances on the ground (Akasofu, 2012). During the substorm onset there is a sudden localized brightening of the aurora at the equatorward edge of the auroral oval somewhere between 18 and 3 MLT and 55° and 74° magnetic latitude (Frey et al., 2004). It has been demonstrated that prior to the auroral substorm onset high speed earthward flows occur within the magnetotail (Angelopoulos et al., 2008). At about the same time and geographic location as the auroral onset the H component of the magnetic field sharply decreases, which is associated with an enhancement of the westward electrojet and a sharp drop in the AL index. This sharp drop can be as much as 1000 nT or more with high dB/dt values. Viljanen et al., (2006a) has shown that these changes can be as large as 10.7 nT/s, typically occurring within the first 10–20 min of the substorm onset, but occasionally occurring at other times during the substorm. Weygand (2021) demonstrated that using both a single substorm event and a two-dimensional superposed epoch analysis of substorms that there is sudden increase of dB/dt at substorm onset followed by an expansion poleward, westward, and eastward after the onset during the expansion phase. Fig. 8 (from Weygand, 2021) shows the dB/dt distributions for various times relative to substorm onset. The temporal and spatial development of the dB/dt resembles the temporal and spatial change of the auroral emissions.

Even more common than substorms are magnetic perturbation events (MPEs). MPEs are large rapid changes in the magnetic field with amplitudes $|\Delta B|$ of hundreds of nT, which can appear in any ground magnetic field component, and with durations of about 5–10 min (Viljanen and Tanskanen, 2011; Engebretson et al., 2019a, b; Engebretson et al., 2024). Engebretson et al. (2019a, b) defined MPEs for their statistical studies as events where $dB/dt > 6nT/s$. Engebretson et al., (2021) and Weygand et al., (2021) used a dataset of hundreds of MPEs to show that most MPEs (64–70 %) occurred within

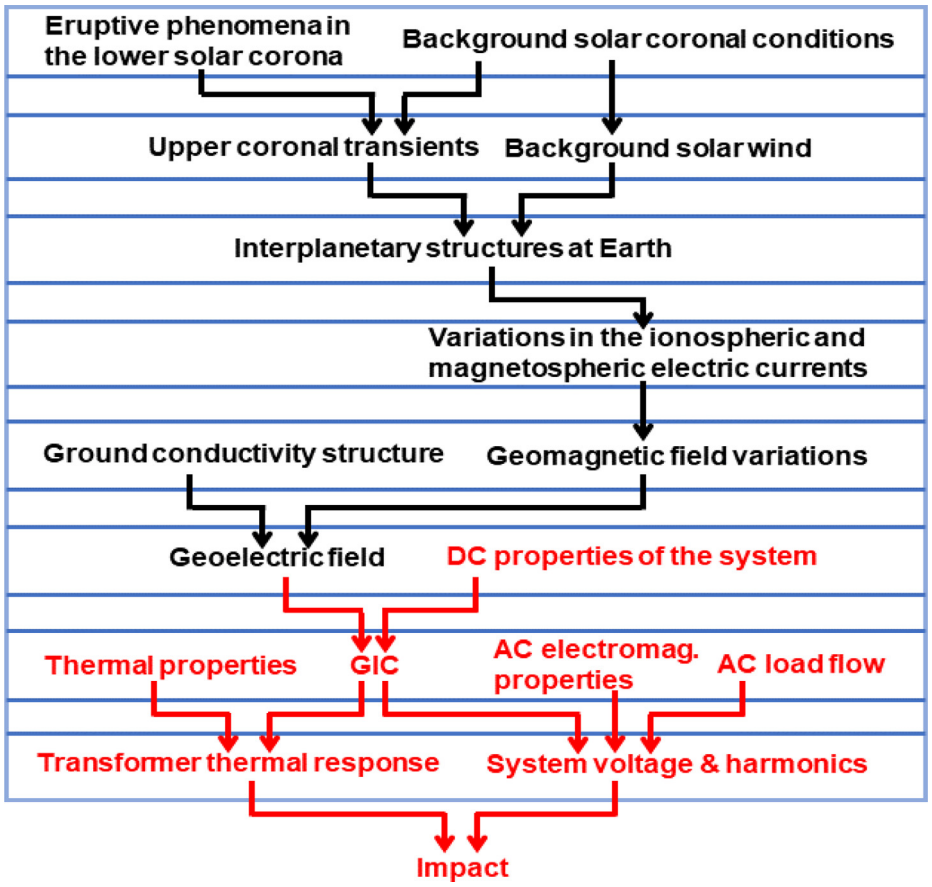

Fig. 7. Space weather chain of events for GICs (. adapted from Pulkkinen et al., 2017)

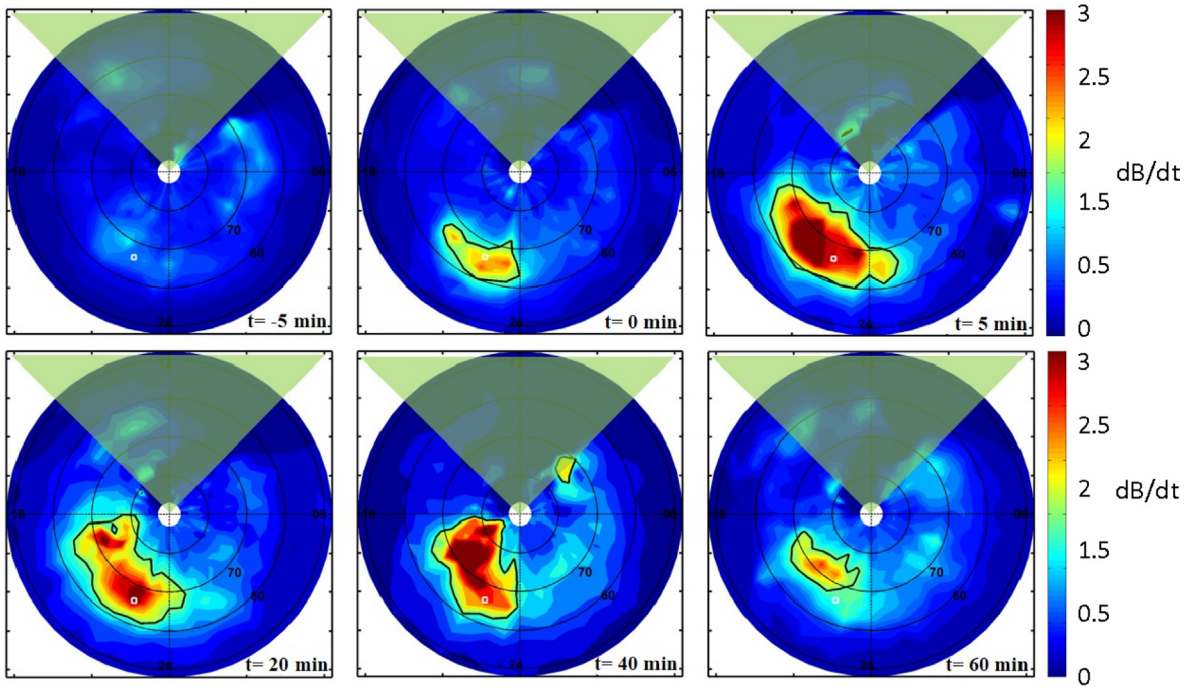

Fig. 8. Two dimensional superposed epoch analysis of the 95 % percentile of the 81 substorms Each panel is in a magnetic coordinate system with 12 magnetic local time (MLT) at the top, 00 MLT at the bottom, 06 MLT on the right, and 18 MLT on the left. From epoch time 0 min (substorm onset) to epoch time 60 min, the area dB/dt that exceeds 1.5 nT/s (black contour in pre-midnight sector) covers a large portion of the pre-midnight sector.

the first 30 min of substorm onset, while 14–20 % occurred 30 min to 60 min after substorm onset, and the remaining 12–14 % occurred at periods over 60 min after substorm onset. Engebretson et al., (2019a) and Weygand et al., (2021) also reported dB/dt values within the dataset as high as about 30 nT/s. A two-dimensional superposed epoch analysis of MPE events centered over southeast Baffin Island showed that the MPEs appeared filamentary with a full-width half-maximum radius of about 275 km (Engebretson et al., 2019b). The origin of these MPEs is not yet known. However, ground based auroral images available for some of the MPEs shown in Weygand et al., (2021) and in Engebretson et al., (2019b) resemble ripples, vortices, and in one case a north–south streamer, all associated with energetic particle injections (Weygand et al., 2021).

Lower latitudes can also experience significant dB/dt. Latitude profiles of geomagnetic disturbances, dB/dt and geoelectric fields show maximum values in the auroral zone but show a secondary peak in the equatorial region (Ngwira et al, 2013a). At lower latitudes, as well as the SSC and main phase of magnetic storms mentioned above, there are also magnetic field variations due to ionospheric currents driven by the ionospheric disturbance dynamo and prompt penetration electric fields. The ionospheric disturbance dynamo magnetic fields are generally slowly varying while the prompt penetration electric fields (PPEF) create rapidly varying magnetic field variations so are more important for geomagnetic induction effects on ground systems. A number of studies (e.g. Adebesin et al., 2016) have shown that the low latitude dB/dt due to PPEF occur simultaneously with the magnetospheric electric field response to solar wind density variations (both increase and decrease). The ionospheric response to PPEF is greater at the latitudes of the equatorial electrojet, producing dB/dt that are larger than at low latitude locations outside this region.

Historical events that produced technological impacts have also been mined for information about the details of the magnetic disturbance that create hazards. The most notable magnetic storm is the Carrington event of 1859, which produced widespread effects on the telegraph system (Boteler, 2006). The effects of this event were described by Tsurutani et al., (2003) and put in a modern context by Cliver and Svalgaard (2004) and Cliver (2006). Major magnetic storms produced large disturbances on the telegraph in 1892 (Love, 2018) and 1909 (Love et al., 2019a). The geomagnetic disturbance in May 1921 caused even more problems, causing fires at telegraph stations in Sweden and the United States (Love et al., 2019b; Hapgood, 2019). In-depth investigations of extreme solar and geomagnetic events in 1938, 1940 and 1946 have recently been provided by Hayakawa et al., (2020, 2021 and 2022).

More recent events have also been the subject of reanalysis as more information became available. In the March 1989 storm, there were no measurements of the solar wind conditions that caused the disturbance. However, Nagatsuma et al., (2015) made use of GOES data to obtain an estimate of the southward interplanetary magnetic field and used this to estimate the solar wind speed. Boteler (2019) inferred two CMEs during this event, and that the second CME hit the Earth's magnetosphere just before the magnetic substorm that caused the blackout of the Hydro-Québec power system, suggesting that the substorm was triggered by the shock of the CME arrival. Although much attention is given to substorms, changes in the convection electrojets are often overlooked or even discounted as a cause of significant GIC when, in fact, they are associated with significant impacts in the March 1940, February 1958 and August 1972 storms, and were likely the cause of the transformer damage in the US in the March 1989 storm (Boteler, 2001). A recent statistical study by Freeman et al., (2019) identified the two-cell DP2 magnetic perturbation caused by magnetospheric convection as the dominant source of hazardous dB/dt $>$ 600 nT/min that is potentially damaging to the U.K. National Grid.

Values of dB/dt recorded during major storms in the last few decades include max dB/dt $\sim$ 11.7 nT/s in March 1989, and max dB/dt $\sim$ 8.0 nT/s in the Halloween storm of 2003, both of which caused power system impacts. The St Patrick's day storm of March 2015 contained strong substorms, as evidenced by a large drop in the AL index and had dB/dt with values of $\sim$ 14.2 nT/s given by Ngwira et al., (2018) and 16.5 nT/s given by Weygand (2021) observed in the northern hemisphere. In the southern hemisphere Carter et al., (2016) obtained measurements on the order of 21 nT/s during the same storm. During the September 2017 storm, the Scandinavian region experienced dB/dt $\sim$ 16.7 nT/s (Dimmock et al., 2019), while areas of North America and Greenland within the auroral oval also experienced large dB/dt values (Ngwira et al., 2018). However, in spite of the larger dB/dt values, none of these later storms produced power system effects like those in 1989 and 2003, illustrating the difficulty in identifying the magnetic disturbance characteristics that are critical for ground infrastructure. Part of the problem is that dB/dt calculated from 1-minute data are reduced because the anti-aliasing filtering for the recordings removes the higher frequency components so cannot be compared to dB/dt calculated from 1-second data (Trichtchenko, 2021). Also, power transformers have a non-linear response to GIC so a simple relation between power system effects and instantaneous values of dB/dt should not be expected.

5.2. Geoelectric fields

The next step in the chain to understanding geomagnetic effects on ground systems is to determine the geoelectric fields produced during geomagnetic disturbances. This is an area that has seen significant development in the last couple of decades. An excellent review by Kelbert (2020) shows the role of Earth conductivity information in understanding GIC risks and includes descriptions of activities in

many countries with active research programs in this area. Because of a lack of information about the spatial structure of the magnetic disturbances and the Earth conductivity structure, geoelectric field calculations were initially only possible by assuming a plane wave source field and a uniform or layered Earth conductivity structure (Pirjola, 1984; Boteler, 1994). However, there has been considerable progress in obtaining information through magnetotelluric (MT) surveys of the surface conductivity structure and in new calculation techniques to make full use of that information.

There is a large community within solid-Earth geophysics concerned with studying the interior of the Earth using MT technique. This technique, pioneered by Cagniard (1953), uses measurements of the magnetic and electric fields at Earth's surface to calculate the Earth transfer function, E/B, as a function of frequency. Different frequencies penetrate to different depths within the Earth because of the 'skin depth' effect, and they are affected by the different conductivities at these depths. Iterative modelling can then be used to obtain a calculated Earth transfer function that closely matches the measured one, thereby giving a model of the Earth conductivity structure. The simplest approach is to use the data from individual sites to estimate a one-dimensional (1-D) model of the Earth conductivity that takes account of the conductivity variation with depth but ignores lateral changes in conductivity. With a line or array of MT sites it is possible to construct 2-D and even 3-D models of the Earth conductivity structure.

MT studies were generally made in areas considered to be geologically interesting and did not necessarily coincide with the locations of power systems; or, if they did, they only covered a small fraction of the area covered by the system. The best that could be done was to identify geologic terrains and assign 1-D conductivity models obtained from MT measurements from anywhere within a terrain to the rest of the region, thereby allowing calculations of geoelectric fields across the whole area of power systems. This approach does not take into account the changes in conductivity structure between different geological regions or at a coastline. The first attempt to include lateral changes in geology was made by using regional conductivity models in a 'piecewise' fashion (Marti et al., 2014), but this ignores the boundary effects. Calculations of geoelectric fields in the vicinity of the conductivity boundary that occurs at the coast was developed by Gilbert (2005, 2015) and Pirjola (2013). More recently this problem has been tackled using finite element modelling (FEM) (Dong et al., 2013; Liu et al., 2018).

Spatial structure of the geomagnetic disturbances also affects the geoelectric fields. The complex image method (CIM) provides a simple technique for calculating geomagnetic and geoelectric fields produced by an electrojet source (Boteler and Pirjola, 1998a; Pirjola et al., 1998; Boteler et al., 2000). The CIM method for interpolation of fields between measurement sites can be combined with the Spherical Elementary Current System technique for determining ionospheric currents from ground-based magnetometer measurements. This has been used with 1-D conductivity models to calculate electric fields (Viljanen et al., 2004) and has been applied by Wei et al., (2013) to calculate geoelectric fields in the US and Canada for the March 1989 and November 2003 storms.

A major step forward in GIC research has been the deployment of extensive MT arrays to provide more comprehensive coverage and allow the development of 3-D conductivity models. Examples of this are the Earthscope array in the United States (Schultz, 2010) and the AusLAMP array in Australia (Marshall et al., 2019). Initially undertaken to understand more about the underlying Earth structure, their value for geomagnetic hazard assessments was soon recognized and now similar array studies are being undertaken in other countries as part of geomagnetic risk studies. The availability of such extensive information has opened up a whole new set of calculation methodologies based on measured MT impedances directly (Love et al., 2019c), MT-derived 3-D conductivity models, and derived impedance tensors. These methods produce averaged models for use by the power industry (EPRI, 2021). The latter approach has been used with source fields derived from SECS analysis of ground magnetic observations (Dimmock et al., 2019) and source fields derived from the Space Weather Modeling Framework (SWMF) (Rosenqvist et al., 2022).

Movement of source currents, and not just the current variations with time, also influences the induction process and production of geoelectric fields. For a moving source, the magnetic field variations seen on the ground will be doppler shifted relative to the frequencies of the source currents (Boteler, 1990). Apatenkov et al., (2020) identified a sequence of current vortex pairs moving eastward with the speed of 0.5–2.5 km/s that fits to the electrodynamics scheme of omega bands. They found that, although the temporal variations of the associated current system are slow, the omega bands can be responsible for strong magnetic variations and GIC due to fast propagation of the source currents.

The actual calculation process for determining geoelectric fields, whether using measured MT impedances or 1-D, 2-D or 3-D models, involves determination of a tensor transfer function, C, relating the geoelectric field components, E_x and E_y, to the rate of change of the magnetic field:

$$[E_y E_x] = [C_{yx} C_{xx}\, C_{yy} C_{yx}][g_y g_x] \tag{6}$$

These calculations are often done using the 'frequency domain' route which involves taking the Fourier transform of the geomagnetic data to obtain the magnetic field spectrum, multiplying each spectral component by the corresponding value of the Earth transfer function to obtain the electric field spectrum, and then doing an inverse Fourier transform to obtain the variations with time of the geoelectric field (Fig. 9).

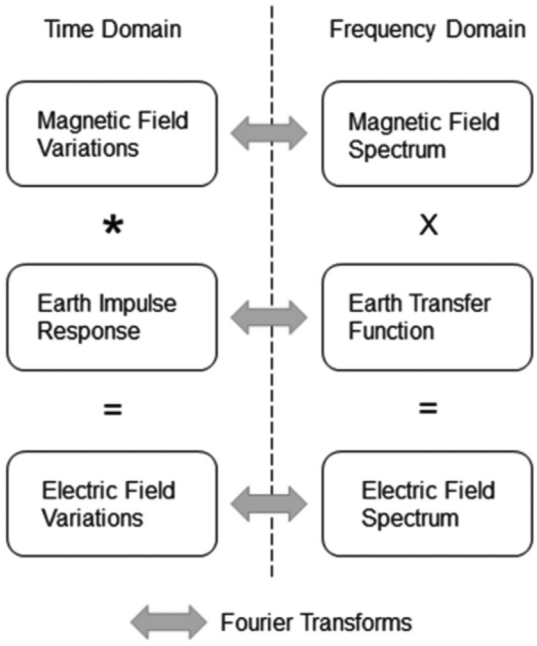

Fig. 9. Schematic of calculations of the geoelectric field using convolution (*) in the time domain or multiplication (X) in the frequency domain.

Alternatively, calculations of the geoelectric field can be done using the 'time domain' route which involves convolving the geomagnetic data with the impulse response of the Earth. In principle, the Earth impulse response is simply the inverse Fourier transform of the Earth Transfer Function; but, in practice, a digital calculation produces an acausal, oscillatory impulse response because of the Gibbs phenomena that a finite spectrum (inevitably used in digital calculations) does not contain sufficient information to reconstruct a clean impulse response (Egbert, 1992; Kelbert et al., 2017). For many years, time domain calculations were limited to an impulse response for a uniform conductivity Earth, for which there is an analytic transform from the transfer function (Pirjola, 2002). However, recently, a new method has been developed using a "causal transform" that enables digital calculations of the impulse response from any Earth transfer function (Boteler and Pirjola, 2022).

5.3. Geomagnetically induced currents (GICs)

5.3.1. Power systems

GIC in long conductors at the Earth's surface are directly driven by electric fields induced in the conductors themselves and are not just currents flowing in from the Earth. The early literature described the driver for GIC as an Earth Surface Potential Gradient, but it has been shown that potential gradients cannot represent realistic electric fields (Boteler and Pirjola, 1998b). To model GIC in a power network the induced electric field integrated along a power line can be represented by a voltage source in the line. This voltage source can also be converted to an equivalent current source, and this is how the source fields are represented in the two GIC modelling methods. These are the Lehtinen-Pirjola method (Lehtinen and Pirjola, 1985) and the Nodal Admittance Matrix (NAM) method (Boteler, 2014), which are mathematically equivalent (Boteler and Pirjola, 2014).

The Lehtinen-Pirjola (LP) method was developed at a time when only a single voltage level in a power system was considered. It directly calculates the GIC flowing to ground at each substation. However, realistic power systems have multiple voltage levels, which lead to many nodes in the network model that are ungrounded and require 'virtual' connections to ground to model GIC. Now a recent modification to the LP method, referred to as the LPm method (Pirjola et al., 2022) replaces the earthing impedance matrix with an earthing admittance matrix. This leads to the equation relating the nodal voltages and the current sources:

$$[J^e] = ([Y^e] + [Y^n])[V^n] \tag{7}$$

where $[Y^e]$ is the earthing admittance matrix and $[Y^n]$ is the LP network admittance matrix. Inversion of the combined matrix and multiplication by the current sources then gives the nodal voltages:

$$[V^n] = ([Y^e] + [Y^n])^{-1}[J^e] \tag{8}$$

These node voltages are then used to calculate the GIC in the transmission lines and the transformer windings. The LPm method removes the need for 'virtual' connections from nodes to ground. It also involves the inversion of a sparse symmetric positive definite matrix allowing efficient techniques, such as Cholesky decomposition, which speeds up computations for large networks (Pirjola et al., 2022).

A recent feature of GIC research has been the increased interest in geomagnetic effects in countries at lower latitudes than those traditionally considered. Transformer damage in New Zealand in November 2001 (Béland and Small, 2004) and in South Africa in the 2003 Halloween storm (Gaunt and Coetzee, 2007) was a surprise. In both cases it was thought that prior exposure to GIC and other power system stresses may have contributed to the failures, which indicates that it is not just the extreme events such as that in March 1989 that present a hazard to power systems. Since then GIC research has expanded greatly with studies in China (Zhang et al.,2012,2015; Liu et al., 2014), Japan (Watari et al., 2009a, 2009b, 2021), Australia (Marshall et al., 2013), New Zealand (Marshall et al., 2012; Divett et al., 2017; 2018; Rodger et al., 2017), Spain (Torta et al., 2012, 2021); Italy (Tozzi et al., 2019), Austria (Bailey et al., 2017), UK (Beggan et al., 2013; Beggan, 2015), Ireland (Blake et al., 2016), France (Kelly at al, 2017), Russia (Sakharov et al., 2009; Belakhovsky et al., 2018), South Africa (Ngwira et al., 2008; Matandirotya et al., 2015; Heyns et al., 2021; Jankee et al., 2022), Uruguay (Carabello et al., 2013; Carabello, 2016), Brazil (Trivedi et al., 2007; Da Silva Barbosa et al., 2015a, b),

Mexico (Carabello et al., 2020), and India (Rajput et al., 2021).

5.3.2. Pipelines

Geomagnetic induction in pipelines is a concern because of the effect it can have on the corrosion prevention systems normally used. These involve injecting a current into the ground to flow back onto the pipe. In this circuit, the pipeline can be considered as the "cathode", and the technique is referred to as "cathodic protection (CP)". The CP current drives the pipe to negative voltage with respect to the surrounding soil. If the pipe-to-soil potential (PSP) is maintained within the "safe" range, between −0.85 V and −1.2 V, it inhibits the electrochemical processes that cause corrosion. However, during geomagnetic disturbances the induced voltages can move the PSP outside the safe range allowing corrosion to occur. This will not have an immediate effect on a pipeline, but the cumulative effect of many storms could reduce the lifetime of a pipeline.

In the pipeline industry, GIC are referred to as "telluric currents" and the 'telluric' PSP variations they cause have now been observed in many parts of the world (see Boteler and Trichtchenko (2015) for a review of telluric observations). Early modelling of geomagnetic induction in pipelines used distributed source transmission line (DSTL) theory and reached the point where it could be used for the design of pipeline CP systems (Rix and Boteler, 2001). The transmission line model of pipeline sections has now been combined with network theory to provide a versatile method for modelling pipeline networks (Boteler, 2013). The modelling shows that the use of higher resistance coatings on pipelines is increasing the impact of geomagnetic induction telluric PSP variations (Boteler, 2007), so that telluric PSP variations are now being observed on new pipelines in regions where they were not noticed before. This has prompted new work on telluric effects, such as that by Viljanen et al., (2006b) in Finland, Fernberg et al., (2007a, b) in Canada, Ingham and Rodger (2018) and Ingham et al., (2022) in New Zealand, Yu et al., (2019) in China, and Larocca et al., (2021) in Argentina. See also the analysis of the interplanetary cause of currents in the Finnish pipeline by Tsurutani and Hajra (2019, 2021a, b).

5.3.3. Railways

Railways are another technological system that has long conductors (the rails) that will be affected by geomagnetic induction. Many railways use track circuits, which apply a voltage between the rails to operate a relay that sets signals to green when a track section is clear. A train entering a track section short-circuits the voltage, causing the relay to drop out and set the signals to red. Sweden had reported signals being set to red during a geomagnetic disturbance in 1982 (Wik et al., 2009). Statistical studies in Russia had found that unexplained signaling anomalies on certain railway lines occurred during times of high geomagnetic activity (Ptitsyna et al., 2008; Eroshenko et al., 2010).

Increased concern about the impacts of High Impact Low Frequency (HILF) events prompted the European Commission's Joint Research Centre, the Swedish Civil Contingencies Agency MSB, the UK Department for Transport, and the NOAA Space Weather Prediction Center to organize a workshop, "Space weather and rail" in London in 2015. This workshop identified vulnerabilities in rail networks via direct impacts on signaling track circuits, and indirectly via dependencies on power, communications, and Global Navigation Satellite Systems (GNSS) (Krausmann et al., 2015).

Further research into geomagnetic effects on railway track circuits was stimulated by the discovery of a 1956 Swedish book about railway signaling problems that contained two sections about geomagnetic interference to railway track circuits. This was written in Swedish, but to make it available to a wider audience, has now been translated into English and published online (Alm, 1956/2020; Lejdström and Svensson, 1956/2020). A new method has been developed for modelling geomagnetic interference to track circuit operation and provides the tools to assess the geomagnetic hazard to railway signaling (Boteler, 2021). This has recently been used to investigate the impact of GIC on railway signaling for electrified lines in the UK (Patterson et al., 2023a,b; 2024).

5.3.4. Submarine cables

Geomagnetic effects on submarine cables go back to the 19th century, but effects on modern cables can be traced to the introduction of coaxial cables with repeaters in the 1950s. During the magnetic storm in February 1958 *trans*-Atlantic telephone calls were heard alternatively as loud squawks and faint whispers as the geomagnetically induced voltage added or subtracted from the driving voltage powering the repeaters (Anderson, 1979). There was a major technological change with the installation of the first trans-Atlantic fibre-optic cable, TAT-8, in 1988. In fibre-optic cables the signals are transmitted over the fibre-optics but there is still a conductor along the cable to carry power to the repeaters. Recordings on the cable during the March 1989 storm showed that it experienced induced voltages up to 700 V (Medford et al., 1989).

Since the introduction of fiber-optic cables there has been a great expansion of submarine cables (they carry > 95 % of international internet traffic), but not much research on possible space weather effects. However, widespread outages of submarine cables would have serious consequences for international communication Jyothi (2021). Further research is needed. Determination of effects on submarine cables is complicated by the need to calculate the electric fields on the seafloor. This is more complicated than calculating the electric fields in Earth's surface as it is necessary to take account of the attenuation of the fields by the conducting seawater. The formulas for the seafloor fields relative to the surface magnetic field were developed by Boteler and Pirjola (2003) and Goto (2015). Recently these have been used to produce a modelling process for

calculating the voltages experienced by submarine cables during a geomagnetic disturbance (Chakraborty et al., 2022; Boteler et al., 2024).

5.4. Assessing and mitigating the GMD hazard

The whole chain of investigations needed to assess the impact of geomagnetic disturbances on ground systems involves many components. This idea was described by Pulkkinen et al., (2017), who said: "The field of GIC has evolved over the past several years from a somewhat separate field of space science research into a full systems science, addressing not only the solar-terrestrial research, but also the engineering and operational hazard mitigation dimensions of the problem." The research progress described above has provided many of the tools for assessing how different systems will respond to extreme geomagnetic disturbances. The remaining questions are related to how large are the events that can be expected and what to do about them.

Just like civil engineers want to know the size of the 1-in-100 year flood when designing a bridge, so electrical engineers want to know the 1-in-100 year geomagnetic disturbance that their ground system has to be designed (or modified) to cope with. Because the events of concern are in the tail of the statistical distribution of magnetic activity, this requires the use of extreme value statistics (Riley et al., 2018; Nikitina et al., 2016; Thomson et al., 2011; Love, 2021). These studies provide estimates of the 1-in-100 year values of geomagnetic activity and how they vary with latitude. Some studies use 1-D earth conductivity models to calculate geoelectric fields and provide extreme value assessments for these. However, this fails to take account of the effect of 3-D conductivity structure and how this affects the geoelectric fields and, in consequence, the GIC. The interaction of localized geomagnetic disturbances with the spatial structure of the earth conductivity needs to be included in these assessments to provide better indication of the extreme values that systems may experience.

The GIC values that occur are very dependent on system characteristics, so a geoelectric field that is critical for one system may not be significant for a neighbouring system. For power systems, a major factor is the voltages used, because higher voltage transmission lines have lower resistance and therefore experience larger GIC than lower voltage lines would have with the same geoelectric field (Zheng et al., 2014). For pipelines, a significant factor has been the use of higher resistance coatings, which have increased the pipe-to-soil potential variations produced by GIC on modern pipelines. In railways, signaling systems using track circuits will experience geomagnetically induced voltages in the rails but whether these affect signal operation depends on how the track circuits are configured, while other systems (e. g. axle counters) are immune from geomagnetic effects (Boteler, 2021). Modern fibre-optic submarine cables are affected by geomagnetic induction into the conductor along the cable used to supply power to the repeaters. Whether this is a problem depends on the ability of the power feed equipment to compensate for the geomagnetically induced voltages and maintain a constant current along the cable.

If a risk assessment has identified that a particular system could be vulnerable to a severe geomagnetic disturbance, then a mitigation strategy is necessary. An engineering solution is preferred by industry, but is not always practical or cost effective. For example, the seemingly obvious solution of putting blocking capacitors in the neutral-ground connection of a transformer to stop the flow of GIC is not without its complications. A good connection to ground from a transformer is still needed to provide protection in the case of lightning strikes and power system faults. Thus, the capacitor has to be sized to deal with the large currents that occur, which greatly increases the cost. Also, blocking GIC at one substation changes the network configuration so that the GIC are now diverted to a different substation; blocking that substation moves the GIC somewhere else, and so on. Therefore, careful simulations of the network are needed before a mitigation strategy can be implemented. On pipelines, blocking the flow of GIC actually increases the problem. Insulating flanges to block GIC were originally included in the design of the Maritimes and Northeast Pipeline in Canada but simulations of geomagnetic induction showed that the insulating flanges did not stop the GIC, they only deflected it into the ground where it flowed round the flange and back onto the pipe. The GIC flowing on and off the pipeline is the cause of the variations in pipe-to-soil potential that are the real concern with regard to pipeline corrosion. As a result of this work the design was changed and the pipeline was subsequently built without insulating flanges (Rix and Boteler, 2001). However, in many cases, engineering solutions are not cost-effective and the engineers are looking for forecasts of GMD and GIC so that special operating procedures can be implemented when necessary to protect their systems.

The modelling described in the previous chapters provides the foundation for improving forecasting of GMD, and work is underway to evaluate models for transition to operations (Pulkkinen et al., 2013). There are still gaps in our knowledge and challenges to provide the forecast lead times that industry would like. However, there is still valuable information that can be used to provide situational awareness for operators of affected systems. Power system operators are unlikely to take action based on current forecasts, so more reliance is placed on real-time data (i. e. "nowcasts"). Methods are now available for time domain calculation of geoelectric fields and are being used to provide real-time mapping of geoelectric fields for power systems (Balch et al., 2018). Real-time simulations of GIC have also been implemented in the control center for the power network in Ontario, Canada (Marti et al., 2013). Power system operators are also investigating combining GMD monitoring with power system parameters to pro-

vide GIC situational awareness for control room operators (Basu et al., 2015; Klauber et al., 2020). Eventually, new interdisciplinary understanding and advanced modeling capabilities will allow for a complete simulation of the processes depicted in Fig. 7 above. This will enable accurate simulations of the chain of events leading to geomagnetic disturbances on the ground starting with their origins in the solar atmosphere.

6. Summary and conclusions

This review has highlighted the gaps in understanding what should be addressed to accurately specify and predict the occurrence of geomagnetic disturbances and their impacts to technical systems. We focus here on geomagnetic disturbances affecting electrical power lines, and other long-line conductors on Earth's surface. Not meant to be a comprehensive review of all prior work, we concentrate on how recent breakthroughs and insights have moved the field forward so that we are now poised for even more profound progress. In particular, new understanding is allowing us to break free from "misconceptions" originating from prior diffuse terminology and nomenclature that may have constrained and biased our perceptions.

The gaps in current understanding are summarized in Table 1, divided according to solar wind driving, geospace coupling, and technical impacts from geomagnetic disturbances. For solar wind driving, the focus is on understanding how the temporal and spatial variabilities in the solar wind are linked to the geomagnetic disturbances that are most impactful to human technologies. For geospace coupling, a range of physical processes must be understood to

Table 1
Key Gaps in Our Understanding of the Physical Processes That Create Hazardous Geomagnetic Disturbances and Associated Effects on Infrastructure.

Solar Wind Driving	
1.1,1	The relative role of direct solar wind drivers, such as interplanetary magnetic field (IMF) direction and strength, plasma density, temperature, and velocity on the generation of currents and energization of plasma in the various coupled magnetospheric regions
1.1.2	The differences in geospace responses to Corotating Interaction Regions, Coronal Mass Ejections, and High-Speed Solar Wind Streams, as well as the importance of prehistory in response to these drivers
1.1.3	The effect of the temporal and spatial extent of solar wind drivers on the resulting geospace current systems and their variability
1.1.4	The differences in geospace current systems for low, moderate or extreme solar wind drivers, and how they may depend on the prehistory of the solar wind driving
1.1.5	The extent to which the solar wind contains information allowing the prediction of geomagnetic disturbances
Geospace Coupling	
1.2.1	The physical processes that determine the partition, storage, and release of magnetic energy in the magnetosphere associated with magnetopause currents, tail currents, ring currents and the coupled ionospheric currents
1.2.2	The physical processes by which solar wind and internal drivers can affect, trigger or excite either waves or instabilities in the coupled geospace system, leading to substorms or magnetic spikes during geomagnetic storms
1.2.3	The large-scale auroral context of geomagnetic disturbances, both in terms of precipitation and currents
1.2.4	The feedback mechanisms linking the various geospace domains and how they affect the storage and release of magnetic energy
1.2.5	The relationship between geomagnetic disturbances and dynamic aurora, such as Omega Bands, Westward Traveling Surges, Wedgelets, Bursty Bulk Flows, and other localized particle injection events
1.2.6	The spatial and temporal development of dB/dt in substorms and substorm-like spikes, and the origins of dB/dt events not related to storms or substorms
1.2.7	The field-aligned current configurations associated with dB/dt, including both filamentary and sheet currents and their temporal variations
1.2.8	The role of Bursty Bulk Flows in the origin and evolution of dB/dt, and the magnetospheric connections to dB/dt events
1.2.9	The circumstances under which height-integrated conductances do not accurately incorporate the physical processes of importance for electrodynamic coupling between the ionosphere and magnetosphere
1.2.10	The energy deposition and resulting conductivity profiles associated with various types of auroral particles and energy spectra
1.2.11	Subauroral space weather effects, including phenomena such as the Sub-Auroral Polarization Stream (SAPS), Subauroral Ion Drifts (SAIDs), STEVE, and their associated features in the conjugate ionosphere
1.2.12	The relation between enhanced electric fields, strong plasma drifts, conductances and field-aligned currents
1.2.13	The physical processes that determine how magnetospheric current systems couple to the upper atmosphere and thereby extract both energy and plasma from the magnetosphere, but also extract heavier plasma from the atmosphere which in turn affects the overall energy content and thus stability of the original magnetospheric currents
1.2.14	The energization processes leading to ion outflow and the associated effects on ionosphere-thermosphere coupling, geospace dynamics, and the development of geomagnetic storms and substorms
Geomagnetic Disturbance Impacts	
1.3.1	The combined impact of the extent, duration, amplitude and repetitiveness of geomagnetic disturbances on vulnerable technological systems
1.3.2	The role of soil, ocean or crustal conductivities on the enhancement or modification of any electric fields induced by the geomagnetic disturbances
1.3.3	The vulnerability of infrastructure to rapid changes in induced electric fields due to variable ionospheric or magnetospheric currents
1.3.4	The quantification of expected impacts associated with rare, extreme GIC characteristics
1.3.5	The quantitative effects of geomagnetic variability on critical infrastructure
1.3.6	The combination of risk factors originating from localized geomagnetic disturbances with structures in the surface and crustal conductivities and/or any exposed structures in the potentially affected infrastructure itself

trace the flow of energy from the solar wind into the magnetosphere and ionosphere at the spatial and temporal scales necessary to quantitatively assess the potentially hazardous impacts of geomagnetic disturbances. For geomagnetic disturbance impacts, we focus on how magnetospheric and ionospheric currents associated with dynamic auroral processes and phenomena couple to geoelectric fields, taking into account the spatially varying conductivity of Earth's crust.

Table 2 summarizes the modeling activities that need to be conducted to accurately simulate geomagnetic disturbances. Here the focus is on developing coupled models that link all the space weather domains, while incorporating the physical processes that regulate the flow of energy through the system. Current and future work will focus on energy flow, coupling processes, and disentangling temporal and spatial variations, such as bursts and spikes. Exploration of alternative modeling approaches is essential, as new modeling capabilities emerge that are better able to handle the spatial and temporal variabilities characterizing hazardous geomagnetic disturbances. Assessment and validation activities for models are important to ensure continuous improvement and quantitative comparison of the different modeling approaches.

Table 3 lists the observational capabilities that will be needed for uncovering physical processes not yet included in current models, for driving and validating space weather models, and for quantifying the impacts to technical systems. New observations and modeling are now allowing us to revisualize long standing pictures of how the solar wind, magnetosphere, ionosphere and thermosphere are connected.

The research, modeling, and observations described in this review and summarized in Tables 1–3 provide a framework for constructing a plan by which the international science community can comprehensively address the growing threat to human technologies caused by geomagnetic disturbances. Though broad in scope and hinging on as yet undiscovered physical processes, it incorporates recent results that have made continued progress and new insights within reach. As many of the physical processes described here are also relevant for addressing other space weather impacts, such as radiation effects, communication and navigation outages, and satellite drag, a comprehensive plan to integrate activities from other ISWAT Clusters is imperative to fill in remaining gaps, as well as to reduce redundant effort. Such integrated plans have been successful in the past in paving the way for the tremendous progress wit-

Table 2
Modeling Activities Needed to Understand and Predict Geomagnetic Disturbances and Their Impacts on Technology.

2.1	Continue the development of multiple models that couple the Sun, solar wind, magnetosphere, plasmasphere, ionosphere, and thermosphere, using a variety of numerical approaches.
2.2	Develop next generation, coupled, multicomponent, multiscale, geospace modeling systems, with each modeling component tailored to include underlying physical processes.
2.3	Identify missing physics that prevent accurate simulation of geomagnetic disturbances at critical spatial and temporal scales.
2.4	Incorporate higher spatial resolution in models to simulate reoccurring explosive magnetotail reconnection, and to reproduce localized and transient phenomena including bursty bulk flows, field aligned current filamentation, and localized spikes in dB/dt.
2.5	Ensure that models accurately account for the transfer of energy from the solar wind into the geospace system and contain appropriate modules to capture spontaneous internal processes of magnetospheric energy release.
2.6	Explore the use of machine learning and artificial intelligence techniques to capture the stochastic nature of small and mid scale geospace phenomena.
2.7	Provide access to advanced simulation capabilities to the space weather community to facilitate research and evaluating potential of new models to improve forecasting capabilities.
2.8	Develop and implement assimilative models, ensemble modeling, and machine learning to identify the conditions under which dB/dt spikes, and other potentially stochastically driven phenomena occur, including the ability to separate those produced by solar wind variations from those produced by internal magnetospheric processes.
2.9	Estimate uncertainties in modeling results due to uncertainties in external drivers and internal parameters.
2.10	Analyze simulation outputs for possible numerical artifacts related to numerical noise and coupling of models with overlapping grids.
2.11	Identify connections between modeled magnetospheric properties, visual aurora, and auroral boundaries to better assess model accuracy and realism.
2.12	Incorporate polar wind and upper atmosphere models into geospace modeling systems available for Runs-on-Request at the CCMC and other modeling centers to facilitate studies of processes leading to ion outflow and its role in the development of substorms.
2.13	Undertake studies that quantify improvements in capabilities to forecast geomagnetic environment variability for timescales ranging from storms (days), substorms (hours) and spikes (minutes), using a well-defined set of archived event data and updated versions of predictive models.
2.14	Address the lack of global datasets ready for model validation, especially at low latitudes.
2.15	Quantitatively assess the ability of models to simulate phenomena of mixed spatial and temporal scales, and their relation to bursts and spikes in magnetosphere and ionosphere response, e. g. bursty bulk flows and transient and filamentary field-aligned currents.
2.16	Conduct focused studies to understand the limitations of using magnetic indices as input to models, and how they may be improved by combining ground-based and space-based current measurements.
2.17	Perform end-to-end modeling of GIC events from their origin on the sun to their effect on susceptible human technology.
2.18	Perform end-to-end, physics-based, risk analysis models that superimpose geomagnetic disturbance variations on localized ground conductivity structures and power networks.
2.19	Conduct so-called "What if" studies to identify potential 'explicit' vulnerabilities for end-user networks, caused by unfortunate occurrences of localized GMD structures 'over-amplifying' effects from structures in either the ground conductivity or the networks themselves.

Table 3
Key Observational Activities Needed to Understand and Predict Geomagnetic Disturbances and Their Impacts on Technology.

3.1	Carry out and combine magnetotelluric measurements to achieve higher spatial resolution and local and global coverage for maps of 3-D ground conductivity.
3.2	Create, expand, and connect magnetic observations to achieve higher spatial and temporal resolution and better global coverage.
3.3	Understand how to effectively combine observations and models to optimize specification of auroral conductances globally.
3.4	Perform coordinated ground-based and space-based experimental campaigns to validate modeled values of auroral electrodynamic parameters and energy transfer rates between the magnetosphere, ionosphere, and lower atmosphere.
3.5	Identify the observations needed to determine whether different energy states of the solar wind-magnetosphere system are only quantitatively, or even qualitatively different, entailing different feedback mechanisms and instabilities (e.g. for extreme cases).
3.6	Identify the observations needed to effectively apply artificial intelligence and machine learning techniques to differentiate the roles of solar wind parameters in driving electric currents.
3.7	Take advantage of new observing capabilities made possible through the deployment of constellations of small satellites to improve spatial coverage, to discriminate between temporal and spatial variations, and to explore regions not previously studied.
3.8	Design a constellation of satellites that will provide continuous coverage of the (normal and expanded) auroral oval at high cadence and spatial resolution, and with the ability to determine the type of particle, mean energy and energy flux of auroral precipitation and the resulting ionospheric electron density and conductivity.
3.9	Develop an international coalition to coordinate ground-based observational assets to enable global, continuous, and real-time geospace measurements (e. g., the SuperMAG / SuperDARN model for multi-instrument networks).
3.10	Develop and improve virtual observatories to include geospace, solar, and solar wind observations that seamlessly assimilate into physics-based, predictive models.
3.11	Undertake Observing System Simulation Experiments (OSSEs) to optimize the scientific outcomes from the unique measurements to be provided by new missions such as the Geospace Dynamics Constellation (GDC), DYNAMIC, HelioSwarm, EZIE, and the Small scale magNetospheric and Ionospheric Plasma Experiment (SNIPE).

nessed in the last decades and establishing a firm foundation for continued progress.

The scope of this review underscores the need for a multidisciplinary approach to mitigating hazards to technical systems from geomagnetic disturbances. Not only does it entail understanding the physical processes governing the behavior of the space domains between the Sun and Earth, but it also drives research on the geology of Earth's surface, and the engineering sciences needed to analyze the impacts to specific human technologies. The multidisciplinary aspects drive the requirements to build a community of scientists across the relevant fields, to ensure effective communication among the various groups, and to ensure that educational activities at academic institutions are well aligned with the intellectual challenges that must be overcome.

Declaration of competing interest

The authors declare that they have no known competing financial interests or personal relationships that could have appeared to influence the work reported in this paper.

Acknowledgements

Regrettably, coauthor Dr. Jennifer Gannon passed away prior to the publication of this paper. Her outstanding contributions to this work and to the study of geomagnetic disturbances and space weather throughout her illustrious career are gratefully acknowledged.

The author team acknowledges the original task definition for a new Space Weather Roadmap and logistical support from COSPAR. This work is part of a bigger effort from ISWAT (International Space Weather Action Teams) by the COSPAR Panel of Space Weather (PSW).

Some individual authors acknowledge the following support:

H.O. - the Swedish Space Agency.

R.R. - NASA Cooperative Agreement 80NSSC21M0180, Partnership for Heliophysics and Space Environment Research (PHaSER).

C.M.N. - NASA grant PHaSER, NASA grant 80NSSC20K1364, and NSF grant 2300579.

V.M. - NASA awards 80NSSC23K0223 and 80NSSC22M0163.

D.S. is supported with PHaSER Cooperative Agreement 80NSSC21M0180.

N.K. is partly funded by ESA contracts SSA P3-SWE-XLV no.4000138311/22/D/AP.

and ESA S2P no.4000134036/21/D/MRP.

J.W. - NASA grant 80NSSC23K0171.

K.N. - NASA grants #80NSSC18K1381 #80NSSC22K0304 #80NSSC23K0899.

and NSF grant #2308853.

J.P.E., J.W.B.E. and M.H. - Grant UKRI/NERC NE/V003070/1.

The work of M.H. is further supported by Schmidt Science Fellows, in partnership with the Rhodes Trust.

References

Adebesin, B.O., Pulkkinen, A., Ngwira, C.M., 2016. The interplanetary and magnetospheric causes of extreme dB/dt at equatorial locations. Geophys. Res. Lett. 43, 11501–11509. https://doi.org/10.1002/2016GL071526.

Ahn, B.-H., Richmond, A.D., Kamide, Y., Kroehl, H.W., Emery, B.A., de la Beaujardiére, O., Akasofu, S.-I., 1998. An ionospheric conductance model based on ground magnetic disturbance data. J. Geophys. Res. 103 (A7), 14769–14780. https://doi.org/10.1029/97JA03088.

Akasofu, S.I., 1964. The development of the auroral substorm. Planet Space Sci. 12, 273–282. https://doi.org/10.1016/0032-0633(64)90151-5.

Akasofu, 1981. Prediction of development of geomagnetic storms using the solar wind-magnetosphere energy coupling function ϵ. Planet. Space Sci. 29, 1151–1158. https://doi.org/10.1016/0032-0633(81)90121-5l.

Akasofu, S. -I. 2012. Auroral Morphology: A Historical Account and Major Auroral Features During Auroral Substorms. In: Keiling, A., Donovan, E., Bagenal, F. and Karlsson, T. (Eds.), Auroral Phenomenology and Magnetospheric Processes: Earth And Other Planets , 29-38. https://doi.org/10.1029/2011GM001156.

Albarran, R.M., Varney, R., Pham, K.H., Lin, D., 2023. Characterization of N+ abundances in the terrestrial polar wind using the multiscale atmosphere-geospace environment. Authorea Preprints. https://doi.org/10.22541/au.170121287.79821817/v1.

Alm, E., 1956/2020. Measures against geomagnetic disturbances in the entire DC track circuit for automatic signaling systems, original publication (in Swedish) Appendix 5F, Betänkande: angående det tekniskautförandet av signalanläggningar vid Statens Järnvägar, 1956; Translation (in English. Infrastructure Resilience Risk Reporter 1 (10), 10–27 https://carleton.ca/irrg/journal/.

Anderson, B.J., Takahashi, K., Toth, B.A., 2000. Sensing global birkeland currents with Iridium engineering magnetometer data. Geophys. Res. Lett. 27 (24), 4045–4048.

Anderson, B.J., Korth, H., Waters, C.L., Green, D.L., Merkin, V.G., Barnes, R.J., Dyrud, L.P., 2014. Development of large-scale Birkeland currents determined from the active magnetosphere and planetary electrodynamics response experiment. Geophys. Res. Lett. 41, 3017–3025. https://doi.org/10.1002/2014GL059941.

Anderson, C.W. 1979 Magnetic storms and cable communications. In: Kennel, C.F., Lanzerotti, L.J., Parker, E.N. (Eds.), Solar System Plasma Physics, Magnetospheres, V. 2, North-Holland, Amsterdam.

Angelopoulos, V., Baumjohann, W., Kennel, C.F., Coroniti, F.V., Kivelson, M.G., Pellat, R., Walker, R.J., Luhr, H., Paschmann, G., 1992. Bursty bulk flows in the inner central plasma sheet. J. Geophys. Res. 97, 4027–4039.

Angelopoulos, V., Kennel, C.F., Coroniti, F.V., Pellat, R., Kivelson, M.G., Walker, R.J., Russell, C.T., Baumjohann, W., Feldman, W.C., Gosling, J.T., 1994. Statistical characteristics of bursty bulk flows events. J. Geophys. Res. 99, 21257–21280.

Angelopoulos, V., McFadden, J.P., Larson, D., Carlson, C.W., Mende, S.B., Frey, H., Phan, T., Sibeck, D.G., Glassmeier, K.-H., Auster, U., Donovan, E., Mann, I.R., Rae, I.J., Russell, C.T., Runov, A., Xhou, X., Kepko, L., 2008. Tail reconnection triggering substorm onset. Science 321 (5891), 931–935. https://doi.org/10.1126/science.1160495.

Apatenkov, S.V., Pilipenko, V.A., Gordeev, E.I., Viljanen, A., Juusola, L., Belakhovsky, V.B., et al., 2020. Auroral omega bands are a significant cause of large geomagnetically induced currents. Geophys. Res. Lett. 47. https://doi.org/10.1029/2019GL086677.

Artemyev, A.V., Angelopoulos, V., Vasko, I.Y., 2019. Kinetic properties of solar wind discontinuities at 1 AU observed by ARTEMIS. J. Geophys. Res.: Space Physics 124, 3858–3870. https://doi.org/10.1029/2019JA026597.

Bailey, R.L., Halbedl, T.S., Schattauer, I., Römer, A., Achleitner, G., Beggan, C.D., Wesztergom, V., Egli, R., Leonhardt, R., 2017. Modelling geomagnetically induced currents in midlatitude Central Europe using a thin-sheet approach. Ann. Geophys. 35 (3), 751–761.

Baker, J.B.H., Zhang, Y., Greenwald, R.A., Paxton, L.J., Morrison, D., 2004. Height-integrated Joule and auroral particle heating in the night side high latitude thermosphere. Geophys. Res. Lett. 31, L09807. https://doi.org/10.1029/2004GL019535.

Balch, C.C., Kelbert, A., Rigler, E.J., Millward, G.H. 2018. NOAA's Regional Geoelectric Field Modeling Capability: Progress toward providing a near real-time map and forecasting capability to improve operational decision making of the U.S. Electrical Power Grid in response to geomagnetic storms, AGU Fall Meeting 2018, abstract #PA24B-09, https://ui.adsabs.harvard.edu/abs/2018AGUFMPA24B..09B/abstract.

Basu, C., Padmanaban, M., Guillon, S., de Montigny, M., Kamwa, I. 2015. Combining multiple sources of data for situational awareness of geomagnetic disturbances, Proc. 2015 IEEE Power & Energy Society General Meeting, Denver, July 2015. doi: 10.1109/PESGM.2015.7286179.

Baumjohann, W., Pellinen, R.J., Opgenoorth, H.J., Nielsen, E., 1981. Joint two-dimensional observations of ground magnetic and ionospheric electric fields associated with auroral zone currents: Current systems associated with local auroral break-ups. Planet. Space Sci. 29 (4), 431–447. https://doi.org/10.1016/0032-0633(81)90087-8.

Beggan, C.D., Beamish, D., Richards, A., Kelly, G.S., Thomson, A.W.P., 2013. Prediction of extreme geomagnetically induced currents in the UK high-voltage network. Space Weather 11, 407–419. https://doi.org/10.1002/swe.20065.

Beggan, C.D., 2015. Sensitivity of geomagnetically induced currents to varying auroral electrojet and conductivity models. Earth Planets Space 67, 24. https://doi.org/10.1186/s40623-014-0168-9.

Belakhovskya, V.B., Pilipenkob, V.A., Sakharova, Y.A., Selivanovc, V.N., 2018. Characteristics of the variability of a geomagnetic field for studying the impact of the magnetic storms and substorms on electrical energy systems. Izv. Phys. Solid Earth 54 (1), 52–65.

Birn, J., Hesse, M., Schindler, K., Zaharia, S., 2009. Role of entropy in magnetotail dynamics. J. Geophys. Res. 114, A00D03. https://doi.org/10.1029/2008JA014015.

Blake, S.P., Gallagher, P.T., McCauley, J., Jones, A.G., Hogg, C., Campanya, J., Beggan, C., Thomson, A.W.P., Kelly, G.S., Bell, D., 2016. Geomagnetically induced currents in the Irish power network during geomagnetic storms. Space Weather 14, 1136–1154. https://doi.org/10.1002/2016SW001534.

Bolduc, L., 2002. GIC observations and studies in the Hydro-Quebec power system. J. Atmos. Sol.-Terr. Phy. 64 (16), 1793–1802.

Boris, J.P. 1970. A physically motivated solution of the Alfvén problem, Tech. Rep. NRL Memo. Rep. 2167, Nav. Res. Lab, Washington, D. C.

Borovsky, J.E., Funsten, H.O., 2003. MHD turbulence in the Earth's plasma sheet: Dynamics, dissipation, and driving. J. Geophys. Res. 108, 1284. https://doi.org/10.1029/2002JA009625, A7.

Borovsky, J.E., Valdivia, J.A., 2018. The earth's magnetosphere: a systems science overview and assessment. Surv. Geophys. 39, 817–859. https://doi.org/10.1007/s10712-018-9487-x.

Borovsky, J.E., Yakymenko, K., 2017. Substorm occurrence rates, substorm recurrence times, and solar wind structure. J. Geophys. Res. Space Physics 122, 2973–2998. https://doi.org/10.1002/2016JA023625.

Boteler, D.H., Pirjola, R.J., 1998a. The complex image method for calculating the magnetic and electric fields produced at the surface of the Earth by the auroral electrojet. Geophys. J. Int. 132, 31–40.

Boteler, D.H., Pirjola, R.J., 1998b. Modelling geomagnetically induced currents produced by realistic and uniform electric fields. IEEE Trans Power Delivery 13, 1303–1308.

Boteler, D.H., Pirjola, R.J., 2003. The magnetic and electric fields produced in the sea during geomagnetic disturbances, Pure Appl. Geophys. 160, 1695–1716.

Boteler, D.H., Pirjola, R.J., 2014. Comparison of methods for modelling geomagnetically induced currents. Ann. Geophys. 32, 1177–1187. https://doi.org/10.5194/angeo-32-1177-2014.

Boteler, D.H., Pirjola, R.J., 2022. Electric field calculations for real-time space weather alerting systems. Geophys. J. Int. 230 (2), 1181–1196. https://doi.org/10.1093/gji/ggac104.

Boteler, D.H. and Trichtchenko, L. 2015. Telluric Influence on Pipelines, Chapter 21, Oil and Gas Pipelines: Integrity and Safety Handbook, In: Winston Revie, R. (Eds.), John Wiley & Sons, Inc., Hoboken. Pp. 275-288.

Boteler, D.H., Pirjola, R., Trichtchenko, L., 2000. On calculating the magnetic and electric fields produced at the earth's surface by a "wide" electrojet. J. Atmos. Solar Terr. Phys. 62, 1311–1315.

Boteler, D.H., Chakraborty, S., Shi, X., Hartinger, M.D., Wang, X., 2024. An examination of geomagnetic induction in submarine cables. Space Weather 22, e2023SW003687. https://doi.org/10.1029/2023SW003687.

Boteler, D.H., 1990. Electromagnetic induction in the Earth due to stationary and moving sources. PAGEOPH 134, 511–526.

Boteler, D.H., 1994. Geomagnetically induced currents: present knowledge and future research. IEEE Transactions in Power Delivery 9, 50–58.

Boteler, D.H. 2001. Space weather effects on power systems. In: Space Weather Geophysical Monograph Series, vol. 125. Washington, DC, USA: American Geophysical Union, Pp. 347 352.

Boteler, D.H., 2006. The super storms of August/September 1859 and their effects on the telegraph system. Adv. Space Res. 38, 159–172.

Boteler, D.H. 2007. Assessing pipeline vulnerability to telluric currents, Paper No 07686, Proc. CORROSION/2007, NACE, Houston, March 2007.

Boteler, D.H., 2013. A new versatile method for modelling geomagnetic induction in pipelines. Geophys. J. Int. 193, 98–109. https://doi.org/10.1093/gji/ggs113.

Boteler, D.H., 2014. Methodology for simulation of geomagnetically induced currents in power systems. J. Space Weather Space Climate 4, A21. https://doi.org/10.1051/swsc/2014018.

Boteler, D.H., 2019. A 21st century view of the March 1989 magnetic storm. Space Weather 17, 1427–1441. https://doi.org/10.1029/2019SW002278.

Boteler, D.H., 2021. Modeling geomagnetic interference on railway signaling track circuits. Space Weather 19, e2020SW002609. https://doi.org/10.1029/2020SW002609.

Brecht, S.H., Lyon, J.G., Fedder, J.A., Hain, K., 1982. A time dependent three dimensional simulation of the Earth's magnetosphere. J. Geophys. Res. 87 (A8), 6098–6108. https://doi.org/10.1029/JA087iA08p06098.

Brekke, A., Moen, J., 1993. Observations of high latitude ionospheric conductances. J. Atmos. Terr. Phys. 55 (11–12), 1493–1512. https://doi.org/10.1016/0021-9169(93)90126-J.

Brittnacher, M., Spann, J., Parks, G., Germany, G., 1997. Auroral observations by the Polar Ultraviolet Imager UVI. Adv. Space Res. 20, 1037–1042.

Burkholder, B.L., Nykyri, K., Ma, X., 2020. Use of the L1 constellation as a multispacecraft solar wind monitor. J. Geophys. Res., Space Physics 125. https://doi.org/10.1029/2020JA027978.

Buzulukova, N., 2018. Extreme Events in Geospace: Origins, Predictability, and Consequences. Elsevier. ISBN: 978-0-12-812700-1, Cambridge, MA, United States.

Béland, J., Small, K., 2004. Space weather effects on power transmission systems: The cases of Hydro-Quebec and Transpower New Zealand Ltd. In: Eaglis, I.A. (Ed.), Effects of Space Weather on Technology Infrastructure. Dordrecht, Netherlands, Kluwer Acad., pp. 287–299.

Cagniard, L., 1953. Basic theory of the magneto telluric method of geophysical prospecting. Geophysics 18, 605–635. https://doi.org/10.1190/1.1437915.

Cameron, T.G., Jackel, B., 2019. Using a numerical MHD model to improve solar wind time shifting. Space Weather 17, 662–671. https://doi.org/10.1029/2019SW002175.

Carabello, R., Sanchez Bettucci, L. and Tancredi, G. 2013. Geomagnetically induced currents in the Uruguayan high-voltage power grid, Geophys. J. Int., vol 195, issue 2, 844–853, Nov 2013, https://doi.org/10.1093/gji/ggt293.

Carabello, R., Gonzalez-Esparza, J.A., Sergeeva, M.A., Pacheco, C.R., 2020. First GIC estimates for the Mexican power grid. Space Weather 8. https://doi.org/10.1029/2019SW002260.

Carabello, R., 2016. Geomagnetically induced currents in Uruguay: 3055 Sensitivity to modelling parameters. Advance Sp. Res. 58 (10), 2067–2075.

Carter, B.A., Yizengaw, E., Pradipta, R., Weygand, J.M., Piersanti, M., Pulkkinen, A., Moldwin, M.B., Norman, R., Zhang, K., 2016. Geomagnetically induced currents around the world during the 17 March 2015 storm. J. Geophys. Res. Space Physics 121, 10496–10507. https://doi.org/10.1002/2016JA023344.

Case, N.A., MacDonald, E.A., Heavner, M., Tapia, A.H., Lalone, N., 2015a. Mapping auroral activity with Twitter. Geophys. Res. Lett. 42, 3668–3676. https://doi.org/10.1002/2015GL063709.

Case, N., et al., 2015b, Aurorasaurus and the St Patrick's Day storm, Astron. Geophys., 56 (3), 3.13-3.14. doi: 10.1093/astrogeo/atv089.

Case, N.A., Kingman, D., MacDonald, E.A., 2016a. A real-time hybrid aurora alert system: Combining citizen science reports with an auroral oval model. Earth Space Sci. 3, 257–265. https://doi.org/10.1002/2016EA000167.

Case, N., et al., 2016b. Determining the Accuracy of Crowdsourced Tweet Verification for Auroral Research, Citizen Sci.: Theory and Practice, 1 (2): 13, pp. 1-9, doi:10.5334/cstp.52.

Cash, M.D., Witters Hicks, S., Biesecker, D.A., Reinard, A.A., de Koning, C.A., Weimer, D.R., 2016. Validation of an operational product to determine L1 to Earth propagation time delays. Space Weather 14, 93–112. https://doi.org/10.1002/2015SW001321.

Chakraborty, S., Boteler, D.H., Shi, X., Murphy, B.S., Hartinger, M.D., Wang, X., Lucas, G., Baker, J.B.H., 2022. Modeling geomagnetic induction in submarine cables. Front. Phys. 10, 1022475. https://doi.org/10.3389/fphy.2022.1022475.

Chen, Y., Tóth, G., Cassak, P., Jia, X., Gombosi, T.I., Slavin, J.A., et al., 2017. Global three-dimensional simulation of Earth's Dayside reconnection using a two-way coupled magnetohydro-dynamics with embedded particle-in-cell model: Initial results. J. Geophys. Res. Space Physics 122 (10), 10318–10335.

Chen, M. W., Lemon, C. L., Hecht, J., Sazykin, S., Wolf, R. A., Boyd, A., & Valek, P. (2019). Diffuse auroral electron and ion precipitation effects on RCM-E comparisons with satellite data during the 17 March 2013 storm. *Journal of Geophysical Research: Space Physics*, *124*(6), 4194-4216, https://doi.org/10.1029/2019JA026545.

Chen, L.-J., Ng, J., Omelchenko, Y., Wang, S., 2021. Magnetopause reconnection and indents induced by foreshock turbulence. Geophys. Res. Lett. 48, e2021GL093029. https://doi.org/10.1029/2021GL093029.

Christensen, A.B. et al., 2003. Initial observations with the Global Ultraviolet Imager (GUVI) in the NASA TIMED satellite mission. J. Geophys. Res. 108 (A12), 1451. https://doi.org/10.1029/2003JA009918.

Ciardi, Lebedev, S.V., Frank, A., Blackman, E.G., Chittenden, J.P., Jennings, C.J., Ampleford, D.J., Bland, S.N., Bott, S.C., Rapley, J., Hall, G.N., Suzuki-Vidal, F.A., Marocchino, A., Lery, T., Stehle, C., 2007. The evolution of magnetic tower jets in the laboratory. Physics of Plasmas 14 (5), , 056501. https://doi.org/10.1063/1.2436479.

Cid, C., Placios, J., Siaz, E., Guerrero, A., Cerrato, Y., 2014. On extreme geomagnetic storms. Space Weather Space Climate 4, A28. https://doi.org/10.1051/swsc/2014026.

Cid, C., Guerrero, A., Saiz, E., Halford, A.J., Kellerman, A.C., 2020. Developing the LDi and LCi geomagnetic indices, an example of application of the AULs framework. Space Weather 18, e2019SW002171. https://doi.org/10.1029/2019SW002171.

Clausen, L.B.N., Ruohoniemi, J.M., Greenwald, R.A., Thomas, E.G., Shepherd, S.G., Talaat, E.R., Bristow, W.A., Zheng, Y., Coster, A.J., Sazykin, S., 2012. Large-scale observations of a subauroral polarization stream by midlatitude SuperDARN radars: instantaneous longitudinal velocity variations. J Geophys Res 117, A05306. https://doi.org/10.1029/2011JA017232.

Cliver, E.W., Svalgaard, L., 2004. The 1859 solar-terrestrial disturbance and the current limits of extreme space weather activity. Solar Phys. 224, 407–422.

Cliver, E.W., 2006. The 1859 space weather event: then and now. Adv. Space Res. 38, 119–129.

Codrescu, M.V., Fuller-Rowell, T.J., Foster, J.C., 1995. On the importance of E-field variability for Joule heating in the high-latitude thermosphere. Geophys. Res. Lett. 22, 2393–2396.

Cosgrove, R.B., Lu, G., Bahcivan, H., Matsuo, T., Heinselman, C.J., McCready, M.A., 2009. Comparison of AMIE-modeled and Sondrestrom-measured Joule heating: A study in model resolution and electric field-conductivity correlation. J. Geophys. Res. 114, A04316. https://doi.org/10.1029/2008JA013508.

Cosgrove, R.B. et al., 2014. Empirical model of Poynting flux derived from FAST data and a cusp signature. J. Geophys. Res 119, 411–430. https://doi.org/10.1002/2013JA019105.

Coumans, V., Gérard, J.-C., Hubert, B., Meurant, M., Mende, S.B., 2004. Global auroral conductance distribution due to electron and proton precipitation from IMAGE-FUV observations. Ann. Geophys. 22, 1595–1611. https://doi.org/10.5194/angeo-22-1595-2004.

Cousins, E.D.P., Matsuo, T., Richmond, A.D., 2015. Mapping high-latitude ionospheric electrodynamics with SuperDARN and AMPERE. J. Geophys. Res 120, 5854ā5870. https://doi.org/10.1002/2014JA020463.

J.C. Coxon, Milan, S.E., and Anderson, B.J. 2018. A review of Birkeland Current research using AMPERE. In: Keiling, A., Marghitu, O., Wheatland, M. (Eds.), Electric Currents in Geospace and Beyond. Pp. 259-278, doi:10.1002/9781119324522.ch16.

Cramer, W.D., Raeder, J., Toffoletto, F.R., Gilson, M., Hu, B., 2017. Plasma sheet injections into the inner magnetosphere: Two-way coupled OpenGGCM-RCM model results. J. Geophys. Res. Space Physics 122, 5077–5091. https://doi.org/10.1002/2017JA024104.

Crowley, G., Hackert, C.L., 2001. Quantification of high latitude electric field variability, Geophys. Res. Lett., 28. Iss. 14, 2783–2786. https://doi.org/10.1029/2000GL012624.

Da Silva Barbosa, C., Alves, L., Caraballo, R., Hartmann, G.A., Papa, A. R.R., Pirjola, R.J., 2015a. Analysis of geomagnetically induced currents at a low-latitude region over the solar cycles 23 and 24: comparison between measurements and calculations. J. Space Weather Space Clim. 5, A35. https://doi.org/10.1051/swsc/2015036.

Da Silva Barbosa, C., Hartmann, G.A., Pinheiro, K.J., 2015b. Numerical modeling of geomagnetically induced currents in a Brazilian transmission line. Adv. Space Res. 55, 1168–1179. https://doi.org/10.1016/j.asr.2014.11.008.

Dang, T., Zhang, B., Yan, M., Lyon, J., Yao, Z., Xiao, S. ... Lei, J., 2023. A New Tool for Understanding the Solar Wind–Venus Interaction: Three-dimensional Multifluid MHD Model. The Astrophysical Journal 945 (2), 91. https://doi.org/10.3847/1538-4357/acba88.

De Michelis, P., Consolini, G., Pignalberi, A., Tozzi, R., Coco, I., Giannattasio, F., Pezzopane, M., Balasis, G., 2021. Looking for a proxy of the ionospheric turbulence with Swarm data. Sci Rep. 11 (1), 6183. https://doi.org/10.1038/s41598-021-84985-1.

De Zeeuw, D.L., Sazykin, S., Wolf, R.A., Gombosi, T.I., Ridley, A.J., To´th, G., 2004. Coupling of a global MHD code and an inner magnetospheric model: Initial results. J. Geophys. Res. 109, A12219. https://doi.org/10.1029/2003JA010366.

Desai, R.T., Eastwood, J.P., Horne, R.B., Allison, H.J., Allanson, O., Watt, C.E.J., et al., 2021. Drift orbit bifurcations and cross-field transport in the outer radiation belt: Global MHD and integrated test-particle simulations. J. Geophys. Res. Space Physics 126, e2021JA029802. https://doi.org/10.1029/2021JA029802.

Dimmock, A.P., Rosenqvist, L., Hall, J.O., Viljanen, A., Yordanova, E., Honkonen, I., et al., 2019. The GIC and geomagnetic response over Fennoscandia to the 7–8 September 2017 geomagnetic storm. Space Weather 17, 989–1010. https://doi.org/10.1029/2018SW002132.

Dimmock, A.P., Welling, D.T., Rosenqvist, L., Forsyth, C., Freeman, M. P., Rae, I.J., et al., 2021. Modeling the geomagnetic response to the September 2017 space weather event over Fennoscandia using the space weather modeling framework: Studying the impacts of spatial resolution. Space Weather 19, e2020SW002683. https://doi.org/10.1029/2020SW002683.

Divett, T., Ingham, M., Beggan, C.D., Richardson, G.S., Rodger, C.J., Thomson, A.W.P., Dalzell, M., 2017. Modeling geoelectric fields and geomagnetically induced currents around New Zealand to explore GIC in the South Island's electrical transmission network. Space Weather 15, 1396–1412.

Divett, T., Richardson, G.S., Beggan, C.D., Rodger, C.J., Boteler, D.H., Ingham, M., Mac Manus, D.H., Thomson, A.W.P., Dalzell, M., 2018. Transformer-level modeling of geomagnetically induced currents in new Zealand's South Island. Space Weather 16 (6), 718–735. https://doi.org/10.1029/2018SW001814.

Dong, B., Danskin, D., Pirjola, R.J., Boteler, D.H., Wang, Z.Z., 2013. Evaluating the applicability of the finite element method for modelling of geoelectric fields. Annales Geophysique 31, 1689–1698. https://doi.org/10.5194/angeo-31-1689-2013.

Dong, C., Wang, L., Hakim, A., Bhattacharjee, A., Slavin, J.A., DiBraccio, G.A., Germaschewski, K., 2019. Global ten-moment multifluid simulations of the solar wind interaction with Mercury: From the planetary conducting core to the dynamic magnetosphere. Geophys. Res. Lett 46, 11584–11596. https://doi.org/10.1029/2019GL083180.

Dungey, J.W., 1961. Interplanetary Magnetic Field and the Aurora1 Zones. Phys. Rev. LEtt. 6, 47–48. https://doi.org/10.1103/PhysRevLett.6.47.

Eastwood, J.P., Biffis, E., Hapgood, M.A., Green, L., Bisi, M.M., Bentley, R.D., Wicks, R., McKinnell, L.-.-A., Gibbs, M., Burnett, C., 2017. The economic impact of space weather: where do we stand? Risk Anal. 37, 206–218. https://doi.org/10.1111/risa.12765.

Ebihara, Y., Nishitani, N., Kikuchi, T., Ogawa, T., Hosokawa, K., Fok, M., 2008. Twodimensional observations of overshielding during a magnetic storm by the Super Dual Auroral Radar Network (SuperDARN) Hokkaido radar. J Geophys Res 113, A01213. https://doi.org/10.1029/2007JA012641.

Echer, E., Gonzalez, W.D., Tsurutani, B.T., 2008. Interplanetary conditions leading to superintense geomagnetic storms (Dst ≤ -250 nT) during solar cycle 23. Geophys. Res. Lett. 35, L06S03. https://doi.org/10.1029/2007GL031755.

Egbert, G.D., 1992. Noncausality of the discrete-time magnetotelluric impulse response. Geophysics 57, 1354–1358. https://doi.org/10.1190/1.1443204.

Eggington, J.W.B., Eastwood, J.P., Mejnertsen, L., Desai, R.R., Chittenden, J.P., 2020. Dipole tilt effect on magnetopause reconnection and the steady-state magnetosphere-ionosphere system: Global MHD simulations. J. Geophys. Res. Space Physics 125, e2019JA027510. https://doi.org/10.1029/2019JA027510.

Eggington, J.W.B., Coxon, J.C., Shore, R.M., Desai, R.T., Mejnertsen, L., Chittenden, J.P., Eastwood, J.P., 2022. Response timescales of the magnetotail current sheet during a geomagnetic storm: Global MHD simulations. Frontiers Astronomy Space Sci. 9. https://doi.org/10.3389/fspas.2022.966164.

El-Alaoui, M., Ashour-Abdalla, M., Walker, R.J., Peroomian, V., Richard, R.L., Angelopoulos, V., Runov, A., 2009. Substorm evolution as revealed by THEMIS satellites and a global MHD simulation. J. Geophys. Res. 114, A08221. https://doi.org/10.1029/2009JA014133.

El-Alaoui, M., Richard, R.L., Ashour-Abdalla, M., Goldstein, M.L., Walker, R.J., 2013. Dipolarization and turbulence in the plasma sheet during a substorm: THEMIS observations and global MHD simulations. J. Geophys. Res.: Space Physics 118, 7752–7761. https://doi.org/10.1002/2013JA019322.

El-Alaoui, M., Walker, R.J., McPherron, R.L., 2023. Effects of the ionospheric conductance on the dynamics of the magnetotail. J. Geophys. Res.: Space Physics 128, e2022JA030259. https://doi.org/10.1029/2022JA030259.

El-Alaoui, M. 2001. Current disruption during November 24, 1996, substorm. J. Geophys. Res. 106(A4), 6229–6245. https://doi.org/10.1029/1999JA000260.

Engebretson, M.J., Pilipenko, V.A., Ahmed, L.Y., Posch, J.L., Steinmetz, E.S., Moldwin, M.B., et al., 2019a. Nighttime magnetic perturbation events observed in Arctic Canada: 1. Survey and statistical analysis. J. Geophys. Res.: Space Physics 124, 7442–7458. https://doi.org/10.1029/2019JA026794.

Engebretson, M.J., Steinmetz, E.S., Posch, J.L., Pilipenko, V.A., Moldwin, M.B., Connors, M.G., et al., 2019b. Nighttime magnetic perturbation events observed in Arctic Canada: 2. Multiple-instrument observations. J. Geophys. Res.: Space Physics 124, 7459–7476. https://doi.org/10.1029/2019JA026797.

Engebretson, M.J., Ahmed, L.Y., Pilipenko, V.A., Steinmetz, E.S., Moldwin, M.B., Connors, M.G., et al., 2021. Superposed epoch analysis of nighttime magnetic perturbation events observed in Arctic Canada. Journal of Geophysical Research: Space Physics 126, e2021JA029465. https://doi.org/10.1029/2021JA029465.

Engebretson, M.J., Yang, L., Steinmetz, E.S., Pilipenko, V.A., Moldwin, M.B., McCuen, B.A., et al., 2024. Extreme geomagnetic disturbances (GMDs) observed in Eastern Arctic Canada: Occurrence characteristics and solar cycle dependence. Journal of Geophysical Research: Space Physics 129, e2023JA031643. https://doi.org/10.1029/2023JA031643.

Eroshenko, E.A., Belov, A.V., Boteler, D., Gaidash, S.P., Lobkov, S.L., Pirjola, R., Trichtchenko, L., 2010. Effects of strong geomagnetic storms on Northern railways in Russia. Adv. Space Res. 46, 1102–1110. https://doi.org/10.1016/j.asr.2010.05.017.

Evans, C.R., Hawley, J.F., 1988. Simulation of magnetohydrodynamic flows - a constrained transport method. Astrophys. J. 332, 659–677. https://doi.org/10.1086/166684.

Evans, D.S. 1987. Global statistical patterns of auroral phenomena," Proceedings of the Symposium on Quantitative Modeling of Magnetospheric - Ionospheric Coupling Processes, p. 325, Kyoto.

Fang, X., Randall, C., Lummerzheim, D., Solomon, S., Mills, M., Marsh, D., Jackman, C., Wang, W., Lu, G., 2008. Electron impact ionization: A new parameterization for 100 eV to 1 MeV electrons. J. Geophys. Res 113, A09311. https://doi.org/10.1029/2008JA013384.

Fang, X., Randall, C., Lummerzheim, D., Wang, W., Lu, G., Solomon, S., Frahm, R., 2010. Parameterization of monoenergetic electron impact ionization. Geophys. Res. Lett. 37, L22106. https://doi.org/10.1029/2010GL045406.

Fang, X., Lummerzheim, D., Jackman, C., 2013. Proton impact ionization and a fast calculation method. J. Geophys. Res. 118, 53695378. https://doi.org/10.1002/jgra.50484.

Fedder, J.A., Slinker, S.P., Lyon, J.G., Elphinstone, R.D., 1995. Global numerical simulation of the growth phase and the expansion onset for substorm observed by Viking. J. Geophys. Res. 100, 19083–19093.

Fernberg, P.A., Samson, C., Boteler, D.H., Trichtchenko, L., Larocca, P., 2007a. Earth conductivity structures and their effects on geomagnetic induction in pipelines. Ann. Geophys. 25 (1), 207–218.

Fernberg, P.A., Trichtchenko, L., Boteler, D.H., McKee, L. 2007b. Telluric hazard assessment for northern pipelines, Paper No 07654, Proc. CORROSION/2007, NACE, Houston, March 2007.

Finlay, C.C., Olsen, N., Kotsiaros, S. et al., 2016. Recent geomagnetic secular variation from Swarm and ground observatories as estimated in the CHAOS-6 geomagnetic field model. Earth Planet Sp 68, 112. doi: 10.1186/s40623-016-0486-1.

Fiori, R.A.D., Boteler, D.H., Gillies, D.M., 2014. Assessment of GIC risk due to geomagnetic sudden commencements and identification of the current systems responsible. Space Weather 12, 76–91. https://doi.org/10.1002/2013SW000967.

Foster, J.C., Holt, J.M., Musgrove, R.G., Evans, D.S., 1986a. Ionospheric convection associated with discrete levels of particle precipitation. Geophys, Res. Lett. 13, 656–659. https://doi.org/10.1029/GL013i007p00656.

Foster, J.C., Holt, J.M., Musgrove, R.G., Evans, D.S., 1986b. In: Solar Wind Dependencies of High-Latitude Convection and Precipitation, Solar Wind-Magnetosphere Coupling. Terra Scientific Publishing Company, Tokyo, pp. 447–494.

Frank, L.A., Ashour-Abdalla, M., Berchem, J., Raeder, J., Paterson, W. R., Kokubun, S., Yamamoto, T., Lepping, R.P., Coroniti, F.V., Fairfield, D.H., Ackerson, K.L., 1995. Observations of plasmas and magnetic field in Earth's distant magnetotail: Comparison with a global MHD model. J. Geophys. Res. 100, 19177–19190. https://doi.org/10.1029/95JA00571.

Freeman, M.P., Forsyth, C., Rae, I.J., 2019. The influence of substorms on extreme rates of change of the surface horizontal magnetic field in the United Kingdom. Space Weather 17, 827–844. https://doi.org/10.1029/2018SW002148.

Frey, H.U., Mende, S.B., Angelopoulos, V., Donovan, E.F., 2004. Substorm onset observations by IMAGE-FUV. J. Geophys. Res.: Space. Physics 109 (A10). https://doi.org/10.1029/2004JA010607.

Fukushima, N., 1976. Generalized theorem for no ground magnetic effect of vertical currents connected with Pedersen currents in the uniform-conductivity ionosphere. Rep. Ionos. Space Res Japan 30, 35–50.

Fuller-Rowell, T.J., Evans, D.S., 1987. Height-integrated Pedersen and Hall conductivity patterns from the TIROS-NOAA satellite data. J. Geophys. Res. 92, 7606–7618. https://doi.org/10.1029/JA092iA07p07606.

Fuller-Rowell, T.J., D. Rees, S. Quegan, R.J. Moffett, M.V. Codrescu, G. H. Millward (1996), A coupled thermosphere-ionosphere model (CTIM). In: STEP Report, Schunk, R.W. (Ed.), (Scientific Committee on Solar Terrestrial Physics (SCOSTEP), NOAA/NGDC, Boulder, 1996, p. 217.

Gallardo-Lacourt, B., Nishimura, Y., Donovan, E., Gillies, D.M., Perry, G.W., Archer, W.E., et al., 2018. A statistical analysis of STEVE. J. Geophys. Res.: Space Phys. 123, 9893–9905. https://doi.org/10.1029/2018JA025368.

Garcia-Sage, K., T. E. Moore, A. Pembroke, V. G. Merkin, and W. J. Hughes (2015), Modeling the effects of ionospheric oxygen outflow on bursty magnetotail flows, *J. Geophys. Res. Space Physics*, 120, 8723–8737, doi:10.1002/2015JA021228.

Gaunt, C.T. and Coetzee, G. 2007. Transformer failures in regions incorrectly considered to have low GIC-risk, in Proc. IEEE Lausanne Power Tech, Jul. 2007, pp. 807-812, doi: 10.1109/PCT.2007.4538419.

Germany, G.A., Torr, D.G., Richards, P.G., Torr, M.R., John, S., 1994. Determination of ionospheric conductivities from FUV auroral emissions. J. Geophys. Res. 99 (A12), 23297–23305. https://doi.org/10.1029/94JA02038.

Gilbert, J.L., 2005. Modeling the effect of the ocean-land interface on induced electric fields during geomagnetic storms. Space Weather 3, S04A03. https://doi.org/10.1029/2004SW000120.

Gilbert, J.L., 2015. Simplified techniques for treating the ocean–land interface for geomagnetically induced electric fields. IEEE Trans Electromagn Compat 57 (4), 688–692. https://doi.org/10.1109/TEMC.2015.2453196.

Gjerloev, J.W., Hoffman, R.A., Ohtani, S., Weygand, J., Barnes, R., 2010. Response of the auroral electrojet indices to abrupt southward IMF turnings. Ann. Geophys. 28, 1167–1182. https://doi.org/10.5194/angeo-28-1167-2010.

Gjerloev, J.W., Ohtani, S., Iijima, T., Anderson, B., Slavin, J., Le, G., 2011. Characteristics of the terrestrial field-aligned current system. Ann. Geophys. 29, 1713–1729. https://doi.org/10.5194/angeo-29-1713-2011.

Gjerloev, J.W., Waters, C.L., Barnes, R.J., 2018. Deriving global convection maps from SuperDARN measurements. J. Geophys. Res.: Space Physics 123, 2902–2915. https://doi.org/10.1002/2017JA024543.

Gjerloev, J.W., 2009. A global ground-based magnetometer initiative. Eos Trans. AGU 90 (27), 230–231. https://doi.org/10.1029/2009EO270002.

Glocer, A., Tóth, G., Gombosi, T., Welling, D., 2009. Modeling ionospheric outflows and their impact on the magnetosphere, initial results. J. Geophys. Res. 114, A05216. https://doi.org/10.1029/2009JA014053.

Glocer, A., Fok, M., Meng, X., Toth, G., Buzulukova, N., Chen, S., Lin, K., 2013. CRCM + BATS-R-US two-way coupling. J. Geophys. Res. Space Physics 118, 1635–1650. https://doi.org/10.1002/jgra.50221.

Glocer, A., Toth, G., Fok, M.-C., 2018. Including kinetic ion effects in the coupled global ionospheric outflow solution. J. Geophys. Res.: Space Physics 123, 2851–2871. https://doi.org/10.1002/2018JA025241.

Glocer, A., Welling, D., Chappell, C.R., Toth, G., Fok, M.-C., Komar, C., et al., 2020. A case study on the origin of near-Earth plasma. J. Geophys. Res.: Space Physics 125, e2020JA028205. https://doi.org/10.1029/2020JA028205.

Gombosi, T.I., Tóth, G., De Zeeuw, D.L., Hansen, K.C., Kabin, K., Powell, K.G., 2002. Semi-relativistic magnetohydrodynamics and physics-based convergence acceleration. J. Comput. Phys. 177, 176–205. https://doi.org/10.1006/jcph.2002.7009.

Gombosi, T. I., D. L. De Zeeuw, K. G. Powell, A. J. Ridley, I. V. Sokolov, Q. F. Stout, and G. Toth, 2003. Adaptive Mesh Refinement for Global Magnetohydrodynamic Simulation edited by J. Buchner, C.T. Dum, M. Scholer (Eds.): LNP 615, pp. 247–274, 2003. Springer-Verlag Berlin Heidelberg 2003.

Gopalswamy, N., Yashiro, S., Akiyama, S., 2007. Geoeffectiveness of halo coronal mass ejections. J. Geophys. Res. 112, A06112. https://doi.org/10.1029/2006JA012149.

Gordeev, E., Sergeev, V., Tsyganenko, N., Kuznetsova, M., Rastäetter, L., Raeder, J., Tóth, G., Lyon, J., Merkin, V., Wiltberger, M., 2017. The substorm cycle as reproduced by global MHD models. Space Weather 15, 131–149. https://doi.org/10.1002/2016SW001495.

Goto, T., 2015. Numerical studies of geomagnetically induced electric field on seafloor and near coastal zones incorporated with heterogeneous conductivity distributions. Earth, Planets and Space 67, 193. https://doi.org/10.1186/s40623-015-0356-2.

Greenwald, R.A., Baker, K.B., Dudeney, J.R., et al., 1995. DARN/SuperDARN. Space Sci Rev 71, 761–796. https://doi.org/10.1007/BF00751350.

Grocott, A., Milan, S.E., Baker, J.B.H., Freeman, M.P., Lester, M., Yeoman, T.K., 2011. Dynamic subauroral ionospheric electric fields observed by the Falkland Islands radar during the course of a geomagnetic storm. J Geophys Res 116 (A1), 1202. https://doi.org/10.1029/2011JA016763.

Gronoff, G., Arras, P., Baraka, S., Bell, J.M., Cessateur, G., Cohen, O., et al., 2020. Atmospheric escape processes and planetary atmospheric evolution. J. Geophys. Res.: Space Physics 125, e2019JA027639. https://doi.org/10.1029/2019JA027639.

Grubbs II, G., Michell, R., Samara, M., Hampton, D., Jahn, J.-M., 2018. Predicting electron population characteristics in 2-D using multispectral ground-based imaging. Geophys. Res. Lett. 45 (1), 15–20. https://doi.org/10.1002/2017GL075873.

Hapgood, M., 2019. The great storm of May 1921: an exemplar of a dangerous space weather event. Space Weather 17 (7), 950–975. https://doi.org/10.1029/2019SW002195.

Hardy, D.A., Gussenhoven, M.S., Holeman, E., 1985. A statistical model of auroral electron precipitation. J. Geophys. Res. 90, 4229–4248. https://doi.org/10.1029/JA090iA05p04229.

Hardy, D.A., Gussenhoven, M.S., Brautigam, D., 1989. A statistical model of auroral ion precipitation. J. Geophys. Res. 94 (A1), 370–392. https://doi.org/10.1029/JA094iA01p00370.

Hasegawa, H., Nakamura, T.K.M., Gershman, D.J., Nariyuki, Y., Viñas, A.F., Giles, B.L., et al., 2020. Generation of turbulence in Kelvin-Helmholtz vortices at the Earth's magnetopause: Magnetospheric Multiscale observations. J. Geophys. Res.: Space Phys. 125, e2019JA027595. https://doi.org/10.1029/2019JA027595.

Hayakawa, H., Ebihara, Y., Pevtsov, A.A., Bhaskar, A., Karachik, N., Oliveira, D.M., 2020. Intensity and time series of extreme solar-terrestrial storm in 1946 March. Month. Not. Roy. Astr. Soc. 497 (4), 5507–5517. https://doi.org/10.1093/mnras/staa1508.

Hayakawa, H., Hattori, K., Pevtsov, A.A., Ebihara, Y., Shea, M.A., McCracken, K.G., Daglis, I.A., Bhaskar, A.T., Ribeiro, P., Knipp, D. J., 2021. The intensity and evolution of the extreme solar and geomagnetic storms in 1938 January. Astrophysical J. 909, 197. https://doi.org/10.3847/1538-4357/abc427.

Hayakawa, H., Oliveira, D.M., Shea, M.A., Smart, D.F., Blake, S.P., Hattori, K., Bhaskar, A.T., Curto, J.J., Franco, D.R., Ebihara, Y., 2022. The extreme solar and geomagnetic storms on 1940 March 20–25. Mon. Not. Roy. Astr. Soc. 517, 1709–1723. https://doi.org/10.1093/mnras/stab3615.

Heyns, M.J., Lotz, S.I., Gaunt, C.T., 2021. 'Geomagnetic pulsations driving geomagnetically induced currents. Space Weather 19 (2). https://doi.org/10.1029/2020sw002557.

Holt, J.M., Evans, J.V., Oliver, W.L., Wand, R.H., 1984. In: Millstone Hill Observations of Ionospheric Convection, Physics of Space Plasmas. Scientific Publishers Inc, Cambridge, Mass, pp. 53–72.

Holt, J.M., Wand, R.H., Evans, J.V., Oliver, W.L., 1987. Empirical models for the plasma convection at high latitudes from Millstone Hill observations. J. Geophys. Res. 92 (A1), 203–212. https://doi.org/10.1029/JA092iA01p00203.

Honkonen, I., Rastätter, L., Grocott, A., Pulkkinen, A., Palmroth, M., Raeder, J., Ridley, A.J., Wiltberger, M., 2013. On the performance of global magnetohydrodynamic models in the Earth's magnetosphere. Space WeatherVolume 11 (5), 313–326. https://doi.org/10.1002/swe.20055.

Honkonen, I., van de Kamp, M., Hoppe, T., Kauristie, K., 2022. Over 20-year global magnetohydrodynamic simulation of Earth's magnetosphere. Space Weather 20, e2022SW003196. https://doi.org/10.1029/2022SW003196.

Huang, Y., Richmond, A.D., Deng, Y., Roble, R., 2012. Height distribution of Joule heating and its influence on the thermosphere. J. Geophys. Res. 117, A08334. https://doi.org/10.1029/2012JA017885.

Huba, J.D., Krall, J., 2013a. Modeling the plasmasphere with SAMI3. Geophys. Res. Lett. 40. https://doi.org/10.1029/2012GL054300.

Huba, J.D., Krall, J., 2013b. Impact of Meridional Winds on Equatorial Spread F: Revisited. Geophys. Res. Lett. 40. https://doi.org/10.1002/grl.50292.

Huttunen, K.E.J., Bale, S.D., Salem, C., 2008. Wind observations of low energy particles within a solar wind reconnection region. Ann. Geophys. 26, 2701–2710. https://doi.org/10.5194/angeo-26-2701-2008.

Ilie, R., Liemohn, M.W., Toth, G., Skoug, R.M., 2012. Kinetic model of the inner magnetosphere with arbitrary magnetic field. J. Geophys. Res. 117, A04208. https://doi.org/10.1029/2011JA017189.

Ilie, R., Liemohn, M. and Toth, G. 2014. Two-way self-consistent simulation of the inner magnetosphere driven by realistic electric and magnetic fields, EGU General Assembly Abstracts, 2014.

Ingham, M., Rodger, C.J., 2018. Telluric field variations as drivers of variations in cathodic protection on a natural gas pipeline in New Zealand. Space Weather 16, 1396–1409. https://doi.org/10.1029/2018SW001985.

Ingham, M., Divett, T., Rodger, C.J., Sigley, M., 2022. Impacts of GIC on the New Zealand gas pipeline network. Space Weather 20, e2022SW003298. https://doi.org/10.1029/2022SW003298.

Jackson, B.V., Yu, H.-S., Buffington, A., Hick, P.P., Tokumaru, M., Fujiki, K., Kim, J., Yun, J., 2019. A daily determination of Bz using the Russell-McPherron effect to forecast geomagnetic activity. Space Weather 17 (4), 639–652. https://doi.org/10.1029/2018SW002098.

Janhunen, P., Huuskonen, A., 1993. A numerical ionosphere-magnetosphere coupling model with variable conductivities. J. Geophys. Res. 98 (A6), 9519–9530. https://doi.org/10.1029/92JA02973.

Janhunen, P. 1996. GUMICS-3 – a global ionosphere–magnetosphere coupling simulation with high ionospheric resolution. In: Burke, W., Guyenne, T.-D. (Eds.), Environment Modelling for Space-based Applications, Symposium Proceedings (ESA SP-392). ESTEC, Noordwijk, pp. 233. (18–20 September).

Janhunen, P., Palmroth, M., Laitinen, T., Honkonen, I., Juusola, L., Facsko, G., Pulkkinen, T.I., 2012. The GUMICS-4 global MHD magnetosphere–ionosphere coupling simulation, J. Atmos. and Sol.-Terr. Phys. 80, 48–59. https://doi.org/10.1016/j.jastp.2012.03.006.

Jankee, P., Oyedokun, D., Moltanian, M., Chisepo, H.K. and Heyn, M. 2022. Geomagnetically Induced Currents: Frequency Spectra and Threats to Voltage Stability, IEEE Access, June 2022. doi: 10.1109/ACCESS.2022.3182237.

Jin, Y., Spicher, A., Xiong, C., Clausen, L.B.N., Kervalishvili, G., Stolle, C., Miloch, W.J., 2019. Ionospheric plasma irregularities characterized by the Swarm satellites: Statistics at high latitudes. J. Geophys. Res. Space Phys. 124, 1262–1282. https://doi.org/10.1029/2018JA026063.

Jordanova, V.K., Yu, Y., Niehof, J.T., Skoug, R.M., Reeves, G.D., Kletzing, C.A., Fennell, J.F., Spence, H.E., 2014. Simulations of inner magnetosphere dynamics with an expanded RAM-SCB model and comparisons with Van Allen Probes observations. Geophys. Res. Lett. 41, 2687–2694. https://doi.org/10.1002/2014GL059533.

Jyothi, S.A., 2021. Solar superstorms: planning for an internet apocalypse. In: Proceedings of the 2021 ACM SIGCOMM Conference. August 2021, pp. 692–704. https://doi.org/10.1145/3452296.3472916.

Kaeppler, S.R., Hampton, D.L., Nicolls, M.J., Stromme, A., Solomon, S. C., Hecht, J.H., Conde, M.G., 2015. An investigation comparing ground-based techniques that quantify auroral electron flux and conductance. J. Geophys. Res 120, 9038ă9056. https://doi.org/10.1002/2015JA021396.

Kay, C., Gopalswamy, N., 2017. Using the coronal evolution to successfully forward model CMEs' in situ magnetic profiles. J. Geophys. Res.: Space Physics 122 (12), 11–810. https://doi.org/10.1002/2017JA024541.

Keiling, A., Ramos, C., Vu, N., Angelopoulos, V., Nosé, M., 2022. Statistical properties and proposed source mechanism of recurrent substorm activity with one-hour periodicity. J. Geophys. Res.: Space Physics 127, e2021JA030064. https://doi.org/10.1029/2021JA030064.

Kelbert, A., Balch, C.C., Pulkkinen, A., Egbert, G.D., Love, J.J., Rigler, E.J., Fujii, I., 2017. Methodology for time-domain estimation of storm time geoelectric fields using the 3-D magnetotelluric response tensors. Space Weather 15, 874–894. https://doi.org/10.1002/2017SW001594.

Kelbert, A., 2020. The role of global/regional earth conductivity models in natural geomagnetic hazard mitigation. Surv. Geophys. 41 (1), 115–166. https://doi.org/10.1007/s10712-019-09579-z.

Kelly, G.S., Viljanen, A., Beggan, C., Thomson, A.W.P., 2017. Understanding GIC in the UK and French high-voltage transmission systems during severe magnetic storms. Space Weather 15, 99–114. https://doi.org/10.1002/2016SW001469.

Kepko, L., McPherron, R.L., Amm, O., et al., 2015. Substorm current wedge revisited. Space Sci. Rev. 190, 1–46. https://doi.org/10.1007/s11214-014-0124-9.

Kikuchi, T., Ebihara, Y., Hashimoto, K.K., Kataoka, R., Hori, T., Watari, S., Nishitani, N., 2010. Penetration of the convection and overshielding electric fields to the equatorial ionosphere during a quasiperiodic DP 2 geomagnetic fluctuation event. J Geophys Res 115, A05209. https://doi.org/10.1029/2008JA013948.

Klauber, C., Shetye, K., Overbye, T.J. and Davis, K. 2020. A GIC estimator for electric grid monitoring during geomagnetic disturbances. In: IEEE Transactions on Power Systems, vol. 35, no. 6, pp. 4847-4855, doi: 10.1109/TPWRS.2020.3000746.

Knight, S., 1973. Parallel electric fields. Planet. Space Sci. 21, 741. https://doi.org/10.1016/0032-0633(73)90093-7.

Korth, H., Zhang, Y., Anderson, B.J., Sotirelis, T., Waters, C.L., 2014. Statistical relationship between large-scale upward field-aligned currents and electron precipitation. J. Geophys. Res. Space Physics 119, 6715–6731. https://doi.org/10.1002/2014JA019961.

Kosar, B.C., MacDonald, E.A., Case, N.A., Zhang, Y., Mitchell, E.J., Viereck, R., 2018a. A case study comparing citizen science aurora data with global auroral boundaries derived from satellite imagery and empirical models. J. Atmos. and Sol.-Terr Phys. 177, 274–282. https://doi.org/10.1016/j.jastp.2018.05.006, ISSN 1364-6826.

Kosar, B.C., MacDonald, E.A., Case, N.A., Heavner, M., 2018b. Aurorasaurus database of real-time, crowd-sourced aurora data for space weather research. Earth Space Sci. 5, 970–980. https://doi.org/10.1029/2018EA000454.

Kosch, M.J., Hagfors, T., Schlegel, K., 1998. Extrapolating EISCAT Pedersen conductances to other parts of the sky using ground- based TV auroral images. Ann. Geophys. 16, 583–588 http://www.ann-geophys.net/16/583/1998/.

Krausmann, E., Andersson, E., Russell, T., and Murtagh, W. 2015. Space Weather and Rail: Findings and Outlook, JRC Science and Policy Reports, JRC98155, 22 pp, 2015. doi:10.2788/211456.

Kunduri, B.S.R., Baker, J.B.H., Ruohoniemi, J.M., Thomas, E.G., Shepherd, S.G., Sterne, K.T., 2017. Statistical characterization of the large-scale structure of the subauroral polarization stream. J. Geophys. Res. Space Phys. 122, 6035–6048. https://doi.org/10.1002/2017JA024131.

Kuznetsova, M.M., Hesse, M., Rastätter, L., Taktakishvili, A., Tóth, G., De Zeeuw, D.L., Ridley, A., Gombosi, T.I., 2007. Multiscale modeling of magnetospheric reconnection. J. Geophys. Res. 112, A10210. https://doi.org/10.1029/2007JA012316.

Lam, M.M., Freeman, M.P., Jackman, C.M., Rae, I.J., Kalmoni, N.M.E., Sandhu, J.K., Forsyth, C., 2019. How well can we estimate Pedersen conductance from the THEMIS white-light all-sky cameras? J. Geophys. Res.: Space Phys 124, 2920–2934. https://doi.org/10.1029/2018JA026067.

Lane, C., Acebal, A., Zheng, Y., 2015. Assessing predictive ability of three auroral precipitation models using DMSP energy flux. Space Weather 13, 61ã71. https://doi.org/10.1002/2014SW001085.

Laundal, K.M., Reistad, J.P., Hatch, S.M., Madelaire, M., Walker, S., Hovland, A.Ø., et al., 2022. Local mapping of polar ionospheric electrodynamics. Journal of Geophysical Research: Space Physics 127, e2022JA030356. https://doi.org/10.1029/2022JA030356.

Lehtinen, M., Pirjola, R., 1985. Currents produced in earthed conductor networks by geomagnetically-induced electric fields. Ann. Geophys. 3, 479–484.

Lejdström, B. and Svensson, S. (1956/2020), Calculation of geomagnetic interference voltages in track circuits, original publication (in Swedish) Appendix 6, Betänkande: angående det tekniska utförandet av signalanläggningar vid Statens Järnvägar, 1956. Translation (in English), Infrastructure Resilience Risk Reporter, 1(10), 28-51, https://carleton.ca/irrg/journal/.

Lester, M., 2003. Ionospheric convection and its relevance for space weather. Adv. Space Res. 31 (4), 941–950. https://doi.org/10.1016/SO273- I 177(02)00790- 1.

Lin Y., Duan, X., Zhao, C., Xu, L. 2013. Systems science methodological approaches, Sect. 7.2.2. CRC Press, Boca Raton.

Lin, Y., Wang, X.Y., Lu, S., Perez, J.D., Lu, Q., 2014. Investigation of storm time magnetotail and ion injection using three-dimensional global hybrid simulation. J. Geophys. Res. Space Physics 119, 7413–7432. https://doi.org/10.1002/2014JA020005.

Lin, M.-Y., Ilie, R., Glocer, A., 2020. The contribution of N+ ions to Earth's polar wind. Geophysical Research Letters 47, e2020GL089321. https://doi.org/10.1029/2020GL089321.

Lin, D., Sorathia, K., Wang, W., Merkin, V., Bao, S., Pham, K., et al., 2021. The role of diffuse electron precipitation in the formation of subauroral polarization streams. J. Geophys. Res.: Space Phys. 126, e2021JA029792. https://doi.org/10.1029/2021JA029792.

Lin, D., Wang, W., Merkin, V.G., Huang, C., Oppenheim, M., Sorathia, K., et al., 2022. Origin of dawnside subauroral polarization streams during major geomagnetic storms. AGU Advances 3, e2022AV000708. https://doi.org/10.1029/2022AV000708.

Lin, M.-Y, Ilie, R., and Glocer, A. (2022) How are the N+ions affecting the transport and acceleration of ionospheric outflowing ions, Authorea, January 27, 2020, https://doi.org/10.1002/essoar.10502057.1.

Liu, C., Li, Y., Pirjola, R., 2014. Observations and modeling of GIC in the Chinese large-scale high-voltage power networks. J. Space Weather Space Clim. 4, A03. https://doi.org/10.1051/swsc/2013057.

Liu, J., Angelopoulos, V., Chu, X., Zhou, X.-Z., Yue, C., 2015. Substorm current wedge composition by wedgelets. Geophys. Res. Lett. 42, 1669–1676. https://doi.org/10.1002/2015GL063289.

Liu, H.-L., Bardeen, C.G., Foster, B.T., Lauritzen, P., Liu, J., Lu, G., Wang, W., 2018. Development and validation of the Whole Atmosphere Community Climate Model with thermosphere and ionosphere extension (WACCM-X 2.0). J. Adv. Model. Earth Syst. 10, 381–402. https://doi.org/10.1002/2017MS001232.

Liu, C., Wang, X., Wang, H., Zhao, H., 2018. Quantitative influence of coast effect on geomagnetically induced currents in power grids: a case study. J. Space Weather Space Clim. 8, A60. https://doi.org/10.1051/swsc/2018046.

Longden, N., Chisham, G., Freeman, M.P., Abel, G.A., Sotirelis, T., 2010. Estimating the location of the open-closed magnetic field line boundary from auroral images. Ann. Geophys. 28, 1659–1678. https://doi.org/10.5194/angeo-28-1659-2010.

Loto'aniu, P.T.M., Romich, K., Rowland, W., Codrescu, S., Biesecker, D., Johnson, J., et al., 2022. Validation of the DSCOVR spacecraft mission space weather solar wind products. Space Weather 20, e2022SW003085. https://doi.org/10.1029/2022SW003085.

Love, J.J., Hayakawa, H., Cliver, E.W., 2019a. On the intensity of the magnetic superstorm of September 1909. Space Weather 17, 37–45. https://doi.org/10.1029/2018SW002079.

Love, J.J., Hayakawa, H., Cliver, E.W., 2019b. Intensity and impact of the New York Railroad superstorm of May 1921. Space Weather 17, 1281–1292. https://doi.org/10.1029/2019SW002250.

Love, J.J., Lucas, G.M., Bedrosian, P.A., Kelbert, A., 2019c. Extreme-value geoelectric amplitude and polarization across the northeast United States. Space Weather 17 (3), 379–395. https://doi.org/10.1029/2018SW002068.

Love, J.J., 2018. The electric storm of November 1882. Space Weather 16, 37–46. https://doi.org/10.1002/2017SW001795.

Love, J.J., 2021. Extreme-event magnetic storm probabilities derived from rank statistics of historical Dst intensities for solar cycles 14–24. Space Weather 19, e2020SW002579. https://doi.org/10.1029/2020SW002579.

Luan, X., Wang, W., Burns, A., Solomon, S., Zhang, Y., Paxton, L.J., 2010. Seasonal and hemispheric variations of the total auroral precipitation energy flux from TIMED/GUVI. J. Geophys. Res. 115, A11304. https://doi.org/10.1029/2009JA015063.

Luan, X., Wang, W., Burns, A., Solomon, S., Zhang, Y., Paxton, L.J., Xu, J., 2011. Longitudinal variations of nighttime electron auroral precipitation in both the Northern and Southern Hemispheres from the TIMED global ultraviolet imager. J. Geophys. Res. 116, A03302. https://doi.org/10.1029/2010JA016051.

Lummerzheim, D., Rees, M.H., Craven, J., Frank, L.A., 1991. Ionospheric conductances derived for DE-1 auroral images. J. Atmos. and Terr. Phys. 53, 281–292. https://doi.org/10.1016/0021-9169(91)90112-K.

Lyon, J.G., Brecht, S.H., Huba, J.D., Fedder, J.A., Palmadesso, P.J., 1981. Computer simulation of a geomagnetic substorm. Phys. Rev. Lett. 46, 1038. https://doi.org/10.1103/PhysRevLett.46.1038.

Lyon, J.G., Fedder, J.A., Mobarry, C.M., 2004. The Lyon–Fedder–Mobarry (LFM) global MHD magnetospheric simulation code. J. of Atmos. Sol.-Terr Phys. 66, 1333–1350.

MacDonald, E.A., Case, N.A., Clayton, J.H., Hall, M.K., Heavner, M., Lalone, N., Patel, K.G., Tapia, A., 2015. Aurorasaurus: A citizen science platform for viewing and reporting the aurora. Space Weather 13, 548–559. https://doi.org/10.1002/2015SW001214.

Mannucci, A.J., Verkhoglyadova, O.P., Meng, X., McGranaghan, R., 2018. The role of neutral flow in field-aligned currents. Ann. Geophys. 36, 53–57. https://doi.org/10.5194/angeo-36-53-2018.

Marshall, R.A., Dalzell, M., Waters, C.L., Goldthorpe, P., Smith, E.A., 2012. Geomagnetically induced currents in the New Zealand power network. Space Weather 10, S08003. https://doi.org/10.1029/2012SW000806.

Marshall, R.A., Wang, L., Paskos, G.A., Olivares-Pulido, G., Van Der Walt, T., Ong, C., et al., 2019. Modeling geomagnetically induced currents in Australian power networks using different conductivity models. Space Weather 17, 727–756. https://doi.org/10.1029/2018SW002047.

Marshall, R.A. et al., 2013. Observations of geomagnetically induced currents in the Australian power network. Space Weather 11, 6–16. https://doi.org/10.1029/2012SW000849.

Marti, L., Rezaei-Zare, A. and Yan, A. 2013. "Modelling considerations for the Hydro One real-time GMD management system". 2013 IEEE Power & Energy Society General Meeting, Vancouver, BC, Canada, pp. 1-6, doi: 10.1109/PESMG.2013.6673069.

Marti, L., Yiu, C., Rezaei-Zare, A., Boteler, D., 2014. Simulation of geomagnetically induced currents with piecewise layered-Earth models. IEEE Trans. Power Delivery 29 (4), 1886–1893.

Matandirotya, E., Cilliers, P.J., Van Zyl, R.R., 2015. Modeling geomagnetically induced currents in the South African power transmission network using the finite element method. Space Weather 13, 185–195. https://doi.org/10.1002/2014SW001135.

Matsuo, T., Richmond, A.D., 2008. Effects of high-latitude ionospheric electric field variability on global thermospheric Joule heating and mechanical energy transfer rate. J. Geophys. Res. 113, A07309. https://doi.org/10.1029/2007JA012993.

Matsuo, Tomoko 2020, Recent progress on inverse and data assimilation procedure for high-latitude ionospheric electrodynamics, in Ionospheric Multi-Spacecraft Analysis Tools: Approaches for Deriving Ionospheric Parameters, ed. Malcolm Wray Dunlop and Hermann Luhr; ISSI Scientific Report Series Cham: Springer International Publishing pp. 219-232, URL: doi: 10.1007/978-3-030-26732-2.

McCrea, I., Aikio, A., Alfonsi, L., et al., 2015. The science case for the EISCAT_3D radar. Prog. in Earth and Planet. Sci. 2, 21. https://doi.org/10.1186/s40645-015-0051-8.

McGranaghan, R., Knipp, D.J., Matsuo, T., Godinez, H., Redmon, R.J., Solomon, S.C., Morley, S.K., 2015a. Modes of high-latitude auroral conductance variability derived from DMSP energetic electron precipitation observations: Empirical orthogonal function analysis. J. Geophys. Res 120, 11,013ã11,031. https://doi.org/10.1002/2015JA021828.

McGranaghan, R., Knipp, D.J., Solomon, S., Fang, X., 2015b. A fast, parameterized model of upper atmospheric ionization rates, chemistry, and conductivity. J. Geophys. Res. 120. https://doi.org/10.1002/2015JA021146.

McGranaghan, R., Knipp, D.J., Matsuo, T., Cousins, E., 2016. Optimal interpolation analysis of high-latitude ionospheric Hall and Pedersen conductivities: Application to assimilative ionospheric electrodynamics reconstruction. J. Geophys. Res. 121, 4898ã4923. https://doi.org/10.1002/2016JA022486.

McPherron, R.L., Russell, C.T., Aubry, M.P., 1973. Satellite studies of magnetospheric substorms on August 15, 1968: 9. Phenomenological model for substorms. J. Geophys. Res. 78 (16), 3131–3149. https://doi.org/10.1029/JA078i016p03131.

Medford, L.V., Lanzerotti, L.J., Kraus, J.S., Maclennan, C.G., 1989. Transatlantic earth potential variations during the March 1989 magnetic storms. Geophys. Res. Lett. 16 (10), 1145–1148.

Mejnertsen, L., Eastwood, J.P., Chittenden, J., Masters, A., 2016. Global MHD simulations of Neptune's magnetosphere. J. Geophys. Res.: Space Physics 121, 7497–7513. https://doi.org/10.1002/2015JA022272.

Mejnertsen, L., Eastwood, J.P., Hietala, H., Schwartz, S.J., Chittenden, J. P., 2018. Global MHD simulations of the Earth's bow shock shape and motion under variable solar wind conditions. J. Geophys. Res.: Space Phys. 123, 259–271. https://doi.org/10.1002/2017JA024690.

Merkin, V.G., Lyon, J.G., 2010. Effects of the low-latitude ionospheric boundary condition on the global magnetosphere. J. Geophys. Res. Space Phys. 115 (A), 10202. https://doi.org/10.1029/2010ja015461.

Merkin, V.G., Anderson, B.J., Lyon, J.G., Korth, H., Wiltberger, M., Motoba, T., 2013. Global evolution of Birkeland currents on 10 min timescales: MHD simulations and observations. J. Geophys. Res 118, 4977–4997. https://doi.org/10.1002/jgra.50466.

Merkin, V.G., Panov, E.V., Sorathia, K., Ukhorskiy, A.Y., 2019. Contribution of bursty bulk flows to the global dipolarization of the magnetotail during an isolated substorm. J. Geophys. Res. Space Phys. 124, 8647–8668. https://doi.org/10.1029/2019JA026872.

Michael, A.T., Sorathia, K.A., Merkin, V.G., Nykyri, K., Burkholder, B., Ma, X., et al., 2021. Modeling Kelvin-Helmholtz instability at the high-latitude boundary layer in a global magnetosphere simulation. Geophysical Research Letters 48, e2021GL094002. https://doi.org/10.1029/2021GL094002.

Mishin, E., Nishimura, Y., Foster, J., 2017. SAPS/SAID revisited: A causal relation to the substorm current wedge. J. Geophys. Res. Space Physics 122, 8516–8535. https://doi.org/10.1002/2017JA024263.

Mishra, W., Srivastava, N., Chakrabarty, D., 2015. Evolution and consequences of interacting CMEs of 9–10 November 2012 using STEREO/SECCHI and in situ observations. Solar Phys. 290, 527.

Moen, J., Brekke, A., 1993. The solar flux influence on quiet time conductances in the auroral ionosphere. Geophys Res. Lett. 20, 971.

Morley, S., Freeman, M., Tanskanen, E., 2007. A comparison of the probability distribution of observed substorm magnitude with that predicted by a minimal substorm model. Ann. Geophys. 25, 2427–2437.

Mostafavi, P., Merkin, V.G., Provornikova, E., Sorathia, K., Arge, C.N., Garretson, J., 2022. High-resolution Simulations of the Inner Heliosphere in Search of the Kelvin–Helmholtz Waves. The Astrophysical Journal 925 (2), 181. https://doi.org/10.3847/1538-4357/ac3fb4.

Mostl, C., Rollett, T., Frahm, R.A., et al., 2015. Strong coronal channeling and interplanetary evolution of a solar storm up to Earth and Mars. Nat. Comm. 6, 7135. https://doi.org/10.1038/ncomms8135.

Mukhopadhyay, A., Welling, D.T., Liemohn, M.W., Ridley, A.J., Chakraborty, S., Anderson, B.J., 2020. Conductance model for extreme events: Impact of auroral conductance on space weather forecasts. Space Weather 18, e2020SW002551. https://doi.org/10.1029/2020SW002551.

Mukhopadhyay, A., Xianzhe, J., Welling, D. and Liemohn, M. 2021. Global magnetohydrodynamic simulations: performance quantification of magnetopause distances and convection potential predictions, Astron. Space Sci., 21 April 2021, Sec. Space Physics doi: 10.3389/fspas.2021.637197.

Nagatsuma, T., Kataoka, R., Kunitake, M., 2015. Estimating the solar wind conditions during an extreme geomagnetic storm: a case study of the event that occurred on March 13–14, 1989, Earth. Planets and Space 67, 78. https://doi.org/10.1186/s40623-015-0249-4.

Nakamura, T.K.M., Stawarz, J.E., Hasegawa, H., Narita, Y., Franci, L., Wilder, F.D., et al., 2020. Effects of fluctuating magnetic field on the growth of the Kelvin-Helmholtz instability at the Earth's magnetopause. Journal of Geophysical Research: Space Physics 125, e2019JA027515. https://doi.org/10.1029/2019JA027515.

Newell, P.T., Sotirelis, T., Liou, K., Meng, C.I., Rich, F.J., 2007. A nearly universal solar wind-magnetosphere coupling function inferred from 10 magnetospheric state variables. J. Geophys. Res. 112, A01206. https://doi.org/10.1029/2006JA012015.

Newell, P.T., Sotirelis, T., Wing, S., 2009. Diffuse, monoenergetic, and broadband aurora: The global precipitation budget. J. Geophys. Res. 114, A09207. https://doi.org/10.1029/2009JA014326.

Newell, P.T., Sotirelis, T., Wing, S., 2010. Seasonal variations in diffuse, monoenergetic, and broadband aurora. J. Geophys. Res. 115, A03216. https://doi.org/10.1029/2009JA014805.

Newell, P.T., Liou, K., Zhang, Y., Paxton, L.J., Mitchell, E.J., 2014. OVATION Prime-2013: Extension of auroral precipitation model to higher disturbance levels. Space Weather 12, 368–379. https://doi.org/10.1002/2014SW001056.

Ng, J., Chen, L.-J., Omelchenko, Y., Zou, Y., Lavraud, B., 2022. Hybrid simulations of the cusp and dayside magnetosheath dynamics under quasi-radial interplanetary magnetic fields. J. Geophys. Res. Space Physics 127, e2022JA030359.

Ngwira, C.M., Pulkinen, A., McKinnell, A.-L., Cilliers, P.J., 2008. Improved modelling of geomagnetically induced currents in the South African power network. Space Weather 6, S11004. https://doi.org/10.1029/2008SW000408.

Ngwira, C.M., Pulkkinen, A., Wilder, F.D., Crowley, G., 2013a. Extended study of extreme geoelectric field event scenarios for geomagnetically induced current applications. Space Weather 11, 121–131. https://doi.org/10.1002/swe.20021.

Ngwira, C.M., Pulkkinen, A., Mays, M.L., Kuznetsova, M.M., Galvin, A. B., Simunac, K., Baker, D.N., Li, X., Zheng, Y., Glocer, A., 2013b. Simulation of the 23 July 2012 extreme space weather event: What if this extremely rare CME was Earth-directed? Space Weather 11, 671–679. https://doi.org/10.1002/2013SW000990.

Ngwira, C.M., Pulkkinen, A.A., Bernabeu, E., Eichner, J., Viljanen, A., Crowley, G., 2015. Characteristics of extreme geoelectric fields and their possible causes: Localized peak enhancements. Geophys. Res. Lett. 42. https://doi.org/10.1002/2015GL065061.

Ngwira, C.M., Sibeck, D., Silveria, M.V.D., Georgiou, M., Weygand, J. M., Nishimura, Y., Hampton, D., 2018. A study of intense local dB/dt variations during two geomagnetic storms. Space Weather 16. https://doi.org/10.1029/2018SW001911.

Nicolls, M.J., Cosgrove, R., Bahcivan, H., 2014. Estimating the vector electric field using monostatic, multibeam incoherent scatter radar measurements. Radio Sci. 49, 1124ā1139. https://doi.org/10.1002/2014RS005519.

Nikitina, L., Trichtchenko, L., Boteler, D.H., 2016. Assessment of extreme values in geomagnetic and geoelectric field variation for Canada. Space Weather 14. https://doi.org/10.1002/2016SW001386.

Nishida, A., Maezawa, K., 1971. Two basic modes of interaction between the solar wind and the magnetosphere. J. Geophys. Res. 76 (10), 2254–2264. https://doi.org/10.1029/JA076i010p02254.

Nishida, A., 1966. The origin of fluctuations in the equatorial electrojet; a new type of geomagnetic variation. Ann. Geophys. 22, 478–484.

Nishida, A., 1968a. Coherence of geomagnetic DP 2 fluctuations with interplanetary magnetic variations. J. Geophys. Res. 73 (17), 5549–5559. https://doi.org/10.1029/JA073i017p05549.

Nishida, A., 1968b. Geomagnetic Dp 2 fluctuations and associated magnetospheric phenomena. J. Geophys. Res. 73 (5), 1795–1803. https://doi.org/10.1029/JA073i005p01795.

Nishimura, Y., Gallardo-Lacourt, B., Zou, Y., Mishin, E., Knudsen, D.J., Donovan, E.F., et al., 2019. Magnetospheric signatures of STEVE: Implications for the magnetospheric energy source and interhemispheric conjugacy. Geophys. Res. Lett. 46, 5637–5644. https://doi.org/10.1029/2019GL082460.

Nishitani, N., Ruohoniemi, J.M., Lester, M., et al., 2019. Review of the accomplishments of mid-latitude super dual auroral radar network (SuperDARN) HF radars. Prog Earth Planet Sci 6, 27. https://doi.org/10.1186/s40645-019-0270-5.

Nykyri, K., Grison, B., Cargill, P.J., Lavraud, B., Lucek, E., Dandouras, I., Balogh, A., Cornilleau-Wehrlin, N., Rème, H., 2006. Origin of the turbulent spectra in the high-altitude cusp: Cluster spacecraft observations. Ann. Geophys. 24, 1057–1075. https://doi.org/10.5194/angeo-24-1057-2006.

Nykyri, K., Ma, X., Dimmock, A., Foullon, C., Otto, A., Osmane, A., 2017. Influence of velocity fluctuations on the Kelvin-Helmholtz instability and its associated mass transport. J. Geophys. Res. Space Physics 122, 9489–9512. https://doi.org/10.1002/2017JA024374.

Nykyri, K., Bengtson, M., Angelopoulos, V., Nishimura, Y.T., Wing, S., 2019. Can enhanced flux loading by high-speed jets lead to a substorm? Multipoint detection of the Christmas Day substorm onset at 08: 17 UT, 2015. J. Geophys. Res.: Space Phys. 124, 4314–4340. https://doi.org/10.1029/2018JA026357.

Odenwald, S., 2015. Solar Storms:2000 Years of HumanCalamity! CreateSpace Independent Publishing Platform, San Bernardino, CA.

Ogino, T., Walker, R.J., Ashour-Abdalla, M., Dawson, J.M., 1985. An MHD simulation of By dependent magnetospheric convection and field-aligned currents during northward IMF. J. Geophys. Res. 90 (10), 935.

Ohtani, S., Gjerloev, J.W., 2020. Is the substorm current wedge an ensemble of wedgelets?: Revisit to midlatitude positive bays. J. Geophys. Res.: Space Phys. 125, e2020JA027902. https://doi.org/10.1029/2020JA027902.

Oksavik, K., Greenwald, R.A., Ruohoniemi, J.M., Hairston, M.R., Paxton, L.J., Baker, J.B.H., Gjerloev, J.W., Barnes, R.J., 2006. First observations of the temporal/spatial variation of the sub-auroral polarization stream from the SuperDARN Wallops HF radar. Geophys Res Lett 33, L12104. https://doi.org/10.1029/2006GL026256.

Oliveira, D.M., Arel, D., Raeder, J., Zesta, E., Ngwira, C.M., Carter, B. A., et al., 2018. Geomagnetically induced currents caused by interplanetary shocks with different impact angles and speeds. Space Weather 16, 636–647. https://doi.org/10.1029/2018SW001880.

Oliveira, D.M., Weygand, J.M., Zesta, E., Ngwira, C.M., Hartinger, M. D., Xu, Z., et al., 2021. Impact angle control of local intense dB/dt variations during shock-induced substorms. Space Weather 19, e2021SW002933. https://doi.org/10.1029/2021SW002933.

Omelchenko, Y.A., Chen, L.-J., Ng, J., 2021. 3D space-time adaptive hybrid simulations of magnetosheath high-speed jets. J. Geophys. Res. Space Physics 126, e2020JA029035.

Opgenoorth, H.J., Pellinen, R.J., Kaila, K.U., Maurer, H., Kueppers, F., Heikkila, W.J., Tanskanen, P., 1980. Ground based observations of an onset of localised field-aligned currents during auroral breakup around magnetic midnight. J. Geophys. / Zeitschrift F. Geophysik 48, 101–115.

Palin, L., Jacquey, C., Opgenoorth, H., Connors, M., Sergeev, V., et al., 2015. Three-dimensional current systems and ionospheric effects associated with small dipolarization fronts. J. Geophys. Res., Space Phys. 120 (5), 3739–3757. https://doi.org/10.1002/2015JA021040.

Palin, L., Opgenoorth, H.J., Agren, K., Zivkovic, T., Sergeev, V.A., et al., 2016. Modulation of the substorm current wedge by bursty bulk flows: 8 September 2002—Revisited. J. Geophys. Res.: Space Phys. 121 (5), 4466–4482. https://doi.org/10.1002/2015JA022262.

Palmroth, M., Pulkkinen, T.I., Janhunen, P., Wu, C.-C., 2003. Stormtime energy transfer in global MHD simulation. J. Geophys. Res. 108 (A1), 1048. https://doi.org/10.1029/2002JA009446.

Palmroth, M., Ganse, U., Pfau-Kempf, Y., Battarbee, M., Turc, L., Brito, T., Grandin, M., Hoilijoki, S., Sandroos, A., von Alfthan, S., 2018. Vlasov methods in space physics and astrophysics. Living Rev. Comput. Astrophys. 4, 1. https://doi.org/10.1007/s41115-018-0003-2.

Patterson, C.J., Wild, J.A., Boteler, D.H., 2023a. Modeling the impact of geomagnetically induced currents on electrified railway signaling systems in the United Kingdom. Space Weather 21, e2022SW003385. https://doi.org/10.1029/2022SW003385.

Patterson, C.J., Wild, J.A., Boteler, D.H., 2023b. Modeling "wrong side" failures caused by geomagnetically induced currents in electrified railway signaling systems in the UK. Space Weather 21, e2023SW003625. https://doi.org/10.1029/2023SW003625.

Patterson, C.J., Wild, J.A., Beggan, C.D., Richardson, G.S., Boteler, D. H., 2024. Modelling electrified railway signaling misoperations during extreme space weather events in the UK. Sci Rep 14, 1583. https://doi.org/10.1038/s41598-024-51390-3.

Pembroke, A., Toffoletto, F., Sazykin, S., Wiltberger, M., Lyon, J., Merkin, V., Schmitt, P., 2012. Initial results from a dynamic coupled magnetosphere-ionosphere-ring current model. J. Geophys. Res. 117, A02211. https://doi.org/10.1029/2011JA016979.

Pham, K., Zhang, B., Sorathia, K., Dang, T., Wang, W., Merkin, V., et al., 2022. Thermospheric density perturbations produced by traveling atmospheric disturbances during August 2005 storm. J. Geophys. Res.: Space Physics 127 (2), , e2021JA030071. https://doi.org/10.1029/2021JA030071.

Pirjola, R., Viljanen, A., 1998. Complex image method for calculating electric and magnetic fields produced by an auroral electrojet of finite length. Ann. Geophys. 16 (11), 1434–1444. https://doi.org/10.1007/s00585-998-1434-6.

Pirjola, R.J., Boteler, D.H., Tuck, L., Marsal, S., 2022. The Lehtinen-Pirjola method modified for efficient modelling of geomagnetically induced currents in multiple voltage levels of a power network. Ann. Geophys. 40, 205–215. https://doi.org/10.5194/angeo-40-205-2022.

Pirjola, R., 1984. Estimation of the electric field on the earth's surface during a geomagnetic variation. Geophysica 20 (2), 89–103.

Pirjola, R., 2002. Review on the calculation of the surface electric and magnetic fields and geomagnetically induced currents in ground based technological systems. Surv. Geophys. 23, 71–90.

Pirjola, R., 2013. Practical model applicable to investigating the coast effect of the geoelectric field in connection with studies of geomagnetically induced currents. Adv Appl Phys 1 (1), 9–28.

Poedts, S., Kochanov, A., Lani, A., et al., 2020. The virtual space weather modelling centre. J. Space Weather Space Clim. 10, 14. https://doi.org/10.1051/swsc/2020012.

Powell, K.G., Roe, P.L., Linde, T.J., Gombosi, T.I., DeZeeuw, D.L., 1999. A solution-adaptive upwind scheme for ideal magnetohydrodynamics. J. Comp. Phys. 154, 284.

Ptitsyna, N.G., Kasinskii, V.V., Villoresi, G., Lyahov, N.N., Dorman, L.I., 2008. Geomagnetic effects on mid-latitude railways: A statistical study of anomalies in the operation of signaling and train control equipment on the East-Siberian Railway. Adv. Space Res. 42, 1510–1514.

Pulkkinen, A., Rastätter, L., Kuznetsova, M., Singer, H., Balch, C., Weimer, D., Toth, G., Ridley, A., Gombosi, T., Wiltberger, M., Raeder, J., Weigel, R., 2013. Community-wide validation of geospace model ground magnetic field perturbation predictions to support model transition to operations. Space Weather 11, 369–385. https://doi.org/10.1002/swe.20056.

Pulkkinen, A., Bernabeu, E., Thomson, A., Viljanen, A., Pirjola, R., Boteler, D., et al., 2017. Geomagnetically induced currents: science, engineering, and applications readiness. Space Weather 15, 828–856. https://doi.org/10.1002/2016SW001501.

Qian, L., Burns, A.G., Emery, B.A., Foster, B., Lu, G., Maute, A., Richmond, A.D., Roble, R.G., Solomon, S.C. and Wang, W. (2014). The NCAR TIE-GCM. In Modeling the Ionosphere–Thermosphere System (eds J. Huba, R. Schunk and G. Khazanov). https://doi.org/10.1002/9781118704417.ch7.

Raeder, J., Walker, R.J., Ashour-Abdalla, M., 1995. The structure of the distant geomagnetic tail during long periods of northward IMF. Geophys. Res. Lett. 22, 349.

Raeder, J., Berchem, J., Ashour-Abdalla, M., 1998. The Geospace Environment Modeling Grand Challenge: Results from a global geospace circulation model. J. Geophys. Res. 103 (14), 787.

Raeder, J., Wang, Y.L. and Fuller-Rowell, T. 2001. Geomagnetic storm simulation with a coupled magnetosphere— ionosphere—thermosphere model, in Space Weather, ed. by P. Song, G. Siscoe, H.J. Singer. AGU Geophys. Monogr. Ser., vol. 125 (American Geophysical Union, Washington, 2001), p. 377.

Raeder, J., 2003. Global magnetohydrodynamics—A tutorial. In: Büchner, J., Dum, C.T., Scholer, M. (Eds.), Space Plasma Simulation. Springer, Berlin, pp. 212–246.

Raeder, J., Larson, D., Li, W., Kepko, E.L., Fuller-Rowell, T., 2008. Openggcm simulations for the themis mission. Space Sci. Rev. 2008 (141), 535–555. https://doi.org/10.1007/s11214-008-9421-5.

Rajput, V.N., Boteler, D.H., Rana, N., Saiyed, M., Anjana, S., Shah, M., 2021. Insight into impact of geomagnetically induced currents on power systems: Overview, challenges and mitigation. Electric Power Syst. Res. 192, 106927. https://doi.org/10.1016/j.epsr.2020.106927.

Raptis, S., Karlsson, T., Vaivads, A., Lindberg, M., Johlander, A., Trollvik, H., 2022. On magnetosheath jet kinetic structure and plasma properties. Geophys. Res. Lett. 49, e2022GL100678. https://doi.org/10.1029/2022GL100678.

Rastätter, L., Tóth, G., Kuznetsova, M.M., Pulkkinen, A., 2014. CalcDeltaB: An efficient postprocessing tool to calculate groundâ level magnetic perturbations from global magnetosphere simulations. Space Weather 12 (9), 553–565. https://doi.org/10.1002/2014SW001083.

Rastätter, L., Shim, J.S., Kuznetsova, M.M., Kilcommons, L.M., Knipp, D.J., Codrescu, M., Fuller-Rowell, T., Emery, B., Weimer, D.R., Cosgrove, R., et al., 2016. GEM-CEDAR challenge: Poynting flux at DMSP and modeled Joule heat. Space Weather 14, 113–135. https://doi.org/10.1002/2015SW001238.

Redmon, R.J., Peterson, W.K., Andersson, L., Kihn, E.A., Denig, W.F., Hairston, M., Coley, R., 2010. Vertical thermal O+ flows at 850 km in dynamic auroral boundary coordinates. J. Geophys. Res. 115, A00J08. https://doi.org/10.1029/2010JA015589.

Redmon, R.J., Peterson, W.K., Andersson, L., Richards, P.G., 2012. Dawnward shift of the dayside O^+ outflow distribution: The importance of field line history in O^+ escape from the ionosphere. J. Geophys. Res. 117, A12222. https://doi.org/10.1029/2012JA018145.

Redmon, R.J., Peterson, W.K., Andersson, L., Richards, P.G., Yau, A. W., 2014. An assessment of the role of soft electron precipitation in global ion upwelling. J. Geophys. Res. Space Physics 119, 7665–7678. https://doi.org/10.1002/2014JA020061.

Redmon, R.J., Denig, W.F., Kilcommons, L.M., Knipp, D.J., 2017. New DMSP database of precipitating auroral electrons and ions. J. Geophys. Res 122, 9056–9067.

Rees, M.H., 1963. Auroral ionization and excitation by incident energetic electrons'. Planetary Space Sci. 11, 1209.

Reiff, P.H., 1984. Models of Auroral-Zone Conductances. In: Magnetospheric Currents, T.A. Potemra. https://doi.org/10.1029/GM028p0180.

Richmond, A.D., Ridley, E.C., Roble, R.G., 1992. A thermosphere/ionosphere general circulation model with coupled electrodynamics. Geophys. Res. Lett. 19 (6), 601–604. https://doi.org/10.1029/92GL00401.

Richmond, A.D., 1992. Assimilative mapping of ionospheric electrodynamics. Adv. Spa. Res. 12 (6), 59–68.

Ridley, A., Gombosi, T., Zeeuw, D.L., Clauer, C., Richmond, A., 2003. Ionospheric control of the magnetospheric configuration: Neutral winds. J. Geophys. Res. 108, 2002JA009 464.

Ridley, A.J., Gombosi, T.I., DeZeeuw, D.L., 2004. Ionospheric control of the magnetosphere: conductance. Ann. Geophys. 22, 567–584. https://doi.org/10.5194/angeo-22-567-2004.

Ridley, A.J., Deng, Y., Toth, G., 2006. The global ionosphere-thermosphere model. J. Atmos. Sol. Terr. Phys. 68, 839ä864. https://doi.org/10.1016/j.jastp.2006.01.008.

Ridley, A.J., De Zeeuw, D.L., Rastätter, L., 2016. Rating global magnetosphere model simulations through statistical data-model comparisons. Space Weather 14, 819–834. https://doi.org/10.1002/2016SW001465.

Riley, P., Ben-Nun, M., Linker, J.A., Owens, M.J., Horbury, T.S., 2017. Forecasting the properties of the solar wind using simple pattern recognition. Space Weather 15 (3), 526–540.

Riley, P., Baker, D., Liu, Y.D., Verronen, P., Singer, H., Güdel, M., 2018. Extreme space weather events: From cradle to grave. Space Sci. Rev. 214 (1), 21. https://doi.org/10.1007/s11214-017-0456-3.

Rix, B.C. and Boteler, D.H. 2001. Telluric current considerations in the CP design for the Maritimes and Northeast Pipeline, Paper 01317, Proceedings, CORROSION 2001, NACE, Houston, March 11-16.

Robinson, R.M., Vondrak, R.R., 1984. Measurements of E-region ionization and conductivity produced by solar illumination at high latitudes. J. Geophys. Res. 89 (A6), 3951–3956. https://doi.org/10.1029/JA089iA06p03951.

Robinson, R.M., Zanetti, L.J., 2019. Auroral energy flux and Joule heating derived from global maps of field-aligned currents. Geophys. Res. Lett. 48. https://doi.org/10.1029/2020GL091527.

Robinson, R.M., Vondrak, R.R., Miller, K., Dabbs, T., Hardy, D., 1987. On calculating ionospheric conductances from the flux and energy of precipitating electrons. J. Geophys. Res. 92, 2565.

Robinson, R.M., Zhang, Y., Anderson, B.J., Zanetti, L.J., Korth, H., Fitzmaurice, A., 2018. Statistical relations between field-aligned currents and precipitating electron energy flux. Geophys. Res. Lett. 45, 8738–8745. https://doi.org/10.1029/2018GL078718.

Robinson, R.M., Kaeppler, S.R., Zanetti, L., Anderson, B., Vines, S.K., Korth, H., Fitzmaurice, A., 2020. Statistical relations between auroral electrical conductances and field-aligned currents at high latitudes. J. Geophys. Res 125, e2020JA028008.

Robinson, R.M., Zanetti, L., Anderson, B., Vines, S., Gjerloev, J., 2021. Determination of auroral electrodynamic parameters from AMPERE field-aligned current measurements. Space Weather 19, e2020SW002677. https://doi.org/10.1029/2020SW002677.

Rodger, C.J., MacManus, D.H., Dalzell, M., Thomson, A.W., Clarke, E., Petersen, T., Clilverd, M.A., Divett, T., 2017. Long-term geomagnetically induced current observations from New Zealand: Peak current estimates for extreme geomagnetic storms. Space Weather 15 (11), 1447–1460, 495.

Rosenqvist, L., Fristedt, T., Dimmock, A.P., Davidsson, P., Fridström, R., Hall, J.O., et al., 2022. 3D modeling of geomagnetically induced currents in Sweden—validation and extreme event analysis. Space Weather 20, e2021SW002988.

Rostoker, G. 1991. Some Observational Constraints for Substorm Models. In: Kan, J.R., Potemra, T.A., Kokubun, S. and Iijima, T. (Eds.), Magnetospheric Substorms. doi.org/10.1029/GM064p0061.

Sakharov, Ya. A., Danilin, A.N., Ostafiychuk, R.M., Katkalov, Yu. V., Kudryashova, N.V. 2009. Geomagnetically induced currents in the power systems of the Kola peninsula at solar minimum, Proc. 8th Int. Symp. on Electromagnetic Compatibility and Electromagnetic Ecology, St. Petersburg, pp. 237–238.

Sarkar, R., Gopalswamy, N., Srivastava, N., 2020. An Observationally constrained analytical model for predicting the magnetic field vectors of interplanetary coronal mass ejections at 1 au. Astrophys J 888 (2), 121.

Savani, N.P., Vourlidas, A., Szabo, A., Mays, M.L., Richardson, I.G., Thompson, B.J., Pulkkinen, A., Evans, R., Nieves-Chinchilla, T., 2015. Predicting the magnetic vectors within coronal mass ejections arriving at Earth: 1. Initial Architecture. Space Weather 13 (6), 374–385.

Sazykin, S., Wolf, R.A., Spiro, R.W., Gombosi, T.I., De Zeeuw, D.L., and Thomsen, M.F. 2002. Interchange instability in the inner magnetosphere associated with geosynchronous particle flux decreases, Geophys. Res. Lett., 29(10), 1448, doi:10.1029/2001GL014416. (Correction, Geophys. Res. Lett., 29(16), 1778, doi:10.1029/2002GL015846.).

Schultz, A., 2010. EMscope: A continental scale magnetotelluric observatory and data discovery resource. Data Sci. J. 8, IGY6–IGY20.

Schunk, R. and Nagy, A. 2009. Frontmatter. In Ionospheres: Physics, Plasma Physics, and Chemistry (Cambridge Atmospheric and Space Science Series, pp. I-Vi). Cambridge: Cambridge University Press.

Sciola, A., Toffoletto, F., Alexander, D., Sorathia, K., Merkin, V., Farrish, A., 2021. Incorporating inner magnetosphere current-driven electron acceleration in numerical simulations of exoplanet radio emission. Astrophys. J. 914, 1. https://doi.org/10.3847/1538-4357/abefd9.

Sciola, A., Merkin, V.G., Sorathia, K., Gkioulidou, M., Bao, S., Toffoletto, F., et al., 2023. The contribution of plasma sheet bubbles to stormtime ring current buildup and evolution of its energy composition. Journal of Geophysical Research: Space Physics 128, e2023JA031693. https://doi.org/10.1029/2023JA031693.

Senior, A., Kosch, M., Honary, F., 2008. Comparison of methods to determine auroral ionospheric conductances using ground-based optical and riometer data. Ann. Geophys. 26 (12), 3831–3840. https://doi.org/10.5194/angeo-26-3831-2008.

Sergeev, V.A., Tsyganenko, N.A., Smirnov, M.V., Nikolaev, A.V., Singer, H.J., Baumjohann, W., 2011. Magnetic effects of the substorm current wedge in a "spread-out wire" model and their comparison with ground, geosynchronous, and tail lobe data. J. Geophys. Res. 116, A07218. https://doi.org/10.1029/2011JA016471.

Sergeev, V.A., Nikolaev, A.V., Tsyganenko, N.A., Angelopoulos, V., Runov, A.V., Singer, H.J., Yang, J., 2014. Testing a two-loop pattern of the substorm current wedge (SCW2L). J. Geophys. Res. Space Physics 119, 947–963. https://doi.org/10.1002/2013JA019629.

Shore, R.M., Freeman, M.P., Gjerloev, J.W., 2019. Interplanetary magnetic field control of polar ionospheric equivalent current system modes. Space Weather 17, 976–988. https://doi.org/10.1029/2019SW002161.

Shou, Y., Tenishev, V., Chen, Y., Toth, G., Ganushkina, N., 2021. Magnetohydrodynamic with adaptively embedded particle-in-cell model: MHD-AEPIC. J. Computat. Phys. 446, 110656. https://doi.org/10.1016/j.jcp.2021.110656, ISSN 0021-9991.

Smith, A.W., Forsyth, C., Rae, J., Rodger, C.J., Freeman, M.P., 2021. The impact of sudden commencements on ground magnetic field variability: Immediate and delayed consequences. Space Weather 19 (7), e2021SW002764. https://doi.org/10.1029/2021SW002764.

Smith, A.W., Forsyth, C., Rae, I.J., Garton, T.M., Jackman, C.M., Bakrania, M., et al., 2022. On the considerations of using near real time data for space weather hazard forecasting. Space Weather 20, e2022SW003098. https://doi.org/10.1029/2022SW003098.

Sojka, J.J., McPherron, R.L., van Eyken, A.P., Nicolls, M.J., Heinselman, C.J., Kelly, J.D., 2009. Observations of ionospheric heating during the passage of solar coronal hole fast streams. Geophys. Res. Lett. 36, L19105. https://doi.org/10.1029/2009GL039064.

Solomon, S.C., 2001. Auroral particle transport using Monte Carlo and hybrid methods. J. Geophys. Res. 106, 107.

Sorathia, K.A., Merkin, V.G., Panov, E.V., Zhang, B., Lyon, J.G., Garretson, J., et al., 2020. Ballooning-interchange instability in the near-Earth plasma sheet and auroral beads: Global magnetospheric modeling at the limit of the MHD approximation. Geophys. Res. Lett. 47, e2020GL088227. https://doi.org/10.1029/2020GL088227.

Sorathia, K., Michael, A., Sciola, A., Bao, S., Lin, D., Merkin, S., Ukhorskiy, S., Roedig, C., and Garretson, J. 2023. Global modeling of the mesoscale buildup of the ring current and its role in magnetosphere-ionosphere coupling, EGU General Assembly 2023, Vienna, Austria, 24–28 Apr 2023, EGU23-3445, doi: 10.5194/egusphere-egu23-3445.

Spiro, R.W., Reiff, P.H., Maher Jr., L.J., 1982. Precipitating electron energy flux and auroral zone conductances - An empirical model. J. Geophys. Res. 87, 8215–8227. https://doi.org/10.1029/JA087iA10p08215.

Stamm, J., Vierinen, J., Gustavsson, B., Spicher, A., 2023. A technique for volumetric incoherent scatter radar analysis. Ann. Geophys. 41, 55–67. https://doi.org/10.5194/angeo-41-55-2023.

Stawarz, J.E. et al., 2016. Observations of turbulence in a Kelvin-Helmholtz event on 8 September 2015 by the Magnetospheric Multiscale mission. J. Geophys. Res. Space Physics 121, 11021–11034. https://doi.org/10.1002/2016JA023458.

Strangeway, R.J., Ergun, R.E., Su, Y.-J., Carlson, C.W., Elphic, R.C., 2005. Factors controlling ionospheric outflows as observed at intermediate altitudes. J. Geophys. Res. 110, A03221. https://doi.org/10.1029/2004JA010829.

Strickland, D.J., Book, D.L., Coffey, T.P., Fedder, J.A., 1976. Transport equation techniques for the deposition of auroral electrons'. J. Geophys. Res. 81, 2755.

Strickland, D.J., Jasperse, J.R., Whalen, J.A., 1983. Dependence of auroral FUV emissions on the incident electron spectrum and neutral atmosphere'. J. Geophys. Res. 88, 8051.

Tan, Y., Dang, T., Lei, J., Zhang, B., Wang, W., Yang, Z., 2022. Interplanetary control of high-latitude thermospheric winds: Results from HIWIND and model simulations. J. Geophys. Res.: Space Phys. 127, e2022JA030394. https://doi.org/10.1029/2022JA030394.

Tanaka, T., Nakamizo, A., Yoshikawa, A., Fujita, S., Shinagawa, H., Shimazu, H., Kikuchi, T., Hashimoto, K.K., 2010. Substorm convection and current system deduced from the global simulation. J. Geophys. Res. 115, A05220. https://doi.org/10.1029/2009JA014676.

Tanaka, T., Ebihara, Y., Watanabe, M., Den, M., Fujita, S., Kikuchi, T., Hashimoto, K.K., Kataoka, R., 2017. Global simulation study for the time sequence of events leading to the substorm onset. J. Geophys. Res. Space Physics 122, 6210–6239. https://doi.org/10.1002/2017JA024102.

Tanaka, T., 1994. Finite volume TVD scheme on an unstructured grid system for three-dimensional MHD simulation of inhomogeneous systems including strong background potential fields. J. Comput. Phys. 111, 381. https://doi.org/10.1006/jcph.1994.1071.

Tanaka, T., 1995. Generation mechanisms for magnetosphere-ionosphere current systems deduced from a three-dimensional MHD simulation of the solar wind-magnetosphere-ionosphere coupling process. J. Geophys. Res. 100 (A7), 12057–12074. https://doi.org/10.1029/95JA00419.

Temmer et al., this issue.

Thayer, J.P., Semeter, J., 2004. The convergence of magnetospheric energy flux in the polar atmosphere. J. Atmos. Sol. Terr. Phys. 66, 807ä824. https://doi.org/10.1016/j.jastp.2004.01.035.

Thayer, J.P., 1998. Height-resolved Joule heating rates in the high-latitude E region and the influence of neutral winds. J. Geophys. Res 103 (A1), 471–487.

Thomas, E.G., Shepherd, S.G., 2018. Statistical Patterns of Ionospheric Convection Derived from Mid-latitude, High-Latitude, and Polar SuperDARN HF Radar Observations. J. Geophys. Res. 123, 3196–3216. https://doi.org/10.1002/2018Ja025280.

Thomson, A.W.P., Dawson, E.B., Reay, S.J., 2011. Quantifying extreme behavior in geomagnetic activity. Space Weather 9, S10001. https://doi.org/10.1029/2011SW000696.

Thébault, E., Finlay, C., Toh, H., 2015. Special issue "International Geomagnetic Reference Field—the twelfth generation". Earth Planet Sp 67, 158. https://doi.org/10.1186/s40623-015-0313-0.

Toffoletto, F., Sazykin, S., Spiro, R., et al., 2003. Inner magnetospheric modeling with the rice convection model. Space Science Reviews 107, 175–196. https://doi.org/10.1023/A:1025532008047.

Torta, J.M., Serrano, L., Regué, J.R., Sánchez, A.M., Roldán, E., 2012. Geomagnetically induced currents in a power grid of northeastern Spain. Space Weather 10, S06002. https://doi.org/10.1029/2012SW000793.

Torta, J.M., Marsal, S., Ledo, J., Queralt, P., Canillas-Pérez, V., Piña-Varas, P., et al., 2021. New detailed modeling of GICs in the Spanish power transmission grid. Space Weather 19, e2021SW002805. https://doi.org/10.1029/2021SW002805.

Tozzi, R., De Michaelis, P., Coco, I., Giannattasio, F., 2019. A preliminary risk assessment of geomagnetically induced currents over the Italian territory. Space Weather 17, 46–58. https://doi.org/10.1029/2018SW002065.

Trichtchenko, L., 2021. Frequency consideration in GIC applications. Space Weather 19, e2020SW002694. https://doi.org/10.1029/2020SW002694.

Tsurutani, B.T., Hajra, R., 2021b. The Interplanetary and Magnetospheric causes of Geomagnetically Induced Currents (GICs) > 10 A in the Mäntsälä Finland Pipeline: 1999 through 2019 – Erratum. J. Space Weather Space Clim. 11, 32, a, b doi: 10.1051/swsc/2021015.

Tsurutani, B.T., Gonzalez, W.D., Lakhina, G.S., Alex, S., 2003. The extreme magnetic storm of 1–2 September 1859. J. Geophys. Res. 108, 1268. https://doi.org/10.1029/2002JA009504, A7.

Tsurutani, B.T., Lakhina, G.S., Hajra, R., 2020. The physics of space weather/solar-terrestrial physics (STP): what we know now and what the current future challenges are. Nonlinear Processes Geophys. 27, 75–119. https://doi.org/10.5194/npg-27-75-2020.

Tsurutani, B.T., Hajra, R., 2021a. The interplanetary and magnetospheric causes of geomagnetically induced currents (GICs) > 10 A in the Mäntsälä Finland Pipeline: 1999 through 2019. J. Space Weather Space Clim. 11, 23. https://doi.org/10.1051/swsc/2021001.

Tsyganenko, N.A., Sitnov, M.I., 2007. Magnetospheric configurations from a high-resolution data-based magnetic field model. J. Geophys. Res. 112, A06225. https://doi.org/10.1029/2007JA012260.

Tóth, G., Meng, X., Gombosi, T.I., Ridley, A.J., 2011. Reducing numerical diffusion in magnetospheric simulations. J. Geophys. Res. 116, A07211. https://doi.org/10.1029/2010JA016370.

Tóth, G., Meng, X., Gombosi, T.I., Rastätter, L., 2014. Predicting the time derivative of local magnetic perturbations. J. Geophys. Res. Space Physics 119, 310–321. https://doi.org/10.1002/2013JA019456.

Tóth, G. et al., 2005. Space weather modeling framework: a new tool for the space science community. J. Geophys. Res. 110, A12226. https://doi.org/10.1029/2005JA011126.

Tóth, G. et al., 2012. Adaptive numerical algorithms in space weather modeling. J. Comput. Phys. 231 (3), 870–903. https://doi.org/10.1016/j.jcp.2011.02.006.

Van Leer, B., 1997. Towards the ultimate conservative difference scheme, IV, A new approach to numerical convection. J. of Comp. Phys. 23 (3), 276–299. https://doi.org/10.1016/0021-9991(77)90095-X.

Vandegriff, E., Welling, D., Mukhopadhyay, A. et al., 2022. Forecasting of localized geomagnetic disturbances in global models: Physics and Numerics. Authorea. February 03, 2022. doi: 10.1002/essoar.10510388.1.

Varney, R.H., Wiltberger, M., Lotko, W., 2015. Modeling the interaction between convection and nonthermal ion outflows. J. Geophys. Res. Space Phys. 120, 2353–2362. https://doi.org/10.1002/2014JA020769.

Varney, R.H., Wiltberger, M., Zhang, B., Lotko, W., Lyon, J., 2016a. Influence of ion outflow in coupled geospace simulations: 1. Physics-based ion outflow model development and sensitivity study. J. Geophys. Res. Space Phys. 121, 9671–9687. https://doi.org/10.1002/2016JA022777.

Varney, R.H., Wiltberger, M., Zhang, B., Lotko, W., Lyon, J., 2016b. Influence of ion outflow in coupled geospace simulations: 2. Sawtooth oscillations driven by physics-based ion outflow. J. Geophys. Res. Space Phys. 121, 9688–9700. https://doi.org/10.1002/2016JA022778.

Verkhoglyadova, O.P., Meng, X., Mannucci, A.J., Tsurutani, B.T., Hunt, L.A., Mlynczak, M.G., Hajra, R., Emery, B.A., 2016. Estimation of energy budget of ionosphere-thermosphere system during two CIR-HSS events: Observations and modeling. J. Space Weather Space Clim. 6, A20. https://doi.org/10.1051/swsc/2016013.

Verkhoglyadova, O.P., Meng, X., Mannucci, A.J., Mlynczak, M.G., Hunt, L.A., Lu, G., 2017. Ionosphere-thermosphere energy budgets for the ICME storms of March 2013 and 2015 estimated with GITM and observational proxies. Space Weather 15. https://doi.org/10.1002/2017SW001650.

Vickrey, J.F., Vondrak, R.R., Matthews, S.J., 1981. "The diurnal and latitudinal variation of auroral zone ionospheric conductivity". J. Geophys. Res. 86 (A1), 65–75. https://doi.org/10.1029/JA086iA01p00065.

Viljanen, A., Tanskanen, E., 2011. Climatology of rapid geomagnetic variations at high latitudes over two solar cycles. Ann. Geophys. 29, 1783–1792. https://doi.org/10.5194/angeo-29-1783-2011.

Viljanen, A., Tanskanen, E.I., Pulkkinen, A., 2006a. Relation between substorm characteristics and rapid temporal variations of the ground magnetic field. Annales Geophysicae 24 (2), 725–733, Copernicus GmbH.

Viljanen, A., Pulkkinen, A., Pirjola, R., Pajunpää, K., Posio, P., Koistinen, A., 2006b. Recordings of geomagnetically induced currents and a nowcasting service of the Finnish natural gas pipeline system. Space Weather 4, S10004. https://doi.org/10.1029/2006SW000234.

Viljanen, A. et al., 2004. Fast computation of the geoelectric field using the method of elementary current systems and planar Earth models. Ann. Geophys. 22, 101–113 sref:1432–0576/ag/2004-22-101.

Von Alfthan, S., Pokhotelov, D., Kempf, Y., Hoilijoki, S., Honkonen, I., Sandroos, A., Palmroth, M., 2014. Vlasiator: First global hybrid-Vlasov simulations of Earth's foreshock and magnetosheath. J. Atmos. Sol.-Terr. Phys. 120, 2435. https://doi.org/10.1016/j.jastp.2014.08.012.

Vourlidas, A., 2021. Improving the medium-term forecasting of space weather: A big picture review from a solar observer's perspective. Frontiers Astronomy Space Sci. https://doi.org/10.3389/fspas.2021.651527.

Wallis, D.D., Budzinski, E.E., 1981. Empirical models of height integrated conductivities. J. Geophys. Res. 86, 125–137. https://doi.org/10.1029/JA086iA01p00125.

Wang, Z., Zou, S., 2022. COMPASS: A new COnductance Model based on PFISR And SWARM Satellite observations. Space Weather 20, e2021SW002958. https://doi.org/10.1029/2021SW002958.

Watari, S., Nakamura, S., Ebihara, Y., 2021. Measurement of geomagnetically induced current (GIC) around Tokyo, Japan. Earth, Planets Space 73 (1), 102. https://doi.org/10.1186/s40623-021-01422-3.

Watari, S. et al., 2009a. Measurements of geomagnetically induced current in a power grid in Hokkaido, Japan. Space Weather 7, S03002. https://doi.org/10.1029/2008SW000417.

Watari, S. et al., 2009b. Correction to "Measurements of geomagnetically induced current in a power grid in Hokkaido, Japan". Space Weather 7, S05099. https://doi.org/10.1029/2009SW000484.

Waters, C.L., Anderson, B.J., Liou, K., 2001. Estimation of global field aligned currents using the Iridium System magnetometer data. Geophys. Res. Lett 28, 2165.

Waters, C.L., Anderson, B.J., Green, D.L., Korth, H., Barnes, R.J., Vanhamäki, H., 2020. Science Data Products for AMPERE. In: Dunlop, M., Lühr, H. (Eds.), Ionospheric Multi-Spacecraft Analysis Tools. ISSI Scientific Report Series, vol 17. Springer, Cham. https://doi.org/10.1007/978-3-030-26732-2_7.

Wei, L.H., Homeier, N., Gannon, J.L., 2013. Surface electric fields for North America during historical geomagnetic storms. Space Weather 11, 451–462. https://doi.org/10.1002/swe.20073.

Weimer, D.R., 2001. (2001), An improved model of ionospheric electric potentials including substorm perturbations and application to the GEM November 24, 1996 event. J. Geophys. Res 106, 407.

Weimer, D.R., 2005. Improved ionospheric electrodynamic models and application to calculating Joule heating rates. J. Geophys. Res. 110, A05306. https://doi.org/10.1029/2004JA010884.

Welling, D.T., Liemohn, M.W., 2016. The ionospheric source of magnetospheric plasma is not a black box input for global models. J. Geophys. Res.: Space Phys. 121 (6), 5559–5565.

Welling, D.T., Jordanova, V.K., Glocer, A., Toth, G., Liemohn, M.W., Weimer, D.R., 2015. The two-way relationship between ionospheric outflow and the ring current. J. Geophys. Res. Space Physics 120, 4338–4353. https://doi.org/10.1002/2015JA021231.

Welling, D., Toth, G., Jordanova, V.K., Yu, Y., 2018. Integration of RAM-SCB into the space weather modeling framework. United States. https://doi.org/10.1016/j.jastp.2018.01.007.

Weygand, J.M., Wing, S., 2020. Temporal and spatial development of TEC enhancements during substorms. J. Geophys. Res 125 (3), e2019JA026985.

Weygand, J.M., Amm, O., Angelopoulos, V., Milan, S.E., Grocott, A., Gleisner, H., Stolle, C., 2012. Comparison between SuperDARN flow vectors and equivalent ionospheric currents from ground magnetometer arrays. J. Geophys. Res. 117, A05325. https://doi.org/10.1029/2011JA017407.

Weygand, J.M., Engebretson, M.J., Pilipenko, V.A., Steinmetz, E.S., Moldwin, M.B., Connors, M.G., Nishimura, Y., Lyons, L.R., Russell, C.T., Ohtani, S., Gjerloev, J., 2021. SECS analysis of nighttime magnetic perturbation events observed in Arctic Canada. J. Geophys. Res.: Space Phys. 126, e2021JA029839. https://doi.org/10.1029/2021JA029839.

Weygand, J.M., Bortnik, J., Chu, X., Cao, X., Li, J., Aryan, H., Tian, S., 2022. Magnetosphere-ionosphere coupling between north-south propagating streamers and high-speed earthward flows. J. Geophys. Res. Space Physics 127, e2022JA030741. https://doi.org/10.1029/2022JA030741.

Weygand, J.M., C.M. Ngwira, C.M., and R.R. Arritt, R.F. 2023. The equatorward boundary of the auroral current system during magnetic storms. J. Geophys. Res. Space Physics, 128, e2023JA031510. doi: 10.1029/2023JA031510.

Weygand, J.M., 2021. The temporal and spatial development of dB/dt for substorms. AIMS Geosciences 7 (1), 74–94.

Wik, M., Pirjola, R., Lundstedt, H., Viljanen, A., Wintoft, P., Pulkkinen, A., 2009. Space Weather Events in July 1982 and October 2003 and the effects of geomagnetically induced currents on swedish technical systems. Ann. Geophys. 27 (4), 1775–1787.

Williams, P.J.S., Jones, G.O.L., Jain, A.R., 1984. Method of measuring plasma velocity with EISCAT. J. Atmos. Terr. Phys. 46 (6), 521–530.

Wiltberger, M., Pulkkinen, T.I., Lyon, J.G., Goodrich, C.C., 2000. MHD simulation of the December 10, 1996 substorm. J. Geophys. Res. 106, 27649–27663.

Wiltberger, M., Weigel, R.S., Lotko, W., Fedder, J.A., 2009. Modeling seasonal variations of auroral particle precipitation in a global-scale magnetosphere-ionosphere simulation. J. Geophys. Res. 114, A01204. https://doi.org/10.1029/2008JA013108.

Wiltberger, M. et al., 2017. Effects of electrojet turbulence on magnetosphere-ionosphere simulation of a geomagnetic storm. J. Geophys. Res. Space Physics 122, 5008–5027. https://doi.org/10.1002/2016JA023700.

Winter, L.M., 2019. Geomagnetically induced currents from extreme space weather events. InGeomagnetically induced currents from the Sun to the power grid. American Geophysical Union (AGU), pp. 195–203.

Wolf, R.A., 1983. The quasi-static (slow-flow) region of the magnetosphere. In: Carovillano, R.L., Forbes, J.M. (Eds.), Solar Terrestrial Physics. Norwell, Mass, D. Reidel, pp. 303–368.

Wu, J., Knudsen, D.J., Gillies, D.M., Donovan, E.F., Burchill, J.K., 2017. Swarm observation of field-aligned currents associated with multiple auroral arc systems. J. Geophys. Res.: Space Phys. 122, 10,145–10,156. https://doi.org/10.1002/2017JA024439.

Xi, S., W. Lotko, B. Zhang, O. J. Brambles, J. G. Lyon, V. G. Merkin, and M. Wiltberger (2015), Poynting flux-conserving low-altitude boundary conditions for global magnetospheric models, *J. Geophys. Res.*, 120, 384–400, doi:10.1002/2014JA020470.

Yee, J.H., Gjerloev, J., Wu, D., Schwartz, M.J., 2017. First application of the Zeeman technique to remotely measure auroral electrojet intensity from space. Geophys. Res. Lett. 44, 10134–10139. https://doi.org/10.1002/2017GL074909.

Yee, J.-H., Gjerloev, J. and Wu, D. 2021. Remote sensing of magnetic fields induced by electrojets from space". In: Wang, W., Zhang, Y. and

Paxton, (L.J.), Upper Atmosphere Dynamics and Energetics. (American Geophysical Union AGU). chap. 21. 451–468. doi:10.1002/9781119815631.ch21.

Yermolaev, Y.I., Lodkina, I.G., Nikolaeva, N.S. and Yermolaev, M.Y. 2018. Geoeffectiveness of Solar and Interplanetary Structures and Generation of Strong Geomagnetic Storms, In Extreme Events in Geospace: Origins, Predictability, and Consequences Edited by Buzulukova. Elsevier, doi: 10.1016/B978-0-12-812700-1.00004-2.

Yu, Y., Ridley, A., Welling, D.T., Tóth, G., 2010. Including gap region field-aligned currents and magnetospheric currents in the MHD calculation of ground-based magnetic field perturbations. J. Geophys. Res. 115, A08207. https://doi.org/10.1029/2009JA014869.

Yu, Z., Hao, J., Liu, L., Wang, Z., 2019. Monitoring experiment of electromagnetic interference effects caused by geomagnetic storms on buried pipelines in China. IEEE Access 7, 14603–14610. https://doi.org/10.1109/ACCESS.2019.2893963.

Zhang, Y., Paxton, L.J., 2008. An empirical Kp-dependent global auroral model based on TIMED/GUVI data. J. Atmos. Solar-Terr. Physics 70, 1231.

Zhang, Y., Paxton, L.J., Bilitza, D., Doe, R., 2010. Near real-time assimilation in IRI of auroral peak E-region density and equatorward boundary. Adv. Space Res. 46, 1055–1063.

Zhang, J.J., Wang, C., Tang, B.B., 2012. Modeling geomagnetically induced electric field and currents by combining a global MHD model with a local one-dimensional method. Space Weather 10, S05005. https://doi.org/10.1029/2012SW000772.

Zhang, J.J., Wang, C., Sun, T.R., Liu, C.M., Wang, K.R., 2015. GIC due to storm sudden commencement in low-latitude high-voltage power network in China: Observation and simulation. Space Weather 13. https://doi.org/10.1002/2015SW001263.

Zhang, B., Brambles, O.J., Lotko, W., Ouellette, J.E., Lyon, J.G., 2016. The role of ionospheric O+ outflow in the generation of earthward propagating plasmoids. J. Geophys. Res. Space Physics 121, 1425–1435. https://doi.org/10.1002/2015JA021667.

Zhang, B., Sorathia, K.A., Lyon, J.G., Merkin, V.G., Garretson, J.S., Wiltberger, M., 2019. GAMERA: A three-dimensional finite-volume MHD solver for non-orthogonal curvilinear geometries. The Astrophysical Journal - Supplement Series 244 (1), 20. https://doi.org/10.3847/1538-4365/ab3a4c.

Zhang, B., Delamere, P.A., Yao, Z., Bonfond, B., Lin, D., Sorathia, K.A., et al., 2021. How Jupiter's unusual magnetospheric topology structures its aurora. Sci. Adv. 7 (15), eabd1204. https://doi.org/10.1126/sciadv.abd1204.

Zheng, K., Boteler, D.H., Pirjola, R., Liu, L.G., Becker, R., Marti, L., Boutilier, S. and Guillon, S. 2014. Effects of system characteristics on geomagnetically induced currents". In: IEEE Trans. Power Delivery, 29, 2, 890-898.

Zheng, Y., Jun, I., Tu, W., Shprits, Y., Kim, W., Matthiä, D., Meier, M. M., Tobiska, W.K., Miyoshi, Y., Jordanova, V.K., Ganushkina, N.Y., Tenishev, V. 2023. Overview, Progress and Next Steps for Our Understanding of the Near-Earth Space Radiation and Plasma Environment (G3 Cluster): Science and Applications, submitted to Advances in Space Research.

Zhu, J., Ridley, A.J., 2016. "Investigating the performance of simplified neutral-ion collisional heating rate in a global IT model". J. Geophys. Res. A: Space Phys. 121 (1), 578–588.